

Coulomb-Blockade Oscillations in Quantum Dots and Wires

PROEFSCHRIFT

ter verkrijging van de graad van doctor aan de
Technische Universiteit Eindhoven, op gezag van
de Rector Magnificus, prof. dr. J. H. van Lint,
voor een commissie aangewezen door het College
van Dekanen in het openbaar te verdedigen op
donderdag 5 november 1992 om 16.00 uur

door

ANTONIUS ADRIAAN MARIA STARING

Geboren te Tilburg

Dit proefschrift is goedgekeurd
door de promotoren
prof. dr. J. H. Wolter
en
prof. dr. C. W. J. Beenakker
en door de copromotor
dr. H. van Houten

The work described in this thesis has been carried out at the Philips Research Laboratories Eindhoven as part of the Philips programme.

*aan mijn ouders
aan Lisette*

Contents

1	Introduction	1
1.1	Preface	1
1.2	The two-dimensional electron gas	2
1.3	Split-gate nanostructures	6
1.4	Coulomb blockade and single-electron tunneling	9
	References	17
2	Theory of Coulomb-blockade oscillations	21
2.1	Introduction	21
2.2	Periodicity of the oscillations	25
2.3	Conductance oscillations	31
2.4	Thermopower oscillations	39
	References	44
3	Coulomb-blockade oscillations in disordered quantum wires	47
3.1	Introduction	47
3.2	Split-gate quantum wires	49
3.3	Experimental results	51
3.3.1	Conductance oscillations: Zero magnetic field	53
3.3.2	Conductance oscillations: Quantum Hall effect regime	56
3.3.3	Magnetoconductance	61
3.3.4	Hall resistance	64
3.4	Coulomb-blockade oscillations	65
3.4.1	Periodicity	66
3.4.2	Amplitude and lineshape	67

3.4.3	Multiple segments	69
3.5	Discussion	71
	References	76
4	Coulomb-blockade oscillations in quantum dots	79
4.1	Introduction	79
4.2	Temperature dependence	83
4.3	Periodic envelope of Coulomb-blockade oscillations in the quantum Hall regime	88
4.4	Influence of adiabatically transmitted edge channels on single-electron tunneling through a quantum dot	95
4.5	Coulomb-blockade oscillations in the thermopower of a quantum dot	103
	References	111
	Summary	115
	Samenvatting	117
	List of publications	121
	Dankwoord	125
	Curriculum Vitae	127

Chapter 1

Introduction

1.1 Preface

Fundamental solid-state physics has benefitted greatly from the massive industrial research and development effort towards the miniaturization of semiconductor devices. This effort has produced sophisticated crystal growth and lithographic techniques, which allow fabrication of artificial structures, or “devices”, that exhibit new physical phenomena. These new phenomena occur as the structure size is decreased below some relevant physical length scale. Examples of such phenomena and the associated length scales are quantum interference and the quantum mechanical phase coherence length, ballistic transport and the mean free path, and quantum confinement and the Fermi wave length. In addition, phenomena of single-electron tunneling become important if the device capacitance is so small that the electrostatic charging energy required to add a single electron to the device exceeds the thermal energy.

The branch of physics devoted to the study of these effects has been called “mesoscopic” physics [1], since on these short length scales the devices acquire unusual properties, that are neither those of microscopic objects (atoms and molecules) nor those of macroscopic systems. From a scientific point of view, mesoscopic physics is a rich and rewarding field of research, which has grown rapidly. Although it is scarcely a decade old, a lot has been achieved in this field already, in terms of the variety of phenomena that have been discovered and understood [2, 3].

In the past few years, single-electron tunneling has become one of the foci of attention in mesoscopic physics. In this thesis we describe our contribution to this field, which is a study of the interplay of quantum confinement and single-electron tunneling in semiconductor nanostructures. The nanostructures used for this work are split-gate quantum dots and wires, defined in the two-dimensional electron gas in a GaAs–Al_xGa_{1–x}As heterostructure. Both quantum confinement and single-electron tunneling can be observed in this type of nanostructure at low temperatures (1 K and below). In addition, a strong magnetic field (up to 8 T) is used to alter the quantum confinement, allowing discrimination between effects due to quantum confinement and due to single-electron tunneling. Some of the more subtle effects resulting from the interplay between the two have an energy scale of only 0.1 meV (which is equivalent to a temperature of approximately 100 mK). This is why the experiments are made in a dilution refrigerator.

In this introductory chapter, we will introduce the two-dimensional electron gas, explain the split-gate technique, and give a brief overview of single-electron tunneling. After outlining the contents of the subsequent chapters, we close this chapter with a short discussion on the relevance of single-electron tunneling with respect to device applications.

1.2 The two-dimensional electron gas

The two-dimensional electron gas (2DEG) in a modulation-doped GaAs–Al_xGa_{1–x}As heterostructure [4] provides the starting point for the devices studied in this thesis. Such a heterostructure consists of a sequence of thin layers grown epitaxially on a semi-insulating GaAs substrate, see Fig. 1.1(a). The growth technique of choice is molecular-beam epitaxy since this technique yields the highest quality structures, in terms of purity, interface sharpness and crystalline perfection. As shown in Fig. 1.1(b), the conduction electrons supplied by the donors in the Al_xGa_{1–x}As layer are confined in a narrow potential well at the interface of the GaAs and Al_xGa_{1–x}As. This nearly triangular potential well is formed by the repulsive barrier due to the conduction band offset of approximately 0.3 eV between GaAs and Al_xGa_{1–x}As, and by the attractive electrostatic potential due to the positively charged donors in the Al_xGa_{1–x}As layer. Motion of the electrons in the potential well is quantized perpendicular to the in-

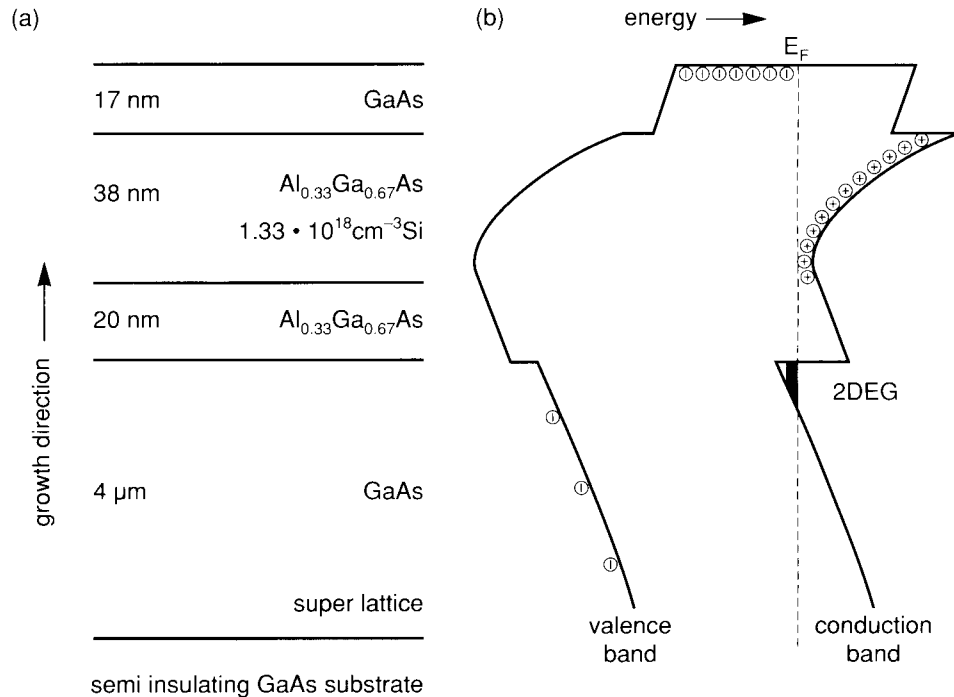


Figure 1.1: Layers of a modulation doped GaAs–Al_xGa_{1–x}As heterostructure (a) and the corresponding band-bending diagram (b). The numbers give typical dimensions.

terface, but is free parallel to the interface. This results in the formation of two-dimensional subbands in the well. Usually the subband associated with the lowest discrete confinement level is populated only.

A 2DEG has several desirable properties. The most important of these may be that the mobility is much greater than is achievable in bulk GaAs. Due to the remote doping scheme the conduction electrons are separated from the ionized donors in the doped Al_xGa_{1–x}As layer, so that scattering from the latter is reduced. Scattering from the ionized donors is further reduced by the insertion of an undoped Al_xGa_{1–x}As spacer layer setting the doped layer back from the heterointerface. Record low-temperature mobilities up to $\mu \gtrsim 10^7$ cm²/Vs have been reported [5], corresponding to elastic mean free paths exceeding $l_e = 0.1$ mm. Another important property of the 2DEG is its low electron density, which can be varied easily by means

of an electric field applied perpendicular to the layers. Usually a metallic gate electrode is deposited on top of the heterostructure for this purpose, in which case isolation is provided automatically by a Schottky barrier. The gate voltage is defined relative to the 2DEG. The density underneath a gate electrode of large area changes linearly with the electrostatic potential ϕ_{gate} of the gate, according to the parallel plate capacitor formula

$$\delta n_s = \frac{\varepsilon}{ed} \delta \phi_{\text{gate}}, \quad (1.1)$$

where $\varepsilon \approx 13\varepsilon_0$ is the static dielectric constant of GaAs, and d is the distance between gate and 2DEG.

An additional advantage of the low electron density is that it leads to a large Fermi wave length. The energy of noninteracting conduction electrons in an unbounded 2DEG is

$$E(k) = \frac{\hbar^2 k^2}{2m}, \quad (1.2)$$

which is isotropic as a function of momentum $\hbar k$. The effective mass in GaAs is $m = 0.067m_0$. The 2D density-of-states

$$\rho_{\text{2D}} = \frac{m}{\pi \hbar^2} \quad (1.3)$$

is *independent* of energy. In equilibrium, the states are occupied according to the Fermi-Dirac distribution

$$f(E - E_F) = \left[1 + \exp \left(\frac{E - E_F}{k_B T} \right) \right]^{-1}. \quad (1.4)$$

At low temperatures T such that $k_B T \ll E_F$, the Fermi energy (or chemical potential) E_F of a 2DEG is thus directly proportional to its sheet density n_s , according to

$$E_F = n_s / \rho_{\text{2D}}. \quad (1.5)$$

The Fermi wave number $k_F \equiv (2mE_F/\hbar^2)^{1/2}$ is related to the density by $k_F = (2\pi n_s)^{1/2}$. Typically, $n_s \sim 3 \times 10^{11} \text{ cm}^{-2}$, so that $E_F \sim 10 \text{ meV}$, and the Fermi wave length $\lambda_F \equiv 2\pi/k_F \sim 50 \text{ nm}$.

One of the most remarkable phenomena exhibited by a 2DEG is the quantum Hall effect [6]. In a strong perpendicular magnetic field B the energy spectrum of the electrons becomes fully discrete, since no free translational motion parallel to B is possible (as in bulk GaAs). Highly degenerate

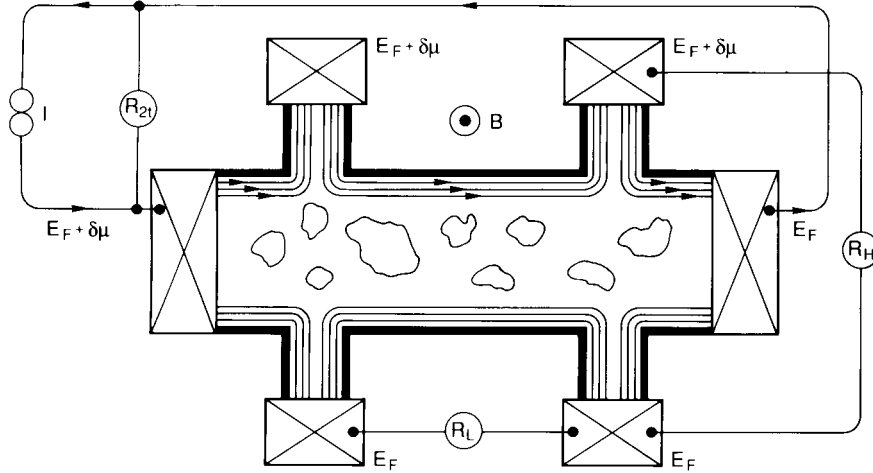


Figure 1.2: Measurement configuration for the Hall resistance R_H , the longitudinal resistance R_L , and the two-terminal resistance R_{2t} . The N_L edge channels at the Fermi level are indicated, with arrows pointing in the direction of motion of edge channels filled by the source contact at chemical potential $E_F + \delta\mu$. The current is carried equally by the edge channels at the upper edge. Localized states in the bulk do not contribute to the conductance. The resulting resistances are $R_{2t} = R_H = h/N_L e^2$, and $R_L = 0$.

Landau levels are formed at energies

$$E_n = (n - \frac{1}{2})\hbar\omega_c , \quad n = 1, 2, \dots , \quad (1.6)$$

where $\omega_c = eB/m$ is the cyclotron frequency. Only a few of these Landau levels, $N_L \sim E_F/\hbar\omega_c$, are populated in a 2DEG. For sufficiently large mobility ($\mu B \gg 1$) and low temperature ($k_B T \ll \hbar\omega_c$) the Hall resistance R_H (see Fig. 1.2) is quantized at values

$$R_H = \frac{h}{ie^2} , \quad i = 1, 2, \dots , \quad (1.7)$$

for magnetic fields such that the Fermi level is in between two Landau levels. Simultaneously, the longitudinal resistance R_L vanishes. The distinction between R_H and R_L is topological: A four-terminal resistance measurement yields R_H if current and voltage contacts alternate along the boundary of

the conductor, and R_L otherwise. Frequently, the resistance is measured using only two contacts. In the quantum Hall effect regime, the two-terminal resistance $R_{2t} = R_H + R_L = R_H$ is quantized at the same value as the Hall resistance.

In the modern theory of the quantum Hall effect [7], the longitudinal and Hall conductance (measured using two pairs of current contacts and voltage contacts) are expressed in terms of transmission probabilities between the contacts for electronic states at the Fermi level. For E_F in between two Landau levels, these states are *edge states* extended along the boundaries of the sample (see Fig. 1.2). Edge states are the quantum-mechanical analog of *skipping orbits* of electrons undergoing repeated specular reflections at the boundary [2]. For a smooth confining potential $V(\mathbf{r})$, the edge states are extended along equipotentials of V at the guiding center energy E_G , defined by

$$E_G = E - (n - \frac{1}{2})\hbar\omega_c , \quad (1.8)$$

for an electron with energy E in the n -th Landau level ($n = 1, 2, \dots$). Since the lowest Landau level has the largest guiding center energy, the corresponding edge state at the Fermi level is located closest to the boundary of the sample, whereas those of the higher Landau levels are situated further towards its center.

The collection of edge states with quantum number n form a 1D subband, which is referred to as an *edge channel*. Each of the N_L edge channels at the Fermi level contributes $2e^2/h$ to the Hall conductance if backscattering is suppressed [2]. This is the case if the Fermi level is in between two bulk Landau levels, so that the states at E_F are those extended along the boundaries only. Backscattering then requires transitions between edge states on *opposite* boundaries, which are usually far apart, and is thus suppressed.

1.3 Split-gate nanostructures

A unique feature of a 2DEG is that it can be given any desired shape using lithographic techniques. The shape is defined by etching a pattern (resulting in permanent removal of the electron gas), or by electrostatic depletion using a patterned gate electrode (which is reversible). A local (partial) depletion of the 2DEG below a gate is associated with a local

increase of the electrostatic potential, relative to the undepleted region. At the boundaries of the gate a potential step is thus induced in the 2DEG. The potential step is smooth, because of the large lateral depletion length (of the order of 100 nm for a step height of 10 meV). This large depletion length is at the basis of the split-gate technique [8], used to define narrow channels of variable width with smooth boundaries.

The fabrication of split-gate devices proceeds in a five step process. First, Ohmic contacts are formed by alloying Au-Ge-Ni into the 2DEG. Second, wet etching is used to define a mesa on the heterostructure, such that the Ohmic contacts are at its edges. Third, the coarse parts of the Ti-Au gates are deposited on the mesa. This part of the gate pattern extends from across the edges of the mesa to a few tens of microns from its center, and is identical for all devices. Fourth, bonding pads are deposited on top of the Ohmic contacts and at the far ends of the gates. These steps can all be carried through using conventional optical lithography. In the fifth step the fine details of the split-gate pattern are fabricated using electron-beam lithography. This allows fabrication of devices with critical dimensions of the order of the Fermi wave length, so that (at least at low temperatures) the transport properties are dominated by quantum size effects. Typically, the lithographic opening of split gates used to define constrictions of variable width into the 2DEG is 300 nm.

One of the simplest devices that may be fabricated using this technique is the quantum point contact [9], which basically is a very short and narrow constriction in the 2DEG, see Fig. 1.3. At low temperatures, the conductance of such a quantum point contact is approximately quantized in units of $2e^2/h$ [10, 11]. Because of the lateral confinement, a series of one-dimensional (1D) subbands is formed in the constriction, each contributing $2e^2/h$ to the conductance [9]. This requires unit transmission probability for all occupied 1D subbands in the constriction, so that the effect can be observed only in the ballistic transport regime, where the length of the constriction is much smaller than the mean free path. In longer constrictions, or quantum wires, it is difficult to obtain conductance quantization. The reason is that quantum wires are much more sensitive to disorder than quantum point contacts. Potential fluctuations due to the random distribution of the remote ionized donors greatly decrease the mean free path within the wire. Indeed, calculations [12] demonstrate that a quantum wire close to pinch off may even break up into a number of separate segments.

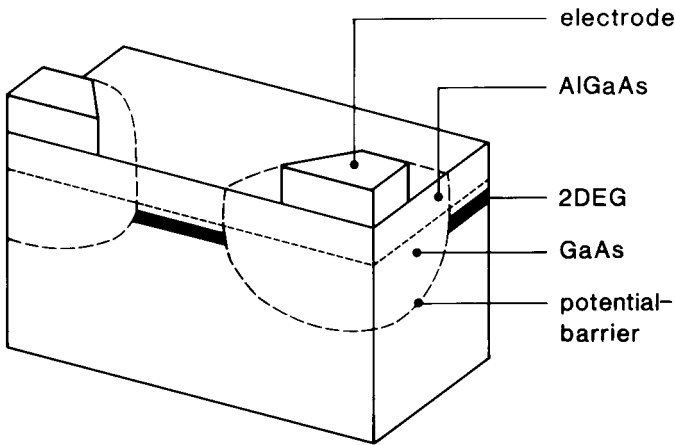


Figure 1.3: Cross section of a split-gate quantum point contact.

If the 2DEG is confined in all directions, a quantum dot is formed. The energy spectrum then is fully discrete, and can be studied by transport experiments if the dot is weakly coupled to wide 2DEG regions by tunnel barriers. Such tunnel barriers may be formed by quantum point contacts, operated close to pinch off (where the conductance $G < 2e^2/h$). An advantage of this technique is that the transparency of the tunnel barrier is adjustable by changing the voltage on the gates defining the point contact. A complication is that the barrier height typically exceeds the Fermi level by only a few meV, and that the thickness of the barrier at the Fermi level is large (on the order of 50 nm). This may lead to a strong dependence of the transparency on the voltage applied across the barrier, hampering a study of nonlinear transport effects intrinsic to a quantum dot.

Measurements of the electrical transport properties of split-gate nanostructures are made at low temperatures, with the devices mounted in the mixing chamber of a dilution refrigerator. This is necessary since the temperature regime for quantum transport in the present devices extends from the millikelvin regime up to a few kelvin. In addition, access to the quantum Hall effect regime is provided by means of a superconducting magnet, capable of generating magnetic fields up to 8 T perpendicular to the

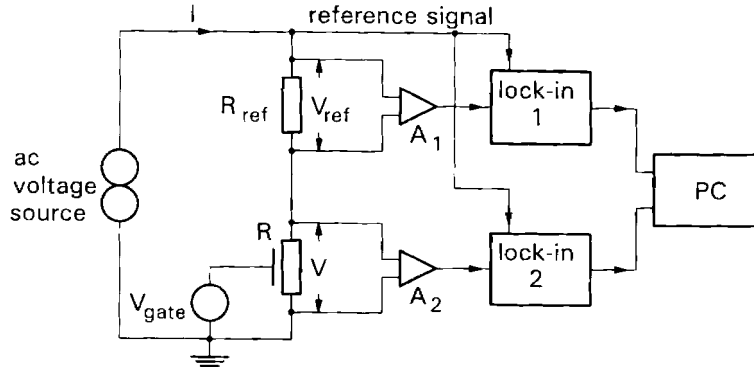


Figure 1.4: Schematic diagram of the measurement circuit. The only part of the circuit at low temperature is the device.

2DEG. As shown schematically in Fig. 1.4, the measurements are made using a double lock-in technique with an excitation voltage below $k_B T/e$ in order to ensure linear response. In the measurement set-up used for the experiments described in this thesis, only the device is at low temperature. The temperature is measured by means of a calibrated germanium resistor, which is positioned inside the mixing chamber, above the main coil of the superconducting magnet. Additional compensation coils keep the magnetic field near zero at that position. In order to reduce electron heating by RF electrical noise as much as possible, low-pass RLC filters are used in the electrical wiring connected to the device. These filters, which have a cut-off frequency of about 1 MHz, are not shown in Fig. 1.4. Primarily, conductance measurements are made, both as a function of gate voltage and as a function of magnetic field.

1.4 Coulomb blockade and single-electron tunneling

The concept of Coulomb blockade refers to the phenomenon that tunneling through a metallic grain with small capacitance may be inhibited at low temperatures and small applied voltages. The reason is that the addition of a single electron to such a system requires an electrostatic charging energy of order $e^2/C \gg k_B T, eV$, where C is its capacitance, T the temperature and V the applied voltage. Basically, this is the explanation first given by

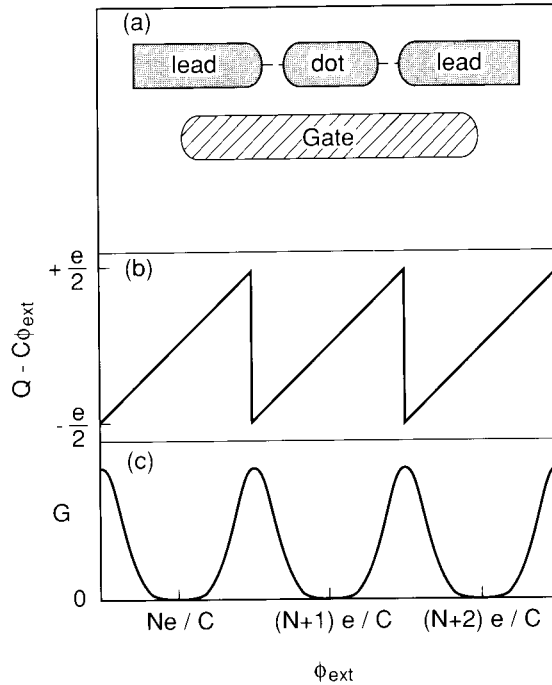


Figure 1.5: (a) Schematic illustration of a confined region (dot) which is weakly coupled to two leads by tunnel barriers. (b) The charge imbalance between dot and lead, which can be maintained due to the Coulomb blockade, oscillates in a sawtooth fashion as a function of the external electrostatic potential difference ϕ_{ext} . (c) Tunneling is possible only near the degeneracy points of the charge imbalance, so that the conductance G exhibits periodic oscillations.

Gorter [13] of an observed [14, 15] anomalous increase of the resistance of thin granular metallic films.

A suitable model system to investigate the Coulomb blockade in more detail consists of a confined region (dot) weakly coupled by tunnel barriers to two leads, see Fig. 1.5(a). An additional gate electrode can be used to control the charge on the dot, which consists of two contributions. The number N of conduction electrons on the dot contributes a charge $Q = -Ne$, which can change by discrete amounts e only. (We assume that the tunnel resistance is large compared to the resistance quantum h/e^2 , so that the number N of electrons on the island may be treated as a sharply

defined classical variable, see chapter 2.) Nearby external charges, e.g., those on the gate, induce a displacement charge $C\phi_{\text{ext}}$ on the dot, which can be varied continuously. Here, C is the capacitance of the dot, and ϕ_{ext} the part of the electrostatic potential difference between dot and leads due to the external charges. Minimization of the absolute value of the charge imbalance $C\phi_{\text{ext}} - Ne$ (under the constraint that N is an integer) determines N at low temperatures. The transition from N to $N+1$ electrons on the dot occurs on reaching a charge imbalance $C\phi_{\text{ext}} - Ne = \frac{1}{2}e$. The additional electron causes the charge imbalance to reverse sign, becoming $-\frac{1}{2}$. Thus, a sawtooth like oscillation of the charge imbalance results [Fig. 1.5(b)]. Tunneling is blocked at low temperatures, except near the points where the charge imbalance jumps from $+\frac{1}{2}e$ to $-\frac{1}{2}e$. Here the electrons can tunnel through the dot, one by one. The Coulomb blockade is lifted, and the (zero bias) conductance exhibits a peak [Fig. 1.5(c)]. These are the “Coulomb-blockade oscillations” [3, 16, 17, 18, 19], which is the central phenomenon studied in this thesis.

In metals, the Coulomb-blockade oscillations are essentially a classical phenomenon [20, 21], since the energy spectrum of the confined region may be treated as a continuum (as was implicitly assumed above). This is not the case in semiconductor nanostructures which have dimensions comparable to the Fermi wave length. In a typical experiment, the confined region or quantum dot contains $N \sim 100$ electrons, with an average energy level spacing $\Delta E \sim 0.1$ meV. At temperatures below a few Kelvin, the level spacing ΔE exceeds the thermal energy $k_B T$, so that transport proceeds by tunneling through a single discrete energy level — a process referred to as resonant tunneling in the absence of charging effects. In semiconductors, one has the opportunity to explore the interplay of resonant tunneling and Coulomb blockade. (The charging energy $e^2/C \sim 0.5$ meV typically is not much greater than the energy level spacing.) In addition, semiconductor nanostructures allow one to study these effects in the quantum Hall effect regime, where the excitation spectrum of a quantum dot is altered completely due to the magnetic quantization ($\hbar\omega_c \sim 1$ meV at $B = 1$ T).

One type of semiconductor nanostructure found to exhibit regular conductance oscillations as a function of gate voltage, is a disordered narrow channel [22, 23, 24, 25, 26, 27]. Originally, an interpretation in terms of a pinned charge-density wave was given for the periodic conductance oscillations in such a quantum wire [22]. As an alternative explanation,

Van Houten and Beenakker [28] suggested that the oscillations are Coulomb-blockade oscillations. As shown in Fig. 1.6(a), a quantum wire may break up into disconnected segments if it is close to pinch-off. Conduction at low temperatures proceeds by tunneling through the barriers delimiting a segment, which plays the role of the confined region in Fig. 1.5. The dominant oscillations in a wire typically have a well-defined periodicity, indicating that a single segment limits the conductance. In addition, some authors have argued that resonant tunneling of noninteracting electrons can explain the periodicity of the oscillations [29, 30]. The work on this thesis was started with the aim to resolve the mechanism of the oscillations by a combined experimental and theoretical study [26, 27].

A second type of nanostructure exhibiting Coulomb-blockade oscillations is a small artificially confined region in a 2DEG (a quantum dot), connected by tunnel barriers either to narrow leads [Fig. 1.6(b)] [31, 32], or to wide electron reservoirs [Fig. 1.6(c)] [33]. In this type of nanostructure, the Coulomb-blockade oscillations can be studied in more detail. However, there is no fundamental distinction between a quantum dot and the disordered quantum wires mentioned above, since a segment of a quantum wire delimited by two particularly strong scattering centers can be viewed as a naturally formed quantum dot. Both types of structure are of interest: Whereas artificially defined quantum dots are more suited to a study of the effect under relatively well-controlled conditions, the significance of the phenomenon of *periodic* conductance oscillations in *disordered* quantum wires lies in its bearing on the general problem of transport in disordered systems. It contradicts the earlier presumed ubiquity of random conductance fluctuations in mesoscopic systems, and directly demonstrates the predominant role of electrostatic interactions in a disordered conductor [34].

Phenomena of single-electron tunneling are not restricted to the Coulomb-blockade oscillations in the linear response conductance discussed so far. For example, in the nonlinear current-voltage characteristics of a double-junction system with very different tunnel rates through the two barriers, steps are found in the current as a function of the source-drain voltage [18, 35, 36]. This “Coulomb staircase” has been observed both in metallic systems [16, 17], and in quantum dots [32]. Recently, radio-frequency modulation of the source-drain voltage or of the tunnel rates has been used to synchronize tunneling of single electrons through the system. It is possible to realize “turn-stile clocking” or “pumping” of a current

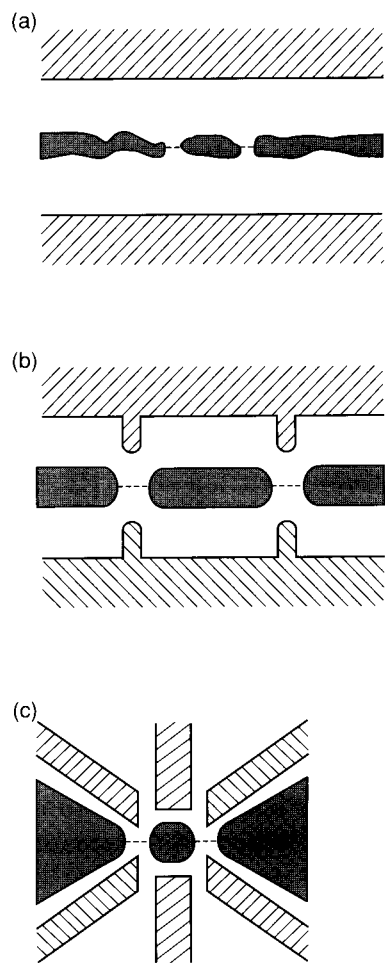


Figure 1.6: Schematic top-view of three semiconductor nanostructures exhibiting Coulomb-blockade oscillations. Hatched regions denote gates, electron gas regions are shaded, and dashed lines indicate tunneling paths. (a) Disordered quantum wire with a single conductance limiting segment. (b) Quantum dot in a narrow channel. (c) Quantum dot between wide regions with separate sets of gates to modulate the tunnel barriers and to vary the external potential of the dot.

$I = ef$, where f is the modulation frequency, through a metallic array of junctions [37, 38] or a quantum dot [39].

In this thesis, however, we will be concerned primarily with the Coulomb-blockade oscillations in semiconductor nanostructures in the regime of linear response. Apart from the conductance, we will also address the thermopower. In chapter 2, the theory of Coulomb-blockade oscillations is outlined following Refs. [40, 41, 42]. This theory remains within the “orthodox” model of the Coulomb blockade [3], in which the number of electrons on the dot is assumed to be a good quantum number. Second-order processes such as tunneling through virtual states [43, 44] and cotunneling [45] are not taken into account. In chapter 3 we present results of a study of Coulomb-blockade oscillations in disordered quantum wires [27]. It is found that the periodic oscillations observed in many of the wires can be interpreted consistently within the frame work of Coulomb-blockade oscillations. Some aspects are not yet resolved fully, however, in particular the detailed magnetic field dependence of the oscillations. In chapter 4 several new aspects of the Coulomb-blockade oscillations in the conductance of quantum dots are discussed. The temperature dependence is examined in section 4.2. At low temperatures, the peak height is found to increase with decreasing temperature, which is characteristic of the resonant tunneling regime. The conductance minima are not suppressed exponentially, indicative of the importance of second-order processes in our devices. In sections 4.3 and 4.4 the effect of a magnetic field on the Coulomb-blockade oscillations is investigated. Whereas the amplitude of the Coulomb-blockade oscillations varies irregularly in the absence of a magnetic field, a periodic modulation of the amplitude has been discovered in the presence of a quantizing magnetic field [46]. This reveals a *cyclic* depopulation of the Landau levels in the dot, in contrast to the sequential depopulation from highest to lowest in a wide 2DEG. This is the subject of section 4.3. The effect on the Coulomb-blockade oscillations of adiabatically transmitted edge channels through the dot, i.e., a conductance of the tunnel barriers greater than e^2/h , is studied in section 4.4. It is shown that even in this regime Coulomb charging of the Landau levels confined to the quantum dot has to be taken into account [47]. Finally, the first observation of Coulomb-blockade oscillations in the *thermopower* of a quantum dot is presented in section 4.5 [48]. These are found to oscillate in a sawtooth like fashion as a function of gate

voltage, in agreement with the theory [41] discussed in chapter 2.

The study of mesoscopic physics is motivated by more than scientific interest. With the extreme miniaturization of transistors in integrated circuits, the regime of classical diffusive transport, in which these devices operate, will break down eventually. Then, mesoscopic effects may become relevant. In addition, the novel transport regimes explored in mesoscopic systems may provide options for innovation of future electronic devices. Since the discovery of quantum ballistic transport many proposals for quantum devices have appeared in the literature, varying from a novel principle of operation for a single transistor, to entire computer architectures in which arrays of quantum devices operate phase coherently. However, most of these proposals have not yet been analyzed critically, with respect to performance, circuit design and technological considerations. Moreover, in order to be commercially attractive, novel devices should offer definite advantages over conventional transistors. In this respect, one of the most stringent requirements is operation at room temperature. Since presently most of mesoscopic physics is in the domain of low-temperature physics, it is obvious that further reduction of device dimensions is required. Then, it is no longer clear whether semiconductors will be a suitable material.

Single-electron tunneling offers the opportunity to realize digital circuits, in which each bit of information is encoded by a single electron. This may in principle allow an unprecedented integration scale, which at the same time remains compatible with the power dissipation requirements of such circuits. (Estimates for circuits with junctions of $10 \times 10 \text{ nm}^2$, considered to be a practical nanolithography limit, yield a value of order 10^9 gates/cm^2 , about 100 times larger than the most optimistic projections for conventional logic circuits [49].) A serious drawback of such circuits, however, is the very low operating temperature, required to obtain an acceptably low digital error rate due to thermally activated tunneling processes. To obtain an error rate of at most 10^{-20} s^{-1} [49], $k_B T$ should be about 70 times smaller than the energy scale $e^2/2C$ of the individual junctions. This implies a temperature limit of only 3 K for circuits with $10 \times 10 \text{ nm}^2$ junctions. Therefore, operation at room temperature of such simple digital circuits is probably not a realistic goal. Better prospects may be offered by neural network type circuits, since these are more fault tolerant, and thus can be operated at higher temperatures than simple digital circuits

with junctions of equal area. Clearly, we are only at the beginning of a challenging field of opportunities.

References

- [1] Y. Imry, in: *Directions in Condensed Matter Physics*, edited by G. Grinstein and G. Mazenko (World Scientific, Singapore, 1986), Vol. 1.
- [2] For a review of theoretical and experimental aspects of quantum transport in semiconductor nanostructures, see: C. W. J. Beenakker and H. van Houten, Solid State Physics **44**, 1 (1991).
- [3] For a review of single-electron tunneling in metals, see: K. K. Likharev, IBM J. Res. Dev. **32**, 144 (1988); D. V. Averin and K. K. Likharev, in: *Mesoscopic Phenomena in Solids*, edited by B. L. Al'tshuler, P. A. Lee, and R. A. Webb (Elsevier, Amsterdam, 1991).
- [4] R. Dingle, H. L. Stormer, A. C. Gossard, and W. Wiegman, Appl. Phys. Lett. **7**, 665 (1978).
- [5] C. T. Foxon, J. J. Harris, D. Hilton, J. Hewett, and C. Roberts, Semicond. Sci. Technol. **4**, 582 (1989).
- [6] *The Quantum Hall Effect*, edited by R. E. Prange and S. M. Girvin (Springer, New York, 1987).
- [7] M. Büttiker, Phys. Rev. B **38**, 9375 (1988).
- [8] T. J. Thornton, M. Pepper, H. Ahmed, D. Andrews, and G. J. Davies, Phys. Rev. Lett. **56**, 1198 (1986).
- [9] H. van Houten, C. W. J. Beenakker, and B. J. van Wees, in: *Nanosstructured Systems*, edited by M. A. Reed (Academic, New York, 1992), a volume of Semiconductors and Semimetals.
- [10] B. J. van Wees, H. van Houten, C. W. J. Beenakker, J. G. Williamson, L. P. Kouwenhoven, D. van der Marel, and C. T. Foxon, Phys. Rev. Lett. **60**, 848 (1988).
- [11] D. A. Wharam, T. J. Thornton, R. Newbury, M. Pepper, H. Ahmed, J. E. F. Frost, D. G. Hasko, D. C. Peacock, D. A. Ritchie, and G. A. C. Jones, J. Phys. C **21**, L209 (1988).
- [12] J. A. Nixon and J. H. Davies, Phys. Rev. B **41**, 7929 (1990).

- [13] C. J. Gorter, Physica **17**, 777 (1951).
- [14] R. Lambeir, A. van Itterbeek, and G. J. van den Berg, Physica **16**, 907 (1950).
- [15] N. Mostovech and B. Vodar, C. R. Acad. Sci. Paris **230**, 934 (1950).
- [16] L. S. Kuz'min and K. K. Likharev, Pis'ma Zh. Eksp. Teor. Fiz. **45**, 389 (1987) [JETP Lett. **45**, 495 (1987)].
- [17] T. A. Fulton and G. J. Dolan, Phys. Rev. Lett. **59**, 109 (1987).
- [18] K. Mullen, E. Ben-Jacob, R. C. Jaklevic, and Z. Schuss, Phys. Rev. B **37**, 98 (1988); M. Amman, K. Mullen, and E. Ben-Jacob, J. Appl. Phys. **65**, 339 (1989).
- [19] L. I. Glazman and R. I. Shekhter, J. Phys. Condens. Matter **1**, 5811 (1989).
- [20] R. I. Shekhter, Zh. Eksp. Teor. Fiz. **63**, 1410 (1972) [Sov. Phys. JETP **36**, 747 (1973)].
- [21] I. O. Kulik and R. I. Shekhter, Zh. Eksp. Teor. Fiz. **68**, 623 (1975) [Sov. Phys. JETP **41**, 308 (1975)].
- [22] J. H. F. Scott-Thomas, S. B. Field, M. A. Kastner, H. I. Smith, and D. A. Antoniadis, Phys. Rev. Lett. **62**, 583 (1989).
- [23] U. Meirav, M. A. Kastner, M. Heiblum, and S. J. Wind, Phys. Rev. B **40**, 5871 (1989).
- [24] S. B. Field, M. A. Kastner, U. Meirav, J. H. F. Scott-Thomas, D. A. Antoniadis, H. I. Smith, and S. J. Wind, Phys. Rev. B **42**, 3523 (1990).
- [25] C. de Graaf, J. Caro, S. Radelaar, V. Lauer, and K. Heyers, Phys. Rev. B **44**, 9072 (1991).
- [26] A. A. M. Staring, H. van Houten, C. W. J. Beenakker, and C. T. Foxon, in: *High Magnetic Fields in Semiconductor Physics III*, edited by G. Landwehr (Springer, Berlin, 1992).

- [27] A. A. M. Staring, H. van Houten, C. W. J. Beenakker, and C. T. Foxon, Phys. Rev. B **45**, 9222 (1992).
- [28] H. van Houten and C. W. J. Beenakker, Phys. Rev. Lett. **63**, 1893 (1989).
- [29] F. M. de Aguiar and D. A. Wharam, Phys. Rev. B **43**, 9984 (1991).
- [30] J. Mašek and B. Kramer (unpublished).
- [31] U. Meirav, M. A. Kastner, and S. J. Wind, Phys. Rev. Lett. **65**, 771 (1990).
- [32] L. P. Kouwenhoven, N. C. van der Vaart, A. T. Johnson, W. Kool, C. J. P. M. Harmans, J. G. Williamson, A. A. M. Staring, and C. T. Foxon, Z. Phys. B **85**, 367 (1991).
- [33] A. A. M. Staring, J. G. Williamson, H. van Houten, C. W. J. Beenakker, L. P. Kouwenhoven, and C. T. Foxon, Physica B **175**, 226 (1991); J. G. Williamson, A. A. M. Staring, H. van Houten, L. P. Kouwenhoven, and C. T. Foxon, in: *Nanostructures and Mesoscopic systems*, edited by W. P. Kirk and M. A. Reed (Academic, Boston, 1992).
- [34] A. L. Efros and B. I. Shklovskii, in: *Electron-Electron Interactions in Disordered Systems*, edited by A. L. Efros and M. Pollak, (North-Holland, Amsterdam, 1985).
- [35] D. V. Averin and A. N. Korotkov, Zh. Eksp. Teor. Fiz. **97**, 1661 (1990) [Sov. Phys. JETP **70**, 937 (1990)]; A. N. Korotkov, D. V. Averin, and K. K. Likharev, Physica B **165 & 166**, 927 (1990); D. V. Averin, A. N. Korotkov, and K. K. Likharev, Phys. Rev. B **44**, 6199 (1991).
- [36] A. Groshev Phys. Rev. B **42**, 5895 (1990); A. Groshev, T. Ivanonv, and V. Valtchinov, Phys. Rev. Lett. **66**, 1082 (1991).
- [37] L. J. Geerligs, V. F. Anderegg, P. A. M. Holweg, J. E. Mooij, H. Pothier, D. Estève, C. Urbina, and M. H. Devoret, Phys. Rev. Lett. **64**, 2691 (1990).

- [38] H. Pothier, P. Lafarge, C. Urbina, D. Estève, and M. H. Devoret, *Europhys. Lett.* **17**, 249 (1992).
- [39] L. P. Kouwenhoven, A. T. Johnson, N. C. van der Vaart, A. van der Enden, C. J. P. M. Harmans, and C. T. Foxon, *Phys. Rev. Lett.* **67**, 1626 (1991).
- [40] C. W. J. Beenakker, *Phys. Rev. B* **44**, 1646 (1991).
- [41] C. W. J. Beenakker and A. A. M. Staring, *Phys. Rev. B*, to be published.
- [42] H. van Houten, C. W. J. Beenakker, and A. A. M. Staring, in: *Single Charge Tunneling*, edited by H. Grabert and M. H. Devoret, NATO ASI Series B (Plenum, New York, 1992).
- [43] D. V. Averin and A. A. Odintsov, *Phys. Lett. A* **140**, 251 (1989); D. V. Averin and Yu. V. Nazarov, *Phys. Rev. Lett.* **65**, 2446 (1990).
- [44] L. I. Glazman and K. A. Matveev, *Pis'ma zh. Eksp. Teor. Fiz.* **51**, 425 (1990) [*JETP Lett.* **51**, 484 (1990)].
- [45] D. V. Averin and Yu. V. Nazarov, in: *Single Charge Tunneling*, edited by H. Grabert and M. H. Devoret, NATO ASI Series B (Plenum, New York, 1992).
- [46] A. A. M. Staring, B. W. Alphenaar, H. van Houten, L. W. Molenkamp, O. J. A. Buyk, M. A. A. Mabesoone, and C. T. Foxon, *Phys. Rev. B*, to be published.
- [47] B. W. Alphenaar, A. A. M. Staring, H. van Houten, O. J. A. Buyk, M. A. A. Mabesoone, and C. T. Foxon, *Phys. Rev. B*, to be published.
- [48] A. A. M. Staring, L. W. Molenkamp, H. van Houten, B. W. Alphenaar, O. J. A. Buyk, M. A. A. Mabesoone, C. W. J. Beenakker, and C. T. Foxon, submitted to *Phys. Rev. Lett.*
- [49] D. V. Averin and K. K. Likharev, in: *Superconducting Devices & Their Applications*, edited by H. Koch and H. Lubbig (Springer, New York, 1992).

Chapter 2

Theory of Coulomb-blockade oscillations

2.1 Introduction

We consider a confined region which is weakly coupled via tunnel barriers to two electron reservoirs. The confined region, or “quantum dot”, has single-electron energy levels at E_p ($p = 1, 2, \dots$), calculated by treating the electron-electron interaction in a mean-field (Hartree) approximation (cf. Ref. [1]). The levels are labeled in ascending order and measured relative to the bottom of the potential well. Each level contains either one or zero electrons. Spin degeneracy can be included by counting each level twice, and other degeneracies can be included similarly. In principle, the position of the levels may depend on the number of electrons in the dot, but for simplicity we will ignore such dependence in what follows. Each reservoir is taken to be in thermal equilibrium, but between the reservoirs there can be a temperature difference $\Delta T = T_l - T_r$. The states in the left (l) and right (r) reservoirs are occupied according to the Fermi-Dirac distributions

$$\begin{aligned} f_l(E - E_F) &= \left[1 + \exp \left(\frac{E - E_F}{k_B T_l} \right) \right]^{-1}, \\ f_r(E - E_F) &= \left[1 + \exp \left(\frac{E - E_F}{k_B T_r} \right) \right]^{-1}, \end{aligned} \tag{2.1}$$

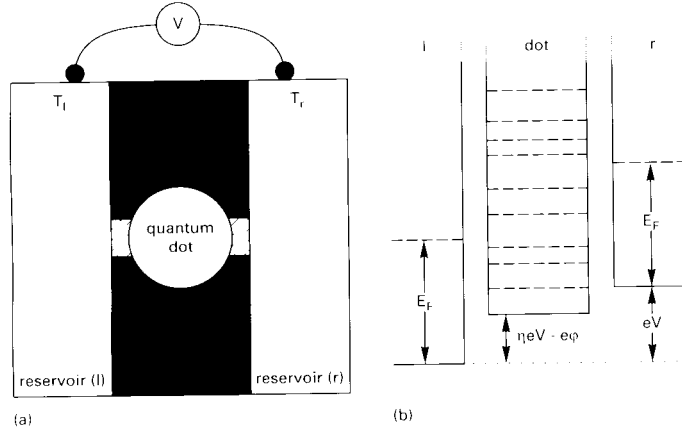


Figure 2.1: (a) Schematic diagram of the quantum dot, tunnel barriers (hatched), and reservoirs. (b) Profile of the electrostatic potential energy (solid curve) along a line through the tunnel barriers. The Fermi levels in the left and right reservoirs, and the discrete energy levels in the quantum dot are indicated (dashed lines).

where the Fermi energy E_F is measured relative to the local conduction band bottom in the reservoirs. In Fig. 2.1 we show schematically a cross-section of the geometry, and the profile of the electrostatic potential energy along a line through the tunnel barriers.

A current I can be passed through the dot by applying a potential difference V between the reservoirs. The linear response conductance G of the dot is defined as $G \equiv I/V$, in the limit $V \rightarrow 0$, given that the reservoirs have equal temperature, i.e., $\Delta T = 0$. Since transport through the dot proceeds by tunneling through its discrete electronic states, it will be clear that for small V a net current can flow for certain values of E_F only (if $\Delta E \gg k_B T$). In the absence of charging effects, a conductance peak due to resonant tunneling occurs if E_F in the reservoirs lines up with one of the energy levels in the dot. This condition is modified by the charging energy.

Because the number N of electrons localized in the dot can take on integer values only, a charge imbalance, and hence a potential difference, can arise between the dot and reservoirs, even if $V = 0$. Following the “orthodox model” of the Coulomb blockade [2], we express the electrostatic potential difference $\phi(Q)$, with $Q = -Ne$, in terms of an effective N -

independent capacitance C between dot and reservoirs,

$$\phi(Q) = \frac{Q}{C} + \phi_{\text{ext}} , \quad (2.2)$$

where ϕ_{ext} is a contribution from external charges (in particular those on a nearby gate electrode). The electrostatic energy $U(N) = \int_0^{-Ne} \phi(Q)dQ$ then takes the form[†]

$$U(N) = \frac{(Ne)^2}{2C} - Ne\phi_{\text{ext}} . \quad (2.3)$$

Recently, McEuen *et al.* [5] have used a semi self-consistent approach to calculate the total ground state energy of the dot in a quantizing magnetic field. This proved to be necessary because the electron gas in the dot in a quantizing magnetic field is divided into compressible (partially filled Landau levels) and incompressible (full Landau levels) regions. The incompressible regions can be thought of as dielectric-like regions separating the metallic-like compressible regions, so that charging effects between the latter regions have to be taken into account. We will ignore such intra-dot electron-electron interaction effects in this chapter, but we will discuss some consequences in chapter 4 (section 4.4).

The tunnel rates from level p to the left and right reservoirs are denoted by Γ_p^l and Γ_p^r , respectively. A possible dependence of the tunnel rates on N is ignored. We assume that both the thermal energy $k_B T$ and the level separation ΔE are much greater than $h\Gamma \equiv h(\Gamma^l + \Gamma^r)$, so that virtual tunnel processes [6, 7] (and the resulting finite width of the transmission resonance through the dot) can be neglected. This assumption allows characterization of the state of the dot by a set of occupation numbers, one for each energy level. Transport through the dot can then be described by rate equations [2]. We also assume that inelastic scattering occurs exclusively in the reservoirs, not in the quantum dot.

[†]To make connection with some of the literature [3, 4] we note that $Q_{\text{ext}} \equiv C\phi_{\text{ext}}$ plays the role of a displacement charge on the dot, which can be varied continuously by means of an external gate voltage. In terms of Q_{ext} one can write

$$U(N) = \frac{(Ne - Q_{\text{ext}})^2}{2C} + \text{constant} ,$$

which is equivalent to Eq. (2.3).

Energy conservation upon tunneling from an initial state p in the dot (containing N electrons) to a final state in the left reservoir at energy $E^{f,l}$ (measured relative to the local conduction band bottom), requires that

$$E^{f,l}(N) = E_p + U(N) - U(N-1) + \eta eV , \quad (2.4)$$

where η is the fraction of the voltage V that drops over the left barrier (see Fig. 2.1). The energy conservation condition for tunneling from an initial state $E^{i,l}$ in the left reservoir to a final state p in the dot is

$$E^{i,l}(N) = E_p + U(N+1) - U(N) + \eta eV , \quad (2.5)$$

where [as in Eq. (2.4)] N is the number of electrons in the dot *before* the tunneling event. Similarly, for tunneling between the quantum dot and the right reservoir we have the conditions

$$E^{f,r}(N) = E_p + U(N) - U(N-1) - (1-\eta)eV , \quad (2.6)$$

$$E^{i,r}(N) = E_p + U(N+1) - U(N) - (1-\eta)eV , \quad (2.7)$$

where $E^{i,r}$ and $E^{f,r}$ are the energies of the initial and final states in the right reservoir.

The stationary current through the dot is given by

$$\begin{aligned} I &= -e \sum_{p=1}^{\infty} \sum_{\{n_i\}} \Gamma_p^l P(\{n_i\}) \left(\delta_{n_p,0} f_l(E^{i,l}(N) - E_F) \right. \\ &\quad \left. - \delta_{n_p,1} [1 - f_l(E^{f,l}(N) - E_F)] \right) \\ &= e \sum_{p=1}^{\infty} \sum_{\{n_i\}} \Gamma_p^r P(\{n_i\}) \left(\delta_{n_p,0} f_r(E^{i,r}(N) - E_F) \right. \\ &\quad \left. - \delta_{n_p,1} [1 - f_r(E^{f,r}(N) - E_F)] \right) . \end{aligned} \quad (2.8)$$

The second summation is over all realizations of occupation numbers $\{n_1, n_2, \dots\} \equiv \{n_i\}$ of the energy levels in the quantum dot, each with stationary probability $P(\{n_i\})$. (The numbers n_i can take on only the values 0 and 1.)

As we discuss in section 2.2, at $T = 0$ the position of the conductance peaks as a function of gate voltage can be determined from a consideration

of the equilibrium properties of the system only [8, 9]. The temperature dependence of the amplitude and width of the Coulomb-blockade oscillations requires solution of the *nonequilibrium* probability distribution $P(\{n_i\})$ from the kinetic equation $\partial P/\partial t = 0$. Beenakker [10] has derived an analytical expression for P in the resonant tunneling regime, which generalizes earlier results by Kulik and Shekhter [11, 12] in the classical regime. An equivalent result has been obtained independently by Meir, Wingreen, and Lee [13], by solving an Anderson model in the limit $k_B T \gg \hbar\Gamma$. In section 2.3, we summarize the main results of Ref. [10] for the amplitude and width of the conductance oscillations. In order to obtain an expression for the thermopower of the dot, the theory of Ref. [10] was extended in Ref. [14] to include single-electron tunneling in response to a temperature difference ΔT across the dot, as well as a potential difference V . This is discussed in section 2.4.

2.2 Periodicity of the oscillations

The probability $P(N)$ to find N electrons in the dot in equilibrium with the reservoirs (at $T = T_l = T_r$) is given by the grand canonical distribution function

$$P(N) = \text{constant} \times \exp \left\{ -\frac{1}{k_B T} [F(N) - N E_F] \right\}, \quad (2.9)$$

where $F(N)$ is the free energy of the dot. At $T = 0$, $P(N)$ generally is nonzero for a *single* value of N only [namely the integer which minimizes the thermodynamic potential $\Omega(N) \equiv F(N) - N E_F$]. In that case, the conductance is suppressed in the limit $T \rightarrow 0$. As pointed out by Glazman and Shekhter [15], a finite conductance is possible only if both $P(N)$ and $P(N+1)$ are nonzero for some N . Then a small applied voltage is sufficient to induce a current, such that electrons pass one by one through the dot, via intermediate states $N \rightarrow N + 1 \rightarrow N \rightarrow N + 1 \rightarrow \dots$. To have both $P(N)$ and $P(N+1)$ nonzero at $T = 0$, it is required that both N and $N+1$ minimize Ω . A necessary condition is $\Omega(N+1) = \Omega(N)$, or

$$F(N+1) - F(N) = E_F. \quad (2.10)$$

This condition is also sufficient, unless Ω has more than one minimum (which is usually not the case).

Equation (2.10) expresses the equality of the electrochemical potential of dot and leads. The usefulness of this result is that it maps the problem of determining the position of the conductance peaks onto the more familiar problem of calculating the electrochemical potential $F(N+1) - F(N)$ of the quantum dot, i.e., the energy cost associated with the addition of a single electron to the dot. This enables, in principle, a study of exchange and correlation effects on conductance oscillations in a quantum dot (e.g. along the lines of work by Bryant [16] and by Maksym and Chakraborty [17]).

At $T = 0$ the free energy $F(N)$ equals the ground-state energy of the dot, for which we take the simplified form $U(N) + \sum_{p=1}^N E_p$. In this approximation, the ground-state energy consists of a separate contribution from the electrostatic energy $U(N)$, which accounts for the charge imbalance, and from the occupied single-electron states in the dot, which accounts for the internal energy. We thus find from Eq. (2.10) that a peak in the low-temperature conductance occurs whenever

$$E_N + U(N) - U(N-1) = E_F , \quad (2.11)$$

for some integer N (where we have relabeled N by $N-1$).

Substitution of Eq. (2.3) into Eq. (2.11) yields

$$E_N^* \equiv E_N + (N - \frac{1}{2}) \frac{e^2}{C} = E_F + e\phi_{\text{ext}} \quad (2.12)$$

as the condition for a conductance peak. The left-hand-side of Eq. (2.12) defines a renormalized energy level E_N^* . The renormalized level spacing $\Delta E^* = \Delta E + e^2/C$ is enhanced above the bare level spacing by the charging energy e^2/C . If $e^2/C \ll \Delta E$, Eq. (2.12) is the usual condition for resonant tunneling. If $e^2/C \gg \Delta E$, Eq. (2.12) describes the periodicity of the classical Coulomb-blockade oscillations in the conductance versus gate voltage [2, 4, 11, 12, 15].

In Fig. 2.2 we have illustrated tunneling of an electron through the dot subject to the conditions set by Eq. (2.12). Initially (left), the dot is occupied by $N-1$ electrons and the condition (2.12) for a conductance peak is satisfied, i.e., $E_N + e^2/2C = E_F + e\phi(N-1)$ [using the shorthand notation $\phi(N)$ for $\phi(-Ne)$]. Here, E_N refers to the lowest *unoccupied* level in the dot (left). If an electron tunnels into this level, the potential difference ϕ between dot and reservoirs decreases by e/C (becoming negative). One now

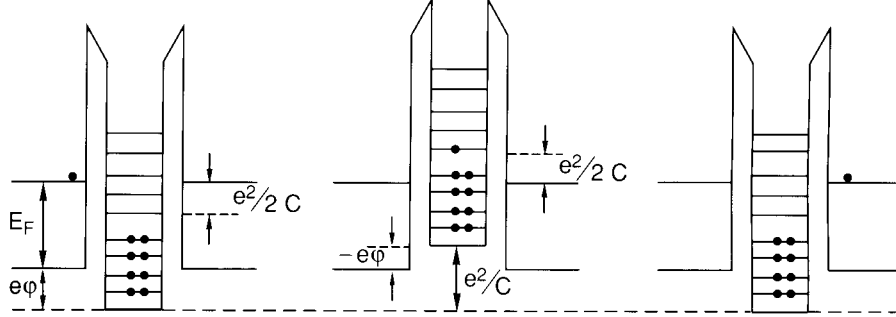


Figure 2.2: Single-electron tunneling through a quantum dot subject to the conditions set by Eq. (2.12), for the case that the charging energy is comparable to the level spacing. An infinitesimally small voltage difference is assumed between the left and right reservoirs.

has $E_N - e^2/2C = E_F + e\phi(N)$, with E_N referring to the highest *occupied* level (middle). Finally, the electron tunnels out of the dot (right), and the potentials and energies are reset to the initial state.

Let us now discuss the periodicity of the oscillations in more detail. Theoretically, it is convenient to consider the case of a variation of the Fermi energy of the reservoirs E_F at constant ϕ_{ext} . According to Eq. (2.12) we find a period

$$\Delta E_F = \Delta E_N^* = \Delta E_N + \frac{e^2}{C}, \quad (2.13)$$

where $\Delta E_N \equiv E_{N+1} - E_N$. In the absence of charging effects, ΔE_F is determined by the irregular spacing ΔE_N of the single-electron levels in the dot. The charging energy e^2/C regulates the spacing once it is larger than the average spacing ΔE of the levels. This is illustrated in Fig. 2.3. In addition, the charging energy *lifts* the spin degeneracy of the levels. This leads to a doublet structure of the oscillations in a plot of G versus E_F , with a spacing that alternates between e^2/C and $e^2/C + \Delta E_N$, where ΔE_N is the spacing between two spin degenerate levels.

Experimentally, one studies the Coulomb-blockade oscillations as a function of gate voltage. To determine the periodicity in that case, one has to consider variations in ϕ_{ext} . In a 2DEG, the external charges are supplied by ionized donors and by a gate electrode (with an electrostatic

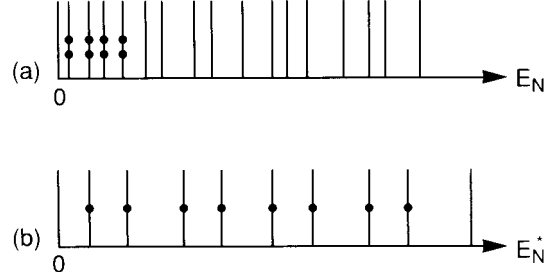


Figure 2.3: The bare energy levels in a quantum dot (a) are spaced much less regular than the renormalized energy levels (b). In addition, the spin degeneracy of the bare levels is lifted by the charging energy (the black dots indicate states occupied by a single electron).

potential difference ϕ_{gate} between gate and 2DEG reservoir). We write

$$\phi_{\text{ext}} = \phi_{\text{donors}} + \alpha\phi_{\text{gate}} , \quad (2.14)$$

where α (as well as C) is a rational function of the capacitance matrix elements of the system, and therefore depends on the geometry. In general, a geometry-specific dependence of E_F and of the set of energy levels E_p on ϕ_{ext} has to be taken into account as well.

We first discuss the case of a quantum dot with wide 2DEG leads. In this geometry, the Fermi energy E_F of the reservoirs is constant, independent of ϕ_{ext} . To clarify the meaning of the parameter α , we model the system of quantum dot, gates, and 2DEG leads by the equivalent circuit of Fig. 2.4. From simple electrostatics[‡] we find $\alpha = C_{\text{gate}}/C$, with $C = C_{\text{dot}} + C_{\text{gate}}$ the capacitance determining the charging energy e^2/C . Thus, the period $\Delta\phi_{\text{gate}}$ obtained from Eqs. (2.12) and (2.14) is

$$\Delta\phi_{\text{gate}} = \frac{e}{C_{\text{gate}}} \left(1 + \frac{\Delta E_N}{e^2/C} \right) . \quad (2.15)$$

[‡]From Eq. (2.2) we find for the charge on the dot $Q = C\phi - C\phi_{\text{ext}} = C\phi - \alpha C\phi_{\text{gate}} + \text{const}$. Alternatively, from the equivalent circuit in Fig. 2.4 we find $Q = Q_{\text{dot}} + Q_{\text{gate}} + Q_{\text{donors}}$, where $Q_{\text{dot}} = C_{\text{dot}}\phi$ is the charge on C_{dot} , $Q_{\text{gate}} = C_{\text{gate}}(\phi - \phi_{\text{gate}})$ is the charge on C_{gate} , and Q_{donors} is the charge on the dot due to the ionized donors. We thus find $C = C_{\text{dot}} + C_{\text{gate}}$ and $\alpha = C_{\text{gate}}/C$.

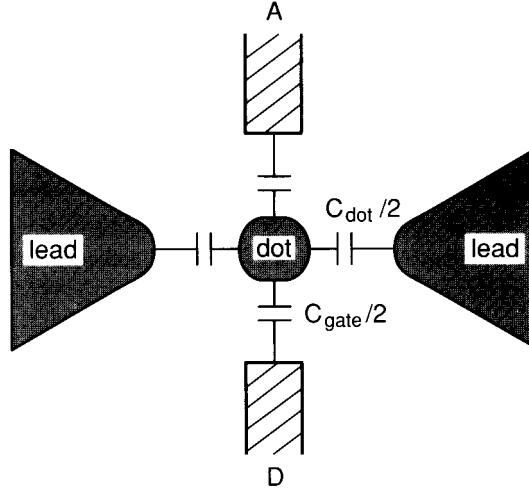


Figure 2.4: Equivalent circuit of the quantum dot, gates (hatched) and 2DEG leads (shaded). The mutual capacitance of dot and leads is C_{dot} , and that of dot and gates is C_{gate} .

If the charging energy dominates, $e^2/C \gg \Delta E$, the oscillations are nearly periodic with period e/C_{gate} .

A more complicated geometry is that of a quantum dot defined within a quantum wire. We model this system by the equivalent circuit shown in Fig. 2.5. The mutual capacitance between gates and leads is much larger than that of dot and gates (C_{gate}) and that of dot and leads (C_{dot}), but does not enter the problem explicitly. However, it has an important consequence for the variation of the Fermi energy in the leads (the reservoirs) with gate voltage. In this geometry, it is reasonable to assume that the electron-gas densities in the dot and leads increase, on average, equally fast with ϕ_{gate} . For equidistant energy levels in the dot we may then assume that $E_F - E_N$ has the same value at each conductance peak. Since the equivalent circuit is essentially identical to that of a quantum dot with wide 2DEG leads, the same electrostatics apply, so that in this geometry we also have $\alpha = C_{\text{gate}}/C$ and $C = C_{\text{dot}} + C_{\text{gate}}$. The period of the oscillations now follows from Eqs. (2.12) and (2.14),

$$\Delta\phi_{\text{gate}} = \frac{e}{C_{\text{gate}}} . \quad (2.16)$$

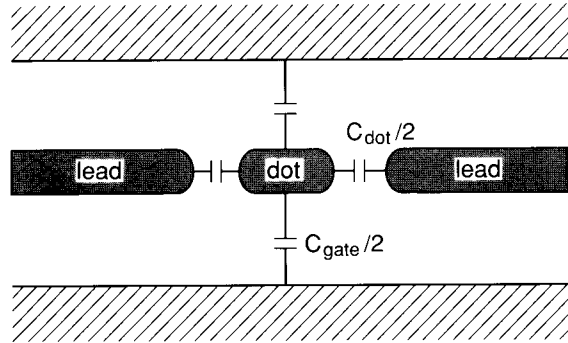


Figure 2.5: Equivalent circuit of a quantum wire containing a quantum dot. The mutual capacitance of dot and leads (shaded) is C_{dot} , and that of dot and gates (hatched) is C_{gate} .

Note that this result applies regardless of the relative magnitudes of the (equidistant) bare level spacing ΔE and the charging energy e^2/C .

In an experiment the gate voltage is the *electrochemical* potential difference V_{gate} between gate and leads, i.e., the difference in Fermi levels, whereas so far we have discussed the period of the oscillations in terms of the *electrostatic* potential difference ϕ_{gate} , i.e., the difference in conduction band bottoms. This only makes a difference for a quantum dot within a quantum wire (Fig. 2.5), since in this geometry the Fermi energy in the leads is not constant, but increases with gate voltage. In one period, the change in Fermi energy in the leads is approximately equal to the change in Fermi energy in the dot. The change in Fermi energy in the (metal) gate is negligible, because the density of states in a metal is much larger than in a 2DEG. We thus find that the oscillation period ΔV_{gate} in the geometry of Fig. 2.5 is

$$\Delta V_{\text{gate}} = \Delta \phi_{\text{gate}} + \frac{\Delta E_F}{e} = \frac{e}{C_{\text{gate}}} + \frac{\Delta E}{e}, \quad (2.17)$$

where the second equality holds for equidistantly spaced levels.

To determine the peak spacing as a function of gate voltage for nonequidistant levels, we approximate the change in E_F with V_{gate} by $\partial E_F / \partial V_{\text{gate}} \sim \Delta E / (e/C_{\text{gate}} + \Delta E)$, where ΔE is the average level spacing.

We then obtain from Eqs. (2.12) and (2.14)

$$\Delta V_{\text{gate}} = \left(\frac{e}{C_{\text{gate}}} + \frac{\Delta E}{e} \right) \frac{\Delta E_N + e^2/C}{\Delta E + e^2/C}. \quad (2.18)$$

The average spacing equals $e/C_{\text{gate}} + \Delta E/e$, in agreement with Eq. (2.17). For equidistant spin-degenerate levels (of spacing $2\Delta E$) we thus find that the peak spacing alternates between two values, corresponding to $\Delta E_N = 0$ and $\Delta E_N = 2\Delta E$. If the charging energy dominates ($e^2/C \gg \Delta E$), one has equal spacing $\Delta V_{\text{gate}}^{(1)} \approx \Delta V_{\text{gate}}^{(2)} \approx e/C_{\text{gate}} + \Delta E/e$, as for non-degenerate levels. In the opposite limit $\Delta E \gg e^2/C$, one finds instead $\Delta V_{\text{gate}}^{(1)} \approx 0$, and $\Delta V_{\text{gate}}^{(2)} \approx 2(e/C_{\text{gate}} + \Delta E/e)$. Thus, the period is effectively doubled, corresponding to the addition of *two* electrons to the dot instead of one. This is characteristic for resonant tunneling of noninteracting electrons through spin-degenerate energy levels. An external magnetic field will resolve the spin degeneracy, leading to a splitting of the conductance peaks which increases with field.

2.3 Conductance oscillations

Equation (2.12) is sufficient to determine the periodicity of the conductance oscillations, but gives no information on their amplitude and width. This requires a solution of a kinetic equation, which has been obtained analytically by Beenakker in Ref. [10]. The equilibrium distribution function of electrons among the energy levels is given by the Gibbs distribution in the grand canonical ensemble:

$$P_{\text{eq}}(\{n_i\}) = \frac{1}{Z} \exp \left[-\frac{1}{k_B T} \left(\sum_{i=1}^{\infty} E_i n_i + U(N) - N E_F \right) \right], \quad (2.19)$$

where $N \equiv \sum_i n_i$ is the number of electrons in the dot, and Z is the partition function,

$$Z = \sum_{\{n_i\}} \exp \left[-\frac{1}{k_B T} \left(\sum_{i=1}^{\infty} E_i n_i + U(N) - N E_F \right) \right]. \quad (2.20)$$

The joint probability $P_{\text{eq}}(N, n_p = 1)$ that the quantum dot contains N electrons *and* that level p is occupied is

$$P_{\text{eq}}(N, n_p = 1) = \sum_{\{n_i\}} P_{\text{eq}}(\{n_i\}) \delta_{N, \sum_i n_i} \delta_{n_p, 1}. \quad (2.21)$$

In terms of this probability distribution, the conductance is given by [10]

$$\begin{aligned} G = \frac{e^2}{k_B T} \sum_{p=1}^{\infty} \sum_{N=1}^{\infty} \frac{\Gamma_p^l \Gamma_p^r}{\Gamma_p^l + \Gamma_p^r} P_{\text{eq}}(N, n_p = 1) \times \\ \times [1 - f(E_p + U(N) - U(N-1) - E_F)]. \end{aligned} \quad (2.22)$$

This particular product of distribution functions expresses the fact that tunneling of an electron from an initial state p in the dot to a final state in the reservoir requires an occupied initial state and empty final state.

We now discuss some limiting cases of the general result (2.22). We first consider the conductance of the individual barriers and the quantum dot in the high temperature limit $k_B T \gg e^2/C, \Delta E$ where neither the discreteness of the energy levels nor the charging energy are important. The conductance then does not exhibit oscillations as a function of gate voltage. The high temperature limit is of interest for comparison with the low temperature results, and because its measurement allows a straightforward estimate of the tunnel rates. The conductance of the quantum dot in the high temperature limit is simply that of the two tunnel barriers in series. We find

$$G = \frac{G^l G^r}{G^l + G^r}, \quad \text{if } \Delta E, e^2/C \ll k_B T \ll E_F. \quad (2.23)$$

The conductances G^l and G^r of the left and right tunnel barriers are given by the thermally averaged Landauer formula

$$G^{l,r} = -\frac{e^2}{h} \int_0^\infty T^{l,r}(E) \frac{df}{dE} dE. \quad (2.24)$$

The transmission probability of a barrier $T(E)$ equals the tunnel rate $\Gamma(E)$ divided by the attempt frequency $\nu(E) = 1/h\rho(E)$,

$$T^{l,r}(E) = h\Gamma^{l,r}(E)\rho(E). \quad (2.25)$$

If the height of the tunnel barriers is large, the energy dependence of the tunnel rates and density-of-states ρ in the dot can be ignored (as long as $k_B T \ll E_F$). The conductance of each barrier then becomes according to Eq. (2.24)

$$G^{l,r} = (e^2/h)T^{l,r} = e^2\rho\Gamma^{l,r} \quad (2.26)$$

(where $T^{l,r}$, ρ , and $\Gamma^{l,r}$ are evaluated at E_F), and the conductance of the dot from Eq. (2.23) is

$$G = e^2\rho \frac{\Gamma^l\Gamma^r}{\Gamma^l + \Gamma^r} = \frac{e^2}{h} \frac{T^l T^r}{T^l + T^r} \equiv G_\infty, \quad \text{if } \Delta E, e^2/C \ll k_B T \ll E_F. \quad (2.27)$$

The validity of the present theory is restricted to the case of negligible quantum fluctuations in the charge on the dot [2]. Since charge leaks out of the dot at a rate $\Gamma^l + \Gamma^r$, the energy levels are sharply defined only if the resulting uncertainty in energy $h(\Gamma^l + \Gamma^r) \ll \Delta E$. In view of Eq. (2.25), with $\rho \sim 1/\Delta E$, this requires $T^{l,r} \ll 1$, or $G^{l,r} \ll e^2/h$. In the resonant tunneling regime of comparable ΔE and $k_B T$, this criterion is equivalent to the criterion $h\Gamma \ll k_B T$ mentioned earlier. In the classical regime $\Delta E \ll k_B T$, the criterion $h\Gamma \ll \Delta E$ dominates. The general criterion $h\Gamma \ll \Delta E, k_B T$ implies that the conductance of the quantum dot $G \ll e^2/h$.

As the temperature is lowered, such that $k_B T < e^2/C$, the Coulomb-blockade oscillations become observable. This is shown in Fig. 2.6. The classical regime $\Delta E \ll k_B T$ was first studied by Kulik and Shekhter [11, 12]. In this regime a continuum of energy levels in the confined central region participates in the conduction. If $\Delta E \ll k_B T \ll e^2/C$, only the terms with $N = N_{\min}$ contribute to the sum in Eq. (2.22), where N_{\min} minimizes the absolute value of $\Delta(N) \equiv U(N) - U(N-1) + \bar{\mu} - E_F$. (Here $\bar{\mu}$ is the equilibrium chemical potential of the dot, measured relative to the bottom of the potential well.) For energy-independent tunnel rates and density-of-states $\rho \equiv 1/\Delta E$, one obtains a line shape of individual conductance peaks given by [10]

$$G/G_{\max} = \frac{\Delta_{\min}/k_B T}{\sinh(\Delta_{\min}/k_B T)} \approx \cosh^{-2}\left(\frac{\Delta_{\min}}{2.5k_B T}\right), \quad (2.28)$$

$$G_{\max} = \frac{e^2}{2\Delta E} \frac{\Gamma^l\Gamma^r}{\Gamma^l + \Gamma^r}, \quad (2.29)$$

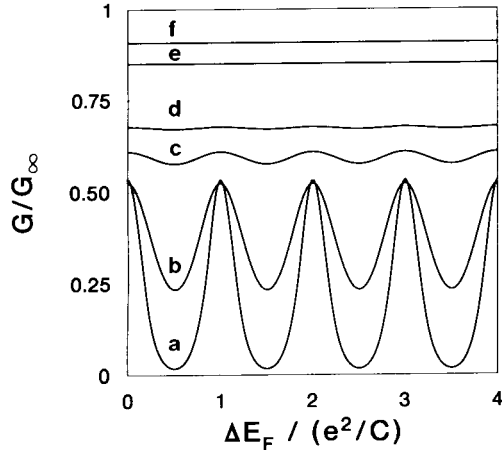


Figure 2.6: Temperature dependence of the Coulomb-blockade oscillations as a function of Fermi energy in the classical regime $k_B T \gg \Delta E$. Curves are calculated from Eq. (2.22) with $\Delta E = 0.01 \times e^2/C$, for $k_B T = 0.075$ (a), 0.15 (b), 0.3 (c), 0.4 (d), 1 (e), and $2 \times e^2/C$ (f). Level-independent tunnel rates are assumed, as well as equidistant nondegenerate energy levels.

using the definition $\Delta_{\min} \equiv \Delta(N_{\min})$. The second equality in Eq. (2.28) is approximate, but holds to better than 1%. A plot of G/G_{\max} versus Δ_{\min} is shown for an isolated peak in Fig. 2.7 (dashed curve).

Whereas the width of the peaks increases with T in the classical regime, the peak height (reached at $\Delta_{\min} = 0$) is temperature independent [compare traces (a) and (b) in Fig. 2.6]. The reason is that the $1/T$ temperature dependence associated with resonant tunneling through a particular energy level is canceled by the T dependence of the number $k_B T / \Delta E$ of levels participating in the conduction. This cancellation only holds if the tunnel rates are energy independent within the interval $k_B T$. A temperature dependence of the peak height may result from a strong energy dependence of the tunnel rates. In such a case one has to use the general result (2.22). This is also required if peaks start to overlap as $k_B T$ approaches e^2/C , or if the dot is nearly depleted ($E_F \lesssim k_B T$). The latter regime does not play a role in metals, but is of importance in semiconductor nanostructures because of the much smaller E_F .

Despite the fact that the Coulomb blockade of tunneling is lifted at a

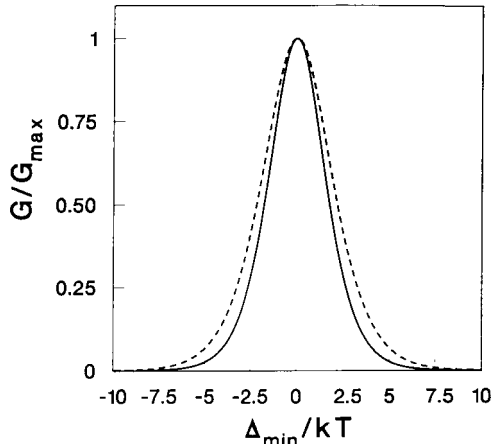


Figure 2.7: Comparison of the lineshape of a thermally broadened conductance peak in the resonant tunneling regime $h\Gamma \ll k_B T \ll \Delta E$ (solid curve) and in the classical regime $\Delta E \ll k_B T \ll e^2/C$ (dashed curve). The conductance is normalized by the peak height G_{\max} , given by Eqs. (2.29) and (2.32) in the two regimes.

maximum of a conductance peak, the peak height G_{\max} in the classical Coulomb-blockade regime $\Delta E \ll k_B T \ll e^2/C$ is a factor of two smaller than the conductance G_{∞} in the high temperature regime $k_B T \gg e^2/C$ of negligible charging energy (in the case of energy-independent tunnel rates). The reason is that the charging energy imposes a correlation between subsequent tunnel events. This correlation, expressed by the series of charge states $Q = -N_{\min}e \rightarrow Q = -(N_{\min} - 1)e \rightarrow Q = -N_{\min}e \rightarrow \dots$, implies that an electron can tunnel from a reservoir into the dot only half of the time [namely only when $Q = -(N_{\min} - 1)e$]. The tunnel probability is therefore reduced by a factor of two compared to the high temperature limit, where no such correlation exists.

The temperature dependence of the maxima of the Coulomb-blockade oscillations as obtained from Eq. (2.22) is plotted in Fig. 2.8. Also shown in Fig. 2.8 are the minima, which are seen to merge with the maxima as $k_B T$ approaches e^2/C . In the resonant tunneling regime $k_B T \lesssim \Delta E$ the peak height increases as the temperature is reduced, due to the diminished thermal broadening of the resonance. The crossover from the classical to the

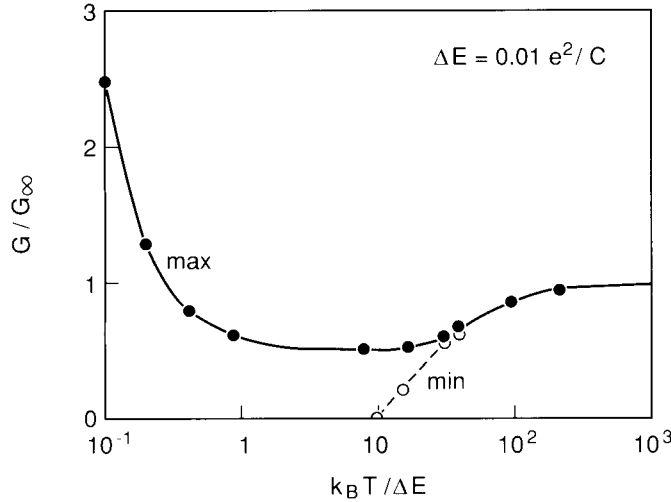


Figure 2.8: Temperature dependence of the maxima (max) and the minima (min) of the Coulomb-blockade oscillations in the conductance, in the regime $h\Gamma \ll k_B T$. The calculation, based on Eq. (2.22), was performed for the case of equidistant nondegenerate energy levels (at separation $\Delta E = 0.01 \times e^2/C$), all with the same tunnel rates Γ^l and Γ^r .

quantum regime is shown in Fig. 2.9 [calculated directly from Eq. (2.22)].

In the case of well-separated energy scales in the resonant tunneling regime ($h\Gamma \ll k_B T \ll \Delta E$), Eq. (2.22) can again be written in a simplified form. Now the single term with $p = N = N_{\min}$ gives the dominant contribution to the sum over p and N , where the integer N_{\min} minimizes the absolute value of

$$\Delta(N) = E_N + U(N) - U(N-1) - E_F \quad (2.30)$$

[cf. Eq. [2.11)]. Using the definition $\Delta_{\min} \equiv \Delta(N_{\min})$, Eq. (2.22) reduces to

$$G/G_{\max} = -4k_B T f'(\Delta_{\min}) = \cosh^{-2} \left(\frac{\Delta_{\min}}{2k_B T} \right), \quad (2.31)$$

$$G_{\max} = \frac{e^2}{4k_B T} \frac{\Gamma_{N_{\min}}^l \Gamma_{N_{\min}}^r}{\Gamma_{N_{\min}}^l + \Gamma_{N_{\min}}^r}. \quad (2.32)$$

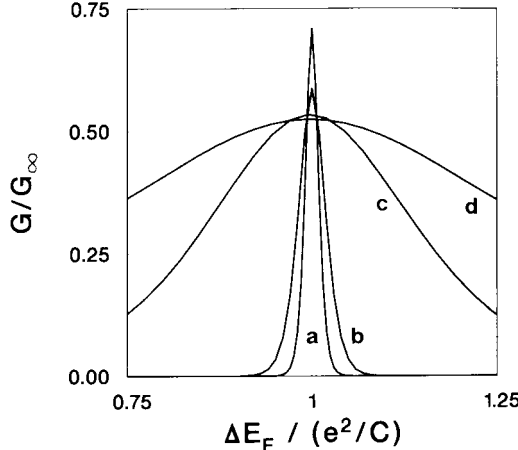


Figure 2.9: Lineshape for various temperatures, showing the crossover from the resonant tunneling regime (a and b) where both the width and the peak height depend on T , to the classical regime (c and d) where only the width of the peak depends on T . Curves are calculated from Eq. (2.22) with $\Delta E = 0.01 \times e^2/C$, and for $k_B T = 0.5$ (a), 1 (b), 7.5 (c), and $15 \times \Delta E$ (d).

As shown in Fig. 2.7, the lineshape in the resonant tunneling regime (full curve) is different from that in the classical regime (dashed curve), if they are compared at equal temperature. Equation (2.31) can be seen as the usual resonant tunneling formula for a thermally broadened resonance, generalized to include the effect of the charging energy on the resonance condition. Equations (2.31) and (2.32) hold regardless of the relative magnitude of ΔE and e^2/C . As illustrated in Fig. 2.8, the peak height in the resonant tunneling regime increases monotonically as $k_B T/\Delta E \rightarrow 0$, as long as $k_B T$ is larger than the resonance width $\hbar\Gamma$.

No theory has been worked out for Coulomb-blockade oscillations in the regime $k_B T \lesssim \hbar\Gamma$ (although the theory of Meir *et al.* [13] is sufficiently general to be applicable in principle). For *noninteracting* electrons, the transmission probability has the Breit-Wigner form [3, 18, 19]

$$G_{\text{BW}} = \mathcal{G} \frac{e^2}{h} \frac{\Gamma^l \Gamma^r}{\Gamma^l + \Gamma^r} \frac{\Gamma}{(\varepsilon/\hbar)^2 + (\Gamma/2)^2}, \quad (2.33)$$

where \mathcal{G} is the degeneracy of the resonant level, and ε is the energy separa-

tion of that level from the Fermi level in the reservoirs. In the presence of inelastic scattering with rate Γ_{in} one has to replace Γ by $\Gamma + \Gamma_{\text{in}}$ [3, 18, 19]. This has the effect of reducing the conductance on resonance by a factor $\Gamma/(\Gamma + \Gamma_{\text{in}})$, and of increasing the width of the peak by a factor $(\Gamma + \Gamma_{\text{in}})/\Gamma$. In contrast, inelastic scattering has no effect on the conductance in the regime $h\Gamma \ll k_B T \ll \Delta E$ [which follows from the fact that the thermal average $-\int G_{\text{BW}} f'(\varepsilon) d\varepsilon \approx \int G_{\text{BW}} d\varepsilon / 4k_B T$ is independent of Γ_{in}]. If inelastic scattering is negligible, and if the two tunnel barriers are equal, then the maximum conductance following from the Breit-Wigner formula is Ge^2/h , a result that may be interpreted as the fundamental contact resistance of a G -fold degenerate state [19, 20]. We surmise that the charging energy will lift the level degeneracy, so that the maximum peak height of the Coulomb-blockade oscillations is $G_{\text{max}} = e^2/h$ for the case of equal tunnel barriers.

A few words on terminology, to make contact with the resonant tunneling literature [3, 19]. The results discussed above pertain to the regime $\Gamma \gg \Gamma_{\text{in}}$, referred to as the “coherent resonant tunneling” regime. In the regime $\Gamma \ll \Gamma_{\text{in}}$ it is known as “coherent sequential tunneling” (results for this regime are given in Ref. [10]). Phase coherence plays a role in both of these regimes, by establishing the discrete energy spectrum in the quantum dot. The classical, or incoherent, regime is entered when $k_B T$ or $h\Gamma_{\text{in}}$ exceed ΔE . The discreteness of the energy spectrum can then be ignored.

We close this section by a discussion of the activation energy of the minima of the conductance oscillations. It is shown in Ref. [10] that G_{min} depends exponentially on the temperature, $G_{\text{min}} \propto \exp(-E_{\text{act}}/k_B T)$, with activation energy

$$E_{\text{act}} = \frac{1}{2}(\Delta E + e^2/C) = \frac{1}{2}\Delta E^*. \quad (2.34)$$

This result holds for equal tunnel rates at two subsequent energy levels. The renormalized level spacing $\Delta E^* = \Delta E + e^2/C$, which according to Eq. (2.13) determines the periodicity of the Coulomb-blockade oscillations as a function of Fermi energy, thus equals twice the activation energy of the conductance minima. The exponential decay of the conductance at the minima of the Coulomb-blockade oscillations results from the suppression of tunneling processes which conserve energy in the intermediate state in the quantum dot. Tunneling via a *virtual* intermediate state is not suppressed at low temperatures, and may modify the temperature dependence

of the minima if $h\Gamma$ is not much smaller than $k_B T$ and ΔE [6, 7]. For $h\Gamma \ll k_B T, \Delta E$ this ‘‘macroscopic quantum tunneling of the charge’’ can be neglected.

2.4 Thermopower oscillations

In the previous sections we have considered a quantum dot that is weakly coupled to two reservoirs of equal temperature. Then, a net current I is passed through the dot in response to an applied potential difference V . If a temperature difference ΔT exists between the reservoirs, the thermo-electric transport coefficients of the dot become relevant, as well as the conductance. It is only recently, that the thermo-electric transport properties of mesoscopic systems have attracted attention [21, 22, 23, 24]. The reason is that these are more difficult to measure on small length scales than the conductance.

A temperature difference ΔT between the reservoirs induces a potential difference V across the dot (the Seebeck effect). The ratio $S \equiv -V/\Delta T$, under conditions of zero electrical current, is the thermopower of the dot. It can be obtained from Eq. (2.8) by solving for $I = 0$. In linear response, the result obtained in Ref. [14] is

$$S = -\frac{e}{k_B T^2 G} \sum_{p=1}^{\infty} \sum_{N=1}^{\infty} \frac{\Gamma_p^l \Gamma_p^r}{\Gamma_p^l + \Gamma_p^r} (E_p + U(N) - U(N-1) - E_F) \times \\ \times P_{\text{eq}}(N, n_p = 1) [1 - f(E_p + U(N) - U(N-1) - E_F)] , \quad (2.35)$$

where G is the conductance of the dot given by Eq. (2.22).

We discuss two limiting cases of the general result (2.35). The first is the classical limit $\Delta E \ll k_B T \ll e^2/C$, in which the discreteness of the energy spectrum in the dot may be ignored, but not the charging energy. Due to the Coulomb-blockade, only the terms with $N = N_{\min}$ where N_{\min} minimizes the absolute value of $\Delta(N) \equiv U(N) - U(N-1) + \bar{\mu} - E_F$ contribute to the sums in the numerator and denominator of Eq. (2.35). (Here $\bar{\mu}$ is the equilibrium chemical potential of the dot, measured relative to the bottom of the potential well.) Equation (2.35) reduces to [14]

$$S = -\frac{1}{2eT} \Delta_{\min} = -\frac{1}{2eT} [(N_{\min} - \frac{1}{2}) \frac{e^2}{C} + \bar{\mu} - e\phi_{\text{ext}} - E_F] , \\ \text{if } \Delta E \ll k_B T \ll e^2/C , \quad (2.36)$$

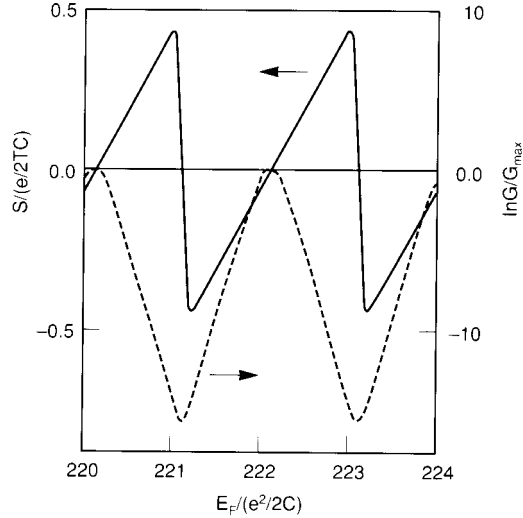


Figure 2.10: Thermopower oscillations as a function of Fermi energy in the classical regime (solid curve). The Coulomb-blockade oscillations in the conductance are shown as well (dotted), on a logarithmic scale. The curves are computed from Eqs. (2.35) and (2.22), for a series of equidistant non-degenerate levels with $\Delta E = 0.005 \times e^2/C$, $k_B T = 0.025 \times e^2/C$, and level-independent tunnel rates.

where $\Delta_{\min} \equiv \Delta(N_{\min})$. According to Eq. (2.36), the thermopower as a function of Fermi energy oscillates around zero in a sawtooth fashion, jumping discontinuously between $\pm e/4CT$ each time N_{\min} changes by one. The peak-to-peak amplitude of the oscillations equals $(e^2/2C)/k_B T$ in units of k_B/e , and is therefore a direct measure of the relative magnitude of the charging and thermal energies. The (positive) slope of the sawtooth $dS/dE_F = 1/2eT$ depends only on the temperature, not on the capacitance.[§] The periodicity of the thermopower oscillations is the same as that of the Coulomb-blockade oscillations in the conductance. To illustrate the sawtooth thermopower-oscillations, we have computed S and G from Eqs. (2.35) and (2.22) for parameters in the classical regime. The results are plotted in Fig. 2.10.

The sawtooth lineshape can be understood from the following quali-

[§]If we consider the thermopower as a function of ϕ_{gate} , however, the slope *does* depend on the capacitance: $dS/d\phi_{\text{gate}} = (C_{\text{gate}}/C)/2T = \alpha/2T$.

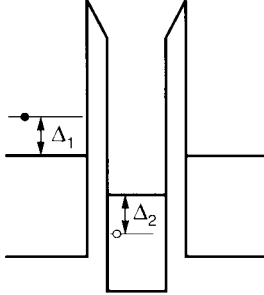


Figure 2.11: Due to the Coulomb blockade, transport through the dot is possible only if an electron with excess energy Δ_1 is created in the reservoir, and a hole with excess energy Δ_2 in the dot, such that $\Delta_1 + \Delta_2 = \Delta_{\min}$.

tative argument. Assuming that the Onsager relations hold for transport through a quantum dot, we find for the thermopower

$$S = \frac{\Pi}{T} = \frac{1}{T} \left. \frac{\partial I_Q}{\partial T} \right|_{\Delta T=0}, \quad (2.37)$$

where $\Pi \equiv (\partial I_Q / \partial T)_{\Delta T=0}$ is the Peltier coefficient, which relates the heat flow I_Q through the dot to the current I . (In Ref. [14] this assumption has been made implicitly, since the effect of the “environment”, i.e. the impedance of the external driving or measuring circuit, was not taken into account [24].) The Peltier coefficient may be interpreted as the energy that is transferred between the reservoirs per transferred carrier. This energy, and thus the thermopower can be determined as follows. Due to the Coulomb blockade, an electron can be transferred through the dot at low temperatures only if an excitation energy Δ_{\min} is supplied to the system. This energy may be used in part to excite an electron in the reservoir to an energy Δ_1 above the Fermi level [with probability $\exp(-\Delta_1/k_B T)$], and in part to excite an electron in the dot so that an empty state is created at an energy Δ_2 below the Fermi level [with probability $\exp(-\Delta_2/k_B T)$], see Fig. 2.11. The excited electron can then tunnel through the dot to the other reservoir via the empty state in the dot, so that the energy Δ_1 is transferred. This process occurs with probability $\exp(-\Delta_{\min}/k_B T)$, independent of Δ_1 . Therefore, the energy that is transferred per electron is

on average $\frac{1}{2}\Delta_{\min}$, so that we obtain $\Pi = \Delta_{\min}/2e$. Combining this result with Eq. (2.37) yields Eq. (2.36), which describes the sawtooth lineshape of the thermopower oscillations.

Although the periodicity of the thermopower and conductance oscillations is the same, the amplitude and lineshape of the thermopower oscillations (2.36) is entirely different from what would follow from a naive application of Mott's rule to Eq. (2.28) for the conductance:

$$\begin{aligned} S_{\text{Mott}} &\equiv -\frac{\pi^2 k_{\text{B}}}{3 e} k_{\text{B}} T \frac{d \ln G}{d E_F} \\ &= -\frac{\pi^2 k_{\text{B}}}{3 e} \left[\cotanh \left(\frac{\Delta_{\min}}{k_{\text{B}} T} \right) - \frac{k_{\text{B}} T}{\Delta_{\min}} \right]. \end{aligned} \quad (2.38)$$

Equation (2.38) would predict an amplitude of order k_{B}/e of the thermopower oscillations which is parametrically smaller (by a factor of order $e^2/Ck_{\text{B}}T$) than the correct result (2.36). Of course, Mott's rule is derived (e.g. in Ref. [25]) for a noninteracting electron gas with a weakly energy-dependent conductance, and is therefore clearly not applicable to the Coulomb-blockade regime. Still, its breakdown even as “a rule of thumb” is noteworthy.

Finally, we briefly discuss the low-temperature limit $k_{\text{B}}T \ll \Delta E$, where the discreteness of the energy spectrum of the dot can be ignored no longer. This is the quantum regime, in which the Coulomb blockade coexists with resonant-tunneling phenomena. We still assume that $k_{\text{B}}T \gg \hbar(\Gamma^l + \Gamma^r)$, so that the levels are thermally broadened only, and Eq. (2.35) applies. In Ref. [14] it is shown that in this limit the discreteness of the spectrum leads to fine structure on the thermopower oscillations. As a function of Fermi energy, the fine structure exhibits a periodicity $\delta E_F = \Delta E_p$ determined by the bare level spacing in the dot. Since the fine structure within a single period of the overall thermopower oscillations occurs at a *constant* number of electrons in the dot, its periodicity directly reflects the excitation spectrum of the dot. (In contrast, the periodicity of the overall thermopower oscillations $\Delta E_F = \Delta E_N^* = \Delta E_N + e^2/C$ is determined by the renormalized level spacing, since the number of electrons in the dot changes by one each period. It thus reflects the addition spectrum of the dot.) We illustrate the development of fine structure on the thermopower oscillations in Fig. 2.12.

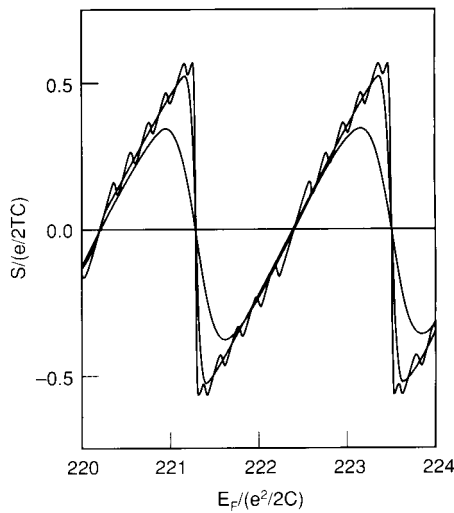


Figure 2.12: Development of fine structure on the thermopower oscillations on lowering the temperature from $k_B T = 0.1, 0.025$, to $0.005 \times e^2/C$. The curves are computed from Eq. (2.35), for a series of equidistant nondegenerate levels with $\Delta E = 0.1 \times e^2/C$, and level-independent tunnel rates.

References

- [1] A. Kumar, S. E. Laux, and F. Stern, Phys. Rev. B **42**, 5166 (1990).
- [2] K. K. Likharev, IBM J. Res. Dev. **32**, 144 (1988); D. V. Averin and K. K. Likharev, in: *Mesoscopic Phenomena in Solids*, edited by B. L. Al'tshuler, P. A. Lee, and R. A. Webb (North-Holland, Amsterdam, 1991). This is a comprehensive review of single-electron tunneling in metals.
- [3] M. Büttiker, Phys. Rev. B **33**, 3020 (1986).
- [4] K. Mullen, E. Ben-Jacob, R. C. Jaklevic, and Z. Schuss, Phys. Rev. B **37**, 98 (1988); M. Amman, K. Mullen, and E. Ben-Jacob, J. Appl. Phys. **65**, 339 (1989).
- [5] P. L. McEuen, E. B. Foxman, J. Kinaret, U. Meirav, M. A. Kastner, N. S. Wingreen, and S. J. Wind, Phys. Rev. B **45**, 11419 (1992).
- [6] D. V. Averin and A. A. Odintsov, Phys. Lett. A **140**, 251 (1989); D. V. Averin and Yu. V. Nazarov, Phys. Rev. Lett. **65**, 2446 (1990).
- [7] L. I. Glazman and K. A. Matveev, Pis'ma Zh. Eksp. Teor. Fiz. **51**, 425 (1990) [JETP Lett. **51**, 484 (1990)].
- [8] C. W. J. Beenakker, H. van Houten, and A. A. M. Staring, Phys. Rev. B **44**, 1657 (1991).
- [9] C. W. J. Beenakker, H. van Houten, and A. A. M. Staring, in: *Granular Nanoelectronics*, edited by D. K. Ferry, J. Barker, and C. Jacoboni (Plenum, New York, 1991).
- [10] C. W. J. Beenakker, Phys. Rev. B **44**, 1646 (1991).
- [11] R. I. Shekhter, Zh. Eksp. Teor. Fiz. **63**, 1410 (1972) [Sov. Phys. JETP **36**, 747 (1973)].
- [12] I. O. Kulik and R. I. Shekhter, Zh. Eksp. Teor. Fiz. **68**, 623 (1975) [Sov. Phys. JETP **41**, 308 (1975)].
- [13] Y. Meir, N. S. Wingreen, and P. A. Lee, Phys. Rev. Lett. **66**, 3048 (1991).

- [14] C. W. J. Beenakker and A. A. M. Staring, Phys. Rev. B, to be published.
- [15] L. I. Glazman and R. I. Shekhter, J. Phys. Condens. Matter **1**, 5811 (1989).
- [16] G. W. Bryant, Phys. Rev. Lett. **59**, 1140 (1987).
- [17] P. A. Maksym and T. Chakraborty, Phys. Rev. Lett. **65**, 108 (1990).
- [18] A. D. Stone and P. A. Lee, Phys. Rev. Lett. **54**, 1196 (1985).
- [19] M. Büttiker, IBM J. Res. Dev. **32**, 63 (1988).
- [20] R. Landauer, in: *Localization, Interaction, and Transport Phenomena*, edited by B. Kramer, G. Bergmann, and Y. Bruynseraede (Springer, Berlin, 1985).
- [21] G. M. Gusev, Z. D. Kvon, and A. G. Pogosov, Pis'ma Zh. Eksp. Teor. Fiz. **51**, 151 (1990) [JETP Lett. **51**, 171 (1990)].
- [22] B. L. Gallagher, T. Galloway, P. Beton, J. P. Oxley, S. P. Beaumont, S. Thoms, and C. D. W. Wilkinson, Phys. Rev. Lett. **64**, 2058 (1990).
- [23] L. W. Molenkamp, H. van Houten, C. W. J. Beenakker, R. Eppenga, and C. T. Foxon, Phys. Rev. Lett. **65**, 1052 (1990); L. W. Molenkamp, Th. Gravier, H. van Houten, O. J. A. Buyk, M. A. A. Mabesoone, and C. T. Foxon, *ibid.* **68**, 3765 (1992).
- [24] M. Amman, E. Ben-Jacob, and J. Cohn, Z. Phys. B **85**, 405 (1991).
- [25] J. M. Ziman, *Principles of the Theory of Solids* (Cambridge University Press, 1972).

Chapter 3

Coulomb-blockade oscillations in disordered quantum wires

3.1 Introduction

The phenomenon investigated experimentally in this chapter was first observed by Scott-Thomas *et al.* [1]. They discovered that at low temperatures a narrow disordered channel in a Si inversion layer may exhibit strikingly regular conductance oscillations as a function of the voltage on the gates used to define the channel. This is in contrast to the aperiodic conductance fluctuations usually observed in such structures [2]. The period of the oscillations differed from device to device, and did not correlate with the channel length. Based on estimates of the sample parameters, it was concluded that each period corresponds to the addition of a single electron to a conductance-limiting segment in the narrow channel. In order to explain their observations, Scott-Thomas *et al.* [1] originally suggested that a charge-density wave or “Wigner crystal” was formed. From a model due to Larkin and Lee [3], and Lee and Rice [4], they inferred that this would lead to a thermally activated conductance because of pinning of the charge-density wave by impurities in the narrow channel. The activation energy would be determined by the most strongly pinned segment of the crystal, and periodic oscillations in the conductance as a function of gate voltage or electron density would reflect the condition that an integer number of electrons is contained between the two impurities delimiting that segment.

As an alternative explanation, it was proposed that the effect is a manifestation of *Coulomb-blockade oscillations* in a semiconductor nanostructure [5]. In the discussion of our experimental results, we limit ourselves to a comparison with the Coulomb-blockade model, discussed in chapter 2 [6, 7, 8]. A discussion of the Wigner-crystal model has been given in Refs. [9] and [10]. The conclusion reached in this chapter is that the Coulomb-blockade model does provide an adequate and consistent description of our experiments. In a low-density quantum wire with weak disorder (no tunnel barriers), however, a Wigner-crystal may well be an appropriate description of the ground state [11].

The Wigner crystal is a manifestation of long-range order neglected in the theory of Coulomb-blockade oscillations. However, both the Coulomb-blockade and the Wigner-crystal models have in common that electron-electron interactions play a central role. In contrast, some authors have argued that resonant tunneling of noninteracting electrons can explain the periodicity of the observed conductance oscillations [12, 13]. One cannot easily discriminate between these models on the basis of the periodicity of the oscillations. Conductance oscillations due to resonant tunneling through nondegenerate levels as well as Coulomb-blockade oscillations both have a periodicity corresponding to the addition of a single electron to the confined region. Other considerations are necessary to demonstrate the inadequacy of a model based on resonant tunneling of noninteracting electrons. The most important of these are the large activation energy of the minima (exceeding the average single-electron level spacing ΔE), and the absence of spin splitting of the peaks in a magnetic field. These considerations will be discussed in detail in this chapter.

Our experimental work has consisted of a study of the conductance of disordered quantum wires defined by a split-gate technique in the two-dimensional electron gas (2DEG) of a GaAs–Al_xGa_{1-x}As heterostructure. We have investigated the effects of temperature and magnetic field on the conductance as a function of gate voltage, as well as the magnetoconductance and the Hall resistance in a cross-shaped narrow channel geometry. In addition, we have varied the channel length, and the degree of disorder.

This chapter is organized as follows. The split-gate quantum wires used in our study are described in section 3.2. An overview of the experimental results is given in section 3.3. We find a rich and complex behavior, with variations from device to device, reflecting the mesoscopic nature of

disordered quantum wires. The most characteristic aspects of our observations, however, are representative of all devices that show the conductance oscillations. The period of the oscillations as a function of gate voltage is explained in section 3.4.1 in terms of the theory of Coulomb-blockade oscillations presented in chapter 2. We can account for the temperature dependence of the lineshape of the oscillations as well, as is discussed in section 3.4.2. The effects of multiple segments in the wire are discussed in section 3.4.3. Finally, we discuss in section 3.5 those aspects of the experimental results that are less well understood.

3.2 Split-gate quantum wires

Our experimental results for the conductance of quasi one-dimensional channels have been obtained using narrow wires, defined by a split-gate technique in the 2DEG in a modulation doped GaAs–Al_xGa_{1-x}As heterostructure. By adjusting the negative gate voltage (applied between the gate on top of the heterostructure and an Ohmic contact to the 2DEG), the channel width W can be controlled in a range from definition (where $W \approx W_{\text{lith}}$, the lithographic width) to pinch off (where W is close to zero). In the regime of interest, which is that close to pinch off, both the electron concentration per unit length and the channel width vary approximately linearly with gate voltage [14].

Starting point for the fabrication of our samples is a GaAs–Al_xGa_{1-x}As heterostructure, which consists of a sequence of layers grown on top of a semi-insulating GaAs substrate by molecular-beam epitaxy. The first layer is a thick buffer layer of pure GaAs. The 2DEG is formed at the interface of this layer with an Al_{0.33}Ga_{0.67}As layer grown on top of it. The latter consists of a 20-nm-thick spacer layer of pure Al_{0.33}Ga_{0.67}As, and a 40-nm-thick Al_{0.33}Ga_{0.67}As layer doped with Si at a concentration of $1.33 \times 10^{18} \text{ cm}^{-3}$. Finally, the heterostructure is capped by a 20-nm-thick undoped GaAs layer.

We have used two sets of samples. In one set (designated by D in Table 3.1), a planar doping layer of Be impurities with a sheet concentration of $2 \times 10^{10} \text{ cm}^{-2}$ was incorporated in the buffer layer during growth, at 25 Å below the heterointerface. This was done in order to introduce strongly repulsive scattering centers in the 2DEG (Be is an acceptor in GaAs). Such scattering centers may act as tunnel barriers in a narrow channel in

Channel	Length (μm)	Period (mV)
$D1$	4.4	2.7
$D2$	6.2	2.1
$D3$	6.3	2.2
$U1$	0.5	
$U2$	6.2	1.0
$U3$	16.7	2.3

Table 3.1: Channel length and period of the conductance oscillations. The D channels are intentionally disordered by means of a planar doping layer of Be near the heterointerface in the GaAs layer. The U channels are unintentionally disordered. Channel $D1$ is the right section and channel $D3$ is the middle section of a miniature Hall-bar [see Fig. 3.1(b)]. The period of the oscillations is given for $T = 1.5$ K and $B = 0$, except for channel $U2$ ($T = 50$ mK and $B = 0$) and for channel $D3$ ($T = 50$ mK and $B = 5$ T). No oscillations were observed in the shortest channel $U1$.

the 2DEG [5]. The other set of samples (designated by U) was undoped, but was nevertheless disordered as well, due to random fluctuations in the distribution of the ionized donors in the $\text{Al}_x\text{Ga}_{1-x}\text{As}$ layer [15].

In the wide regions, the Be-doped samples had an elastic mean free path $l_e \approx 0.7$ μm , deduced from the conductivity at $T = 4.2$ K and the electron sheet density $n_s = 2.9 \times 10^{11} \text{ cm}^{-2}$. For the undoped samples these values were $l_e = 3.9$ μm and $n_s = 3.0 \times 10^{11} \text{ cm}^{-2}$. This mean free path does not describe the transport in the quantum wires near pinch off, when the conductance is limited by a small number of accidentally strong scattering centers. These are due to negatively charged Be acceptors close to the 2DEG, and due to statistical fluctuations in the distribution of the remote ionized donors in the $\text{Al}_x\text{Ga}_{1-x}\text{As}$ layer. The resulting variations in the electrostatic potential are enhanced in a narrow channel because of the reduced screening. Near pinch off, the channel breaks up into a small number of segments separated by potential barriers formed by such scattering centers. This is inferred from our experimental results, and is supported by model calculations of Nixon and Davies [15], in which the random positions of the remote ionized donors are taken into account.

The fabrication of the samples proceeds as follows. First, the heterostructure is mesa-etched into a rectangular shape, and twelve alloyed Au-Ge-Ni Ohmic contacts are formed along its edges. Then, a pattern of six Ti-Au gate electrodes is defined in a two-step process, using optical lithography for the coarse parts and electron-beam lithography for the fine details. These gates can be controlled independently. Figure 3.1 shows scanning electron micrographs of the two narrow-channel geometries studied. When negatively biased, the gates (light lines) subdivide the 2DEG into six wide regions (underneath the dark areas), which are connected by narrow channels. Two Ohmic contacts are attached to each of these wide regions. The first geometry [Fig. 3.1(a)] consists of a set of five narrow channels on a single sample (each of which can be measured independently), while the second [Fig. 3.1(b)] consists of a miniature Hall bar. At the depletion threshold of the 2DEG directly underneath the gates (about -0.3 V), the narrow channels have approximately the lithographic width $W_{\text{lith}} = 0.5 \mu\text{m}$. Close to pinch off the channel width W is reduced to about $0.1 \mu\text{m}$, and the electron density n_s is reduced by about a factor of 2. (The estimate for W is based on typical lateral depletion widths of $0.2 \mu\text{m}/\text{V}$ [14, 15, 16], and that for n_s on an extrapolation of the periodicity of the Shubnikov-de Haas oscillations, measured at several gate voltage values.) The length L of the channels varies (see Table 3.1).

One Be-doped sample (not included in Table 3.1) with channels of width $W_{\text{lith}} = 1 \mu\text{m}$ was studied as well. The results obtained with these channels were similar to those obtained with the narrower channels, except for the pinch-off voltage, which was about twice as large. The periodicity of the dominant oscillations was within the range of values we found in the narrower wires.

3.3 Experimental results

Primarily, we have performed measurements of the conductance as a function of gate voltage, for a number of quantum wires of different length. The experiments were done over a range of temperatures and magnetic fields. In addition, we have measured the conductance and Hall resistance as a function of magnetic field, at fixed gate voltage. A conventional ac lock-in technique was used to measure the conductance, while the gate voltage (or magnetic field) was swept slowly. In order to ensure linear response, the

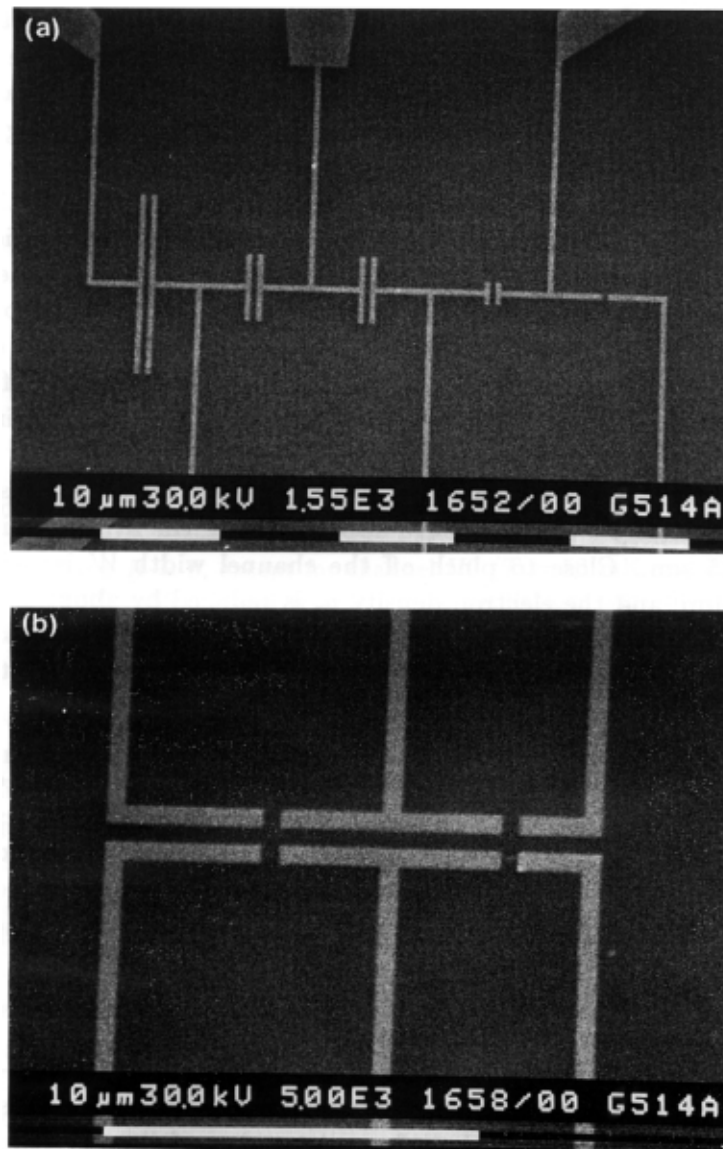


Figure 3.1: Scanning electron micrographs of the two split-gate geometries that we have used. The first (a) defines five narrow channels of increasing length, $L = 0.5, 2.1, 6.2, 6.2$, and $16.7 \mu\text{m}$, respectively. The second (b) defines a miniature Hall bar, with section lengths $L = 4.4, 6.3$, and $2.4 \mu\text{m}$ and side probes having a width of $0.5 \mu\text{m}$. For both geometries, the lithographic channel width is $W_{\text{lith}} = 0.5 \mu\text{m}$.

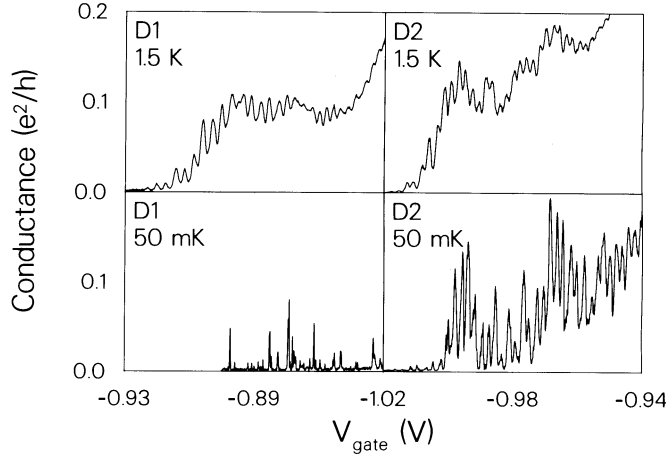


Figure 3.2: Two-terminal conductance versus gate voltage of two intentionally disordered narrow channels (D_1 and D_2) at $T = 1.5$ K and 50 mK.

excitation voltage was kept below $k_B T/e$. We have studied the differential conductance also, using dc bias voltages up to a few mV, but in this chapter we restrict ourselves to the linear response regime. Experimental data are presented for channels D_1 , D_2 , and D_3 , which are intentionally disordered by a planar doping layer of Be, and for channels U_2 and U_3 , which are not intentionally disordered.

3.3.1 Conductance oscillations: Zero magnetic field

In Fig. 3.2 the conductance near pinch off is shown for two Be-doped quantum wires, D_1 and D_2 . At $T = 1.5$ K both channels exhibit well-resolved conductance oscillations, which are *periodic* in the gate voltage. The oscillations appear to be superimposed on a background conductance of approximately $0.1e^2/h$, and have a period $\Delta V_{\text{gate}} \approx 2.7$ mV (D_1) and 2.1 mV (D_2). As the gate voltage is increased the oscillations disappear gradually. Whereas the two conductance traces are relatively similar at $T = 1.5$ K, this is not the case at $T = 50$ mK. In channel D_2 the oscillations become better resolved at this low temperature, while the period is unchanged and the value of the conductance at the maxima remains approximately the same. In contrast, the oscillations in channel D_1 are suppressed at 50 mK,

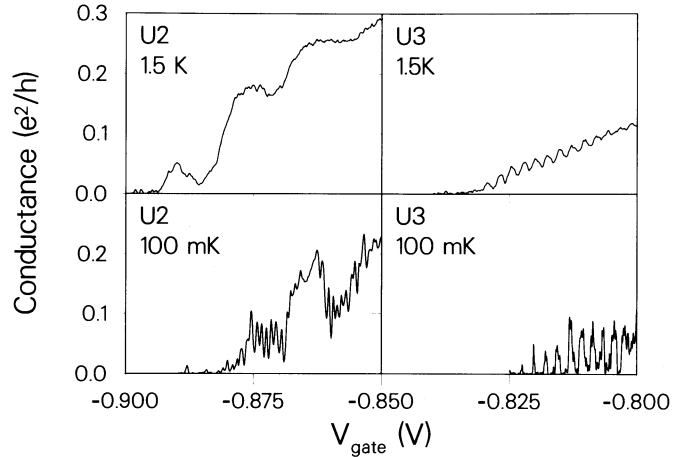


Figure 3.3: Two-terminal conductance versus gate voltage of two unintentionally disordered narrow channels ($U2$ and $U3$) at $T = 1.5 \text{ K}$ and 100 mK .

and an irregular pattern of sharp conductance peaks is observed instead.

In Fig. 3.3 we show a corresponding set of results for two undoped channels, $U2$ and $U3$. At $T = 1.5 \text{ K}$, the periodic conductance oscillations are observed in channel $U3$ only ($\Delta V_{\text{gate}} \approx 2.3 \text{ mV}$). Channel $U2$ shows a slow conductance modulation instead. Both channels show periodic conductance oscillations as the temperature is decreased to 100 mK ($\Delta V_{\text{gate}} \approx 1.0 \text{ mV}$ for $U2$). As is the case in channel $D2$ in Fig. 3.2, the oscillations in channel $U3$ become better resolved on lowering the temperature. In addition, a fine structure develops on these peaks, indicative of a higher-frequency oscillation.

The conductance oscillations for channel $U3$ are shown in more detail in the top panel of Fig. 3.4, for temperatures between 1 and 3 K (the calculated curves in the bottom panel will be explained in section 3.4.2). Note that both the minima and maxima of the oscillations increase with temperature. At $T = 2.5 \text{ K}$ the oscillations are smeared out, but can still be resolved.

The results shown in Figs. 3.2–3.4 are representative of all the channels we have studied, except for the shortest channel ($U1$, $L = 0.5 \mu\text{m}$).

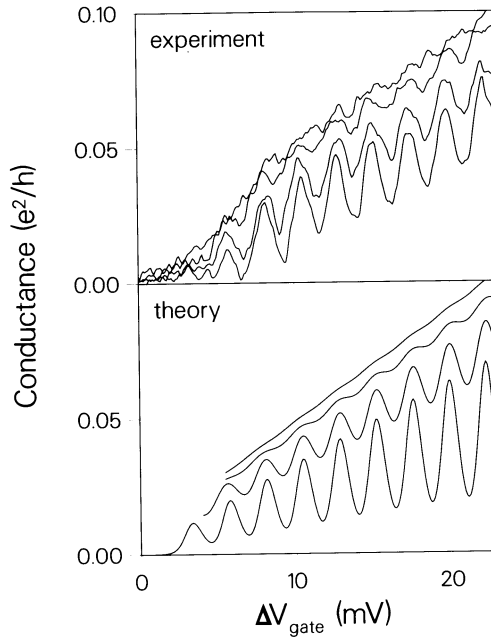


Figure 3.4: Top panel: two-terminal conductance versus gate voltage of channel $U3$ for $T = 3.2, 2.5, 1.6$, and 1 K, from top to bottom. Bottom panel: conductance calculated from Eq. (2.22) for: $e^2/C = 0.6$ meV, $\Delta E = 0.1$ meV, $\alpha = 0.265$, $h\Gamma_p^{l,r} = 0.027pE_p$, and twofold degeneracy.

As evidenced by the conductance, pinch off is typically reached at -1 V $\lesssim V_{\text{gate}} \lesssim -0.8$ V. Periodic conductance oscillations are observed in most of the channels at temperatures of 1.5 K or below, with a period varying between 1 and 3 mV for different channels. We did not find systematic differences between the Be-doped channels and the channels which were not intentionally disordered. The period does not correlate with the length of the channel or the degree of disorder (see Table 3.1), and changes within this range when the sample is thermally cycled. The number of successive oscillations observed is between 20 and 50 for most narrow channels. At very low temperatures (below 100 mK) it is found often that the regular oscillations are replaced by an irregular pattern of sharp conductance peaks.

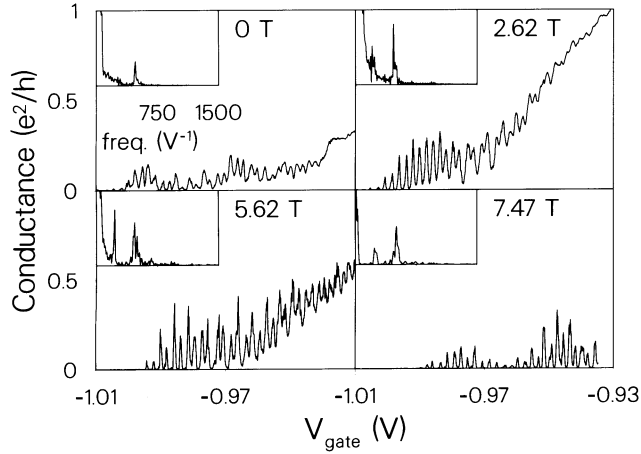


Figure 3.5: Two-terminal conductance versus gate voltage of channel $D2$ at 50 mK in a perpendicular magnetic field. Insets: Fourier spectra of the data. The vertical scale of the Fourier spectra at $B = 0$ and 7.47 T is multiplied by a factor 2.5.

3.3.2 Conductance oscillations: Quantum Hall effect regime

The various effects of a strong magnetic field on the conductance as a function of gate voltage are shown in Figs. 3.5–3.9 for channels $D1$ and $D2$, and in Fig. 3.10 for channel $U2$. Figure 3.5 shows the conductance as a function of gate voltage for channel $D2$, at four values of the magnetic field. We find that the period of the oscillations is *insensitive* to the magnetic field, which is illustrated most clearly by the insets, showing the Fourier spectra of the conductance traces. Each of these exhibits a sharp peak at a B -independent frequency of about 450 V^{-1} (at $B = 7.47 \text{ T}$ the frequency has increased by a few percent). The amplitude of the oscillations and the average conductance depend on the magnetic field in a nonmonotonic fashion. As the magnetic field is increased, both the amplitude and average conductance are enhanced above the zero-field values in magnetic fields of intermediate strength (2.62 and 5.62 T), followed by a decrease in still stronger fields (7.47 T). The conductance peaks do not split, not even in our strongest field of 8 T. In this particular channel, however, a second peak emerges in the Fourier spectrum at approximately half the dominant

frequency as the magnetic field is increased. This second peak is a result of the amplitude modulation of the peaks in the gate-voltage scan, which is seen most clearly in the trace at 5.62 T, where high- and low-conductance peaks alternate in a doubletlike structure. We do not think that the electron spin is responsible for this effect. Some other channels were found to exhibit more than two peaks in the Fourier spectrum. We attribute these multiple periodicities to the presence of more than one segment in the wire. Finally, we note that with increasing magnetic field pinch-off is reached at less negative gate voltages, but that the total number of peaks remains approximately constant.

Figure 3.6 gives the conductance of channel $D1$ at $T = 4.2$ K (a), 1.5 K (b), and 50 mK (c), at various values of the magnetic field. At 4.2 K [Fig. 3.6(a)], the oscillations are almost smeared out in the absence of a magnetic field, and the conductance increases monotonically with gate voltage. Surprisingly, at $B = 1.24$ T the oscillations can be observed clearly at this relatively high temperature. The periodic oscillations can be observed best in the traces at 1.5 K [Fig. 3.6(b)]. The magnetic-field dependence is similar to that of channel $D2$, including the insensitivity of the period to the magnetic field, the absence of spin-splitting, and enhancement of the amplitude and average conductance at intermediate field strengths (1 T $\lesssim B \lesssim 5$ T). In Fig. 3.2 we have shown that at 50 mK, and in the absence of a magnetic field, the periodic oscillations in channel $D1$ are suppressed. This is evident in the zero-field trace in Fig. 3.6(c) as well, where a pattern of irregular conductance peaks is visible, with a typical spacing about five times smaller than the period of the oscillations at 1.5 K. The enhancement of the conductance in fields of intermediate strength is very pronounced at 50 mK, where the conductance near $V_{\text{gate}} \approx -0.8$ V approaches the first quantized Hall plateau ($G = e^2/h$). In the trace at $B = 5.03$ T the step region before the $G = e^2/h$ plateau exhibits quite pronounced oscillations with the same periodicity as those at 1.5 K, but with an amplitude that is almost equal to e^2/h . At more negative gate voltages the regularity of the conductance oscillations is lost. This is also the case in stronger magnetic fields.

In Fig. 3.7 the conductance of channel $D1$ is shown over a wider range of gate voltage, at $B = 2.52$ T and $T = 50$ mK and 1.5 K. At gate voltages below -0.83 V the periodic conductance oscillations can be observed in both traces. As the gate voltage is increased beyond -0.8 V, the conductance

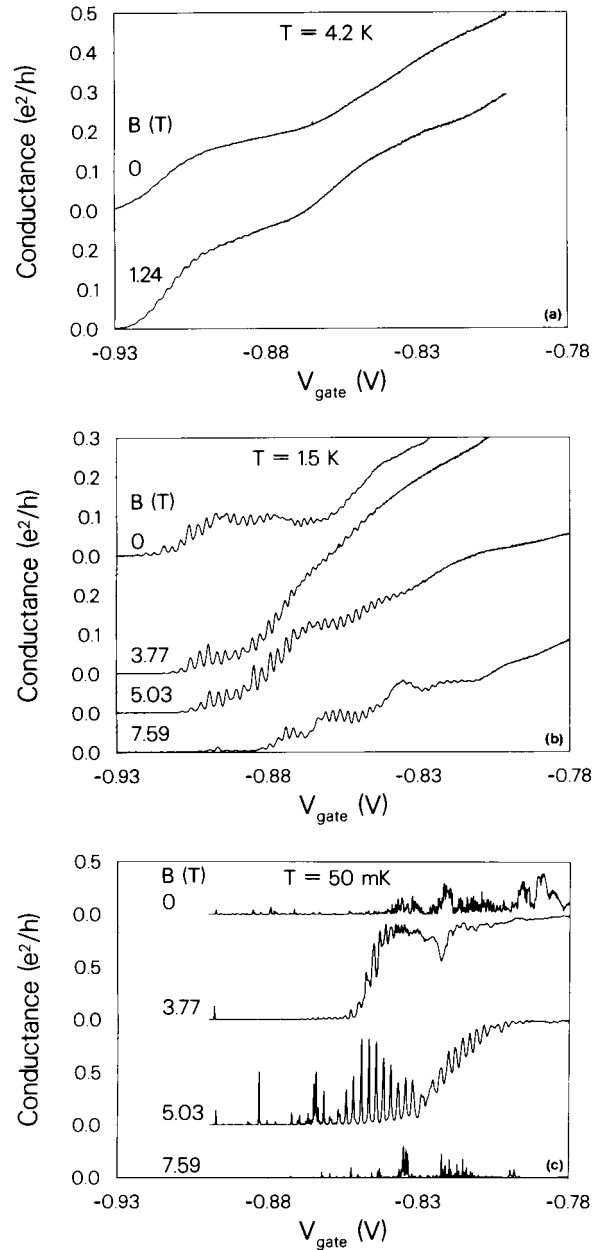


Figure 3.6: Two-terminal conductance versus gate voltage of channel D1 in a perpendicular magnetic field. The temperatures are (a) 4.2 K, (b) 1.5 K, and (c) 50 mK. The curves have been offset for clarity.

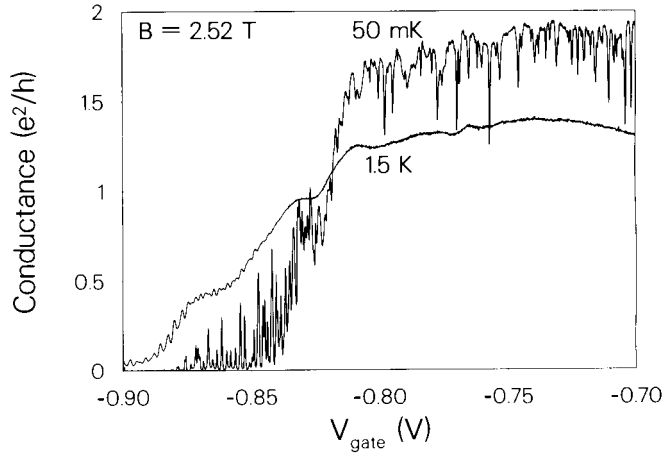


Figure 3.7: Two-terminal conductance versus gate voltage of channel $D1$ at $B = 2.52$ T, for $T = 50$ mK and 1.5 K.

at 50 mK is seen to increase up to a value close to the second quantized Hall plateau at $G = 2e^2/h$. However, a large number of sharp dips in the conductance are observed in this regime. This structure has vanished completely at 1.5 K, and the conductance plateau at $2e^2/h$ is no longer visible. Instead, there is some evidence of a Hall plateau at $G = e^2/h$. In addition, there is a plateau-like feature near $G = \frac{1}{2}e^2/h$, reminiscent of that reported by Timp *et al.* [17] in a four-terminal measurement. Finally, we note that in the regime where the dips occur, the conductance at 1.5 K is below the average conductance at 50 mK, while in the regime of the periodic conductance peaks at more negative gate voltages the ordering is reversed. As discussed in section 3.5, the dips in the conductance at 50 mK can be explained by resonant reflection in the channel.

The left panel of Fig. 3.8 shows the temperature dependence of one of the peaks in the conductance of channel $D1$ at $B = 6.66$ T. At the lowest temperatures, this was one of the most pronounced peaks present in the conductance trace as a function of gate voltage. The peak height increases with decreasing temperature, and reaches a value of $0.6e^2/h$ at $T = 100$ mK. Note the opposite temperature dependence for channel $U3$ at $B = 0$ given in Fig. 3.4. As discussed in section 3.4.2, the reason for this difference is

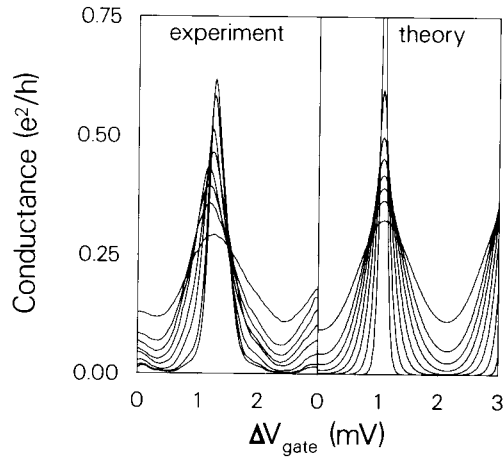


Figure 3.8: Left panel: single conductance peak of channel $D1$ at $B = 6.66$ T. The temperatures are 110, 190, 290, 380, 490, 590, 710, and 950 mK, from highest to lowest peak. Right panel: lineshape calculated from Eq. (2.22) for: $e^2/C = 0.53$ meV, $\Delta E = 0.044$ meV, $\alpha = 0.265$, and $h\Gamma^{l,r} = 0.065$ meV.

that the latter data are in the high-temperature classical regime where $k_B T$ exceeds the average level spacing ΔE of the conductance-limiting segment, whereas the data in Fig. 3.8 are in the low-temperature quantum regime $k_B T \lesssim \Delta E$. The calculated traces in Fig. 3.8, right panel, are discussed in section 3.4.2.

We often have found fine structure developing on the conductance peaks. An example of this behavior is shown in Fig. 3.9, for another peak in the conductance of channel $D1$, at $B = 6.66$ T. For temperatures below 250 mK, the peak is split into a doublet. The amplitudes of both parts increase with decreasing temperature, and become better resolved as well, due to a reduction in width. We have found that conductance peaks which show such fine structure typically are smaller than those that do not (note the difference in vertical scale in Figs. 3.8 and 3.9). As discussed in section 3.4.3, both the occurrence of fine structure, and the fact that it is predominantly associated with the smaller peaks, may be understood from the presence of multiple segments in the wire.

The conductance oscillations in the channels without intentional Be

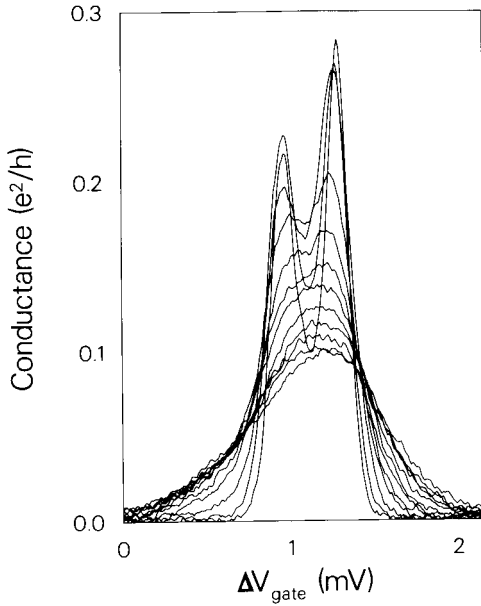


Figure 3.9: Single conductance peak of channel $D1$ at $B = 6.66$ T. The temperatures are 65, 140, 195, 245, 350, 485, 680, and 845 mK, from highest to lowest peak.

doping are enhanced by a magnetic field similar, to those observed in the Be-doped samples. We give one example, in Fig. 3.10, for channel $U2$ at $T = 1$ K. Only the trace at $B = 3.78$ T shows rapid periodic oscillations.

3.3.3 Magnetoconductance

Whereas the conductance as a function of gate voltage at fixed magnetic field shows periodic oscillations, no such behavior is observed when the magnetic field is varied and the gate voltage is fixed. As shown in Fig. 3.11, the duality between variations in the gate voltage and magnetic field, applicable to the quantum ballistic, adiabatic and diffusive transport regimes [16] breaks down in our samples. We have studied the four-terminal longitudinal magnetoconductance G_L , using channel $D3$, which has the miniature Hall-bar geometry shown in the inset of Fig. 3.11(b) [see also Fig. 3.1(b)]. As shown in Fig. 3.11(a), the four-terminal magnetoconductance at $T = 50$

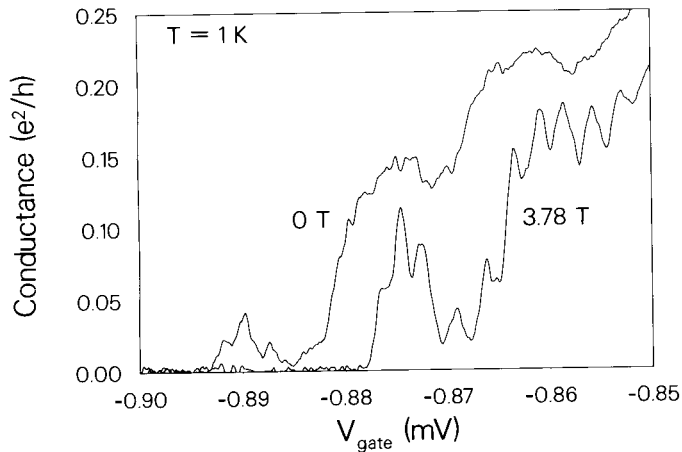


Figure 3.10: Two-terminal conductance versus gate voltage of channel U2 at $T = 1$ K, and $B = 0$ and 3.78 T.

mK exhibits essentially *random* structure, whereas in Fig. 3.11(b) it can be seen that the conductance as a function of gate voltage for the same channel exhibits periodic oscillations. [The two-terminal magnetoconductance does not exhibit periodic oscillations as a function of the magnetic field either (not shown).] The extreme sensitivity of the magnetoconductance to a small change in the gate voltage is not surprising, since the measurements were made for gate voltages in the regime where the conductance oscillates periodically as a function of V_{gate} [at least for the top two panels in Fig. 3.11(a), cf. Fig. 3.11(b)]. Previously, we have interpreted the absence of periodic magnetoconductance oscillations as a manifestation of the Coulomb blockade of the Aharonov-Bohm effect [18, 19]. As we will discuss in section 3.5, reinterpretation may be necessary.

In the bottom panel of Fig. 3.11(a) a magnetoconductance trace obtained at a gate voltage just outside the regime of periodic conductance oscillations is shown (note the difference in vertical scale). The large peaks in the conductance near 2.5 and 6 T in this trace are resistance minima, reminiscent of Shubnikov-de Haas oscillations in the quantum Hall effect regime. The latter can be identified quite well as the channel width is increased further, in which case the resistance at the minima approaches

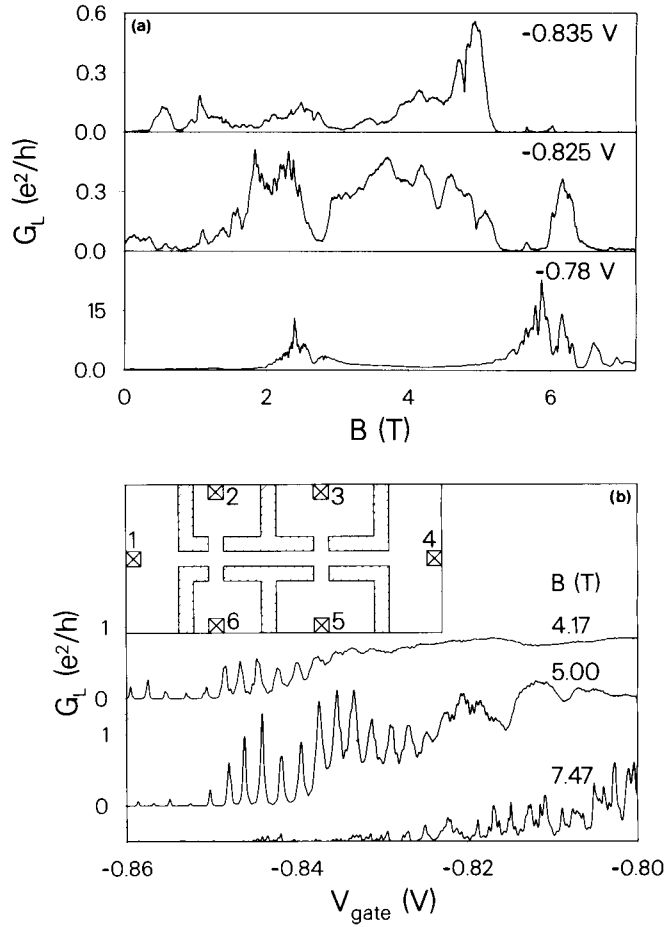


Figure 3.11: (a) Four-terminal longitudinal conductance G_L of channel $D3$ at $T = 50\text{ mK}$ as a function of magnetic field, for three values of the gate voltage. (b) G_L as a function of gate voltage for channel $D3$ at $T = 50\text{ mK}$, for three values of the magnetic field. Inset: schematic top view of the miniature Hall-bar geometry. Contacts 1 and 4 were used as current contacts, and the voltage was measured across contacts 2 and 3.

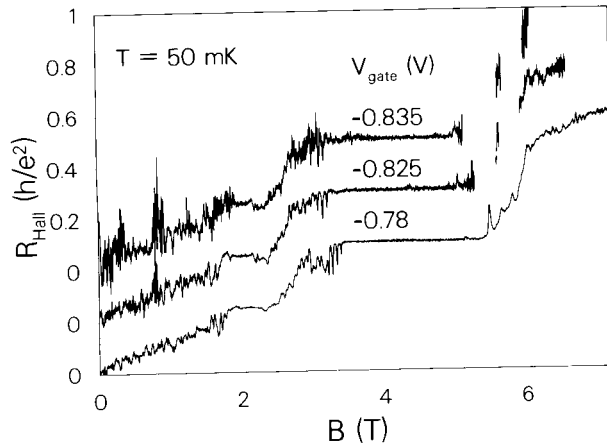


Figure 3.12: Hall resistance of channel $D3$ at $T=50$ mK, for three values of the gate voltage. The Hall resistance cannot be measured when the conductance of the channel is reduced to zero, hence the interruptions in the traces around 6 T. The small channel conductance is also responsible for the poor signal-to-noise ratio of these experimental traces. Contacts 1 and 4 were used as current contacts, and the Hall voltage was measured across contacts 3 and 5 [see inset Fig. 3.11(b)].

zero, and G_L acquires very large values. From a set of measurements of the Shubnikov-de Haas oscillations at several values of the gate voltage, we obtained by extrapolation a value of $n_s \sim 1.5 \times 10^{11} \text{ cm}^{-2}$ for the density in the channel in the regime of periodic conductance oscillations.

3.3.4 Hall resistance

The Hall resistance can be measured within the narrow channel using the miniature Hall-bar geometry of Fig. 3.1(b). The results for channel $D3$ are shown in Fig. 3.12, for the same set of gate voltages as in Fig. 3.11. We find no qualitative differences in traces of the Hall resistance versus magnetic field in the regime of periodic conductance oscillations and traces obtained outside this regime. The Hall resistance cannot be measured in ranges of the magnetic field where the conductance is close to zero (cf. Fig. 3.11). This is the reason for the missing parts in the traces at $V_{\text{gate}} = -0.825$ and -0.835 V in Fig. 3.12.

In all traces in Fig. 3.12, the quantum Hall plateau at $2e^2/h$ can be recognized easily, but the plateau at $4e^2/h$ is less pronounced. (The spin-split plateaus at odd multiples of e^2/h are not resolved in the narrow channels.) In between the plateaus, quasiperiodic oscillations as a function of magnetic field are found (see, for example, near 3 T in the trace at $V_{\text{gate}} = -0.78$ V). We attribute these to an Aharonov-Bohm effect involving resonant reflection, with a mechanism similar to that described in section 3.5 for the dips in the conductance plateau in the trace in Fig. 3.7. Below 2 T the Hall resistance shows random oscillations. For $V_{\text{gate}} = -0.825$ and -0.835 V, these are time dependent and not reproducible (the signal-to-noise ratio in this regime is poor, because of the low conductance of the narrow channel). To the extent that the fluctuations are reproducible, we attribute these to quantum interference effects familiar from other studies of narrow channels [20].

We also have tried to measure the Hall resistance (at fixed magnetic field) as a function of gate voltage. In the regime of periodic conductance oscillations this is very difficult for the same reason mentioned above: The Hall resistance cannot be measured when the two-terminal conductance is reduced to zero. It can therefore not be established experimentally whether periodic oscillations occur in the Hall resistance. One could argue that this question is meaningless.

3.4 Coulomb-blockade oscillations

In this section we analyze those features of our experimental results that may be considered to be generic, rather than sample specific. The most conspicuous are the conductance oscillations periodic in the gate voltage. The value of the period, its insensitivity to a strong magnetic field, and the absence of spin-splitting, can all be understood on the basis of Eq. (2.12) [6] expressing the condition for a conductance peak at $T = 0$, see section 3.4.1. The temperature dependence of the amplitude and width of the oscillations is analyzed in terms of the results of a kinetic theory for the conductance of a quantum dot in the regime of comparable charging energy and level spacing, summarized in chapter 2 (section 2.3) [7]. This is the subject of section 3.4.2. In these two subsections we assume that the Coulomb-blockade oscillations arise from a single conductance-limiting segment. In section 3.4.3 we briefly consider the effects of multiple segments in series.

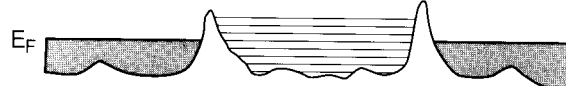


Figure 3.13: Schematic conductance band diagram of a disordered quantum wire containing a conductance-limiting segment (a quantum dot with a discrete energy spectrum). The leads are thought to have a continuous energy spectrum.

3.4.1 Periodicity

We model the conductance-limiting segment in the narrow channel as a naturally formed quantum dot, which is weakly coupled by tunnel barriers to two leads, see Fig. 3.13. The tunnel barriers are thought to be due to two large fluctuations in the potential confining the 2DEG to a quantum wire. As discussed in section 3.1, these fluctuations most likely result from variations in the distribution of the ionized donors in the doped $\text{Al}_x\text{Ga}_{1-x}\text{As}$ layer, and from background impurities. This model is justified by the fact that no correlation is found between the periodicity of the oscillations and the channel length, and that the conductance oscillations are observed when the width is reduced below $W \sim 0.1 \mu\text{m}$, in which case the electron density is $1.5 \times 10^{11} \text{ cm}^{-2}$. A $3 \mu\text{m}$ long channel then contains some 450 electrons.

We analyze this system in terms of the mutual capacitance C_{dot} of dot and leads, and the mutual capacitance C_{gate} of dot and gates, as discussed in chapter 2 (see Fig. 2.5). To calculate C_{dot} and C_{gate} is a rather complicated three-dimensional electrostatic problem, hampered further by the uncertain dimensions of the conductance-limiting segment. Experimentally, a typical spacing of the conductance peaks is $\Delta V_{\text{gate}} \sim 2.3 \text{ mV}$, so that from Eq. (2.16) we estimate $C_{\text{gate}} \sim 0.7 \times 10^{-16} \text{ F}$, ignoring the contribution of the finite level spacing to the period in gate voltage (ΔE is typically much smaller than e^2/C_{gate} , see below). The length L of the segment may be estimated from the gate voltage range between channel definition and pinch-off, $\delta V_{\text{gate}} \sim e n_s W_{\text{lith}} L / C_{\text{gate}}$, where $n_s = 2.9 \times 10^{11} \text{ cm}^{-2}$ is the electron density in the channel at definition. From the above estimate of C_{gate} and using $\delta V_{\text{gate}} \sim 1 \text{ V}$, we find $L \sim 0.3 \mu\text{m}$. The resulting value for the capacitance per unit length C_{gate}/L is consistent with what one would expect for the capacitance per unit length of a wire of diameter W running in the middle of a gap of width W_{lith} in a metallic plane [21] (the thick-

ness of the GaAs and $\text{Al}_x\text{Ga}_{1-x}\text{As}$ layers between gate and 2DEG is small compared to W_{lith}): $C_{\text{gate}}/L \sim 4\pi\epsilon/2\text{arccosh}(W_{\text{lith}}/W) \sim 3 \times 10^{-10} \text{ F/m}$.

The level spacing in the segment is estimated at $\Delta E \sim 2\pi\hbar^2/mLW \sim 0.2 \text{ meV}$ (for a twofold spin degeneracy). Since each oscillation corresponds to the addition of a single electron to the dot, the maximum number of oscillations following from ΔE and the Fermi energy $E_F \sim 5 \text{ meV}$ when the dot is formed is given by $2E_F/\Delta E \sim 50$, consistent with the observations. From the fact that the oscillations are still observable at $T = 1.5 \text{ K}$, albeit with considerable thermal smearing, we deduce that in our experiments $e^2/C + \Delta E \sim 1 \text{ meV}$. Thus, $C \sim 2 \times 10^{-16} \text{ F}$, $C_{\text{dot}} = C - C_{\text{gate}} \sim 1.3 \times 10^{-16} \text{ F}$, and $\alpha \equiv C_{\text{gate}}/C \sim 0.35$. The mutual capacitance of dot and leads (C_{dot}) may be approximated by the self capacitance of the dot, which should be comparable to that of a two-dimensional circular disk [21] of diameter L (which is the largest linear dimension of the elongated conductance-limiting segment), $C_{\text{dot}} \sim 4\epsilon L \sim 1.4 \times 10^{-16} \text{ F}$, consistent with the above estimate.

We conclude that the periodicity of the conductance oscillations in our experiment is explained consistently by the theory for Coulomb-blockade oscillations, in a regime where e^2/C is larger than the bare level spacing ΔE by about a factor of four. According to Eq. (2.17), the period is governed by e/C_{gate} , which exceeds $\Delta E/e$ by an order of magnitude, thus providing part of the explanation of the regularity of the oscillations. A finite temperature $k_B T > \Delta E$ further regulates the spacing of the oscillations, see section 3.4.3.

As an alternative explanation of the conductance oscillations, resonant tunneling of noninteracting electrons has been proposed [12, 13]. As mentioned in section 3.1, we have two arguments for rejecting this explanation. Firstly [18], the measured activation energy of the conductance minima would imply a bare level spacing $\Delta E \sim 1 \text{ meV}$ if charging effects would be absent. Since the Fermi energy E_F is 5 meV or less, such a large level spacing would restrict the possible total number of oscillations in a gate voltage scan to a maximum of $2E_F/\Delta E \sim 10$, considerably less than the number observed experimentally [1, 18]. Secondly, one would expect a spin splitting of the oscillations in a strong magnetic field, which is not observed [9].

3.4.2 Amplitude and lineshape

In Fig. 3.4 we compare a calculation based on Eq. (2.22) with experimental traces for channel $D1$, discussed in section 3.3.1. To obtain good agree-

ment we assume that the tunnel rates for successive spin-degenerate levels increase linearly as $\Gamma_i^l = \Gamma_i^r = 0.027i\Delta E/h$ ($i = 1, 2, \dots$), where $\Delta E = 0.1$ meV is the spacing of these levels. Both the increase of the tunnel rates with energy and the low number of electrons assumed to be present in the dot are necessary for obtaining a good agreement with the experiment. (In the calculation, the first conductance peak corresponds to an occupation of the dot by zero or one electron.) The capacitances were chosen so that $e^2/C = 0.6$ meV and $\alpha = 0.265$. These values are consistent with the estimates given above. The Fermi energy in the leads was assumed to increase with gate voltage such that it is on average equal to the energy of the highest occupied level in the dot at $T = 0$ (cf. section 2.2). The data in Fig. 3.4 are in the classical regime ($k_B T > \Delta E$), where the peak height is roughly independent of temperature, whereas the width of the peaks increases with T . This is reproduced by our calculations.

On lowering the temperature, we enter the resonant tunneling regime $k_B T < \Delta E$. As long as $k_B T > h\Gamma$, the width of the peaks is proportional to T and the peak height is proportional to $1/T$. The peak height thus increases on lowering the temperature, up to a value of order e^2/h , reached when $k_B T$ is of order $h\Gamma$. A theory for the regime $k_B T < h\Gamma$ is not available presently, but we surmise that the maximum peak height is e^2/h , for the case of equal tunnel barriers. This is consistent with our experimental observations, which do not show conductance peaks exceeding this value. [The largest conductance peaks found experimentally approach e^2/h , see Fig. 3.6(c) (channel D1, at 5 T)].

To test to what extent Eq. (2.22) can describe our experimental results in the quantum regime $k_B T \lesssim \Delta E$, we have calculated the peaks shown in the right panel of Fig. 3.8. (The data in the left panel of Fig. 3.8 was obtained in the presence of a magnetic field of 6.66 T, so that we assume no spin degeneracy in the calculation.) Equation (2.22) reproduces the temperature dependence of the peak height and width quite well, for temperatures between 190 and 950 mK. The parameter values used are $e^2/C = 0.53$ meV, $\Delta E = 0.088$ meV, $\alpha = 0.265$, and $h\Gamma^l = h\Gamma^r = 0.065$ meV, which are consistent with the values used for the calculations shown in the bottom panel of Fig. 3.4. The Zeeman spin-splitting energy is not known, due to uncertainties in the g factor, but is taken equal to $\frac{1}{2}\Delta E$ in the calculations. The resulting set of equidistant nondegenerate levels is spaced at 0.044 meV. We note, however, that the parameter values used

imply that $k_B T < h\Gamma$ for the calculated peaks in Fig. 3.4, so that Eq. (2.22) is strictly not valid, and instead a theory should be used which takes the finite broadening of the levels in the quantum dot into account.

The data obtained in the absence of a magnetic field at very low temperatures [see Figs. 3.2 and 3.6(c)] is probably in the quantum regime as well. An analysis of these data is hampered by the presence of multiple segments in the wire, as discussed in section 3.4.3. A strong magnetic field reduces the backscattering probability in the channel, which may explain why the conductance at low T appears to be less affected by the presence of multiple segments. The qualitative agreement between theory and experiment in Figs. 3.4 and 3.8, for a reasonably consistent set of parameter values, and over a wide range of temperatures, supports our interpretation of the conductance oscillations periodic in the gate voltage as Coulomb-blockade oscillations, in the regime where $k_B T < e^2/C$ and $k_B T = \mathcal{O}(\Delta E)$.

3.4.3 Multiple segments

In an attempt to investigate the effects of multiple segments in the wire, we consider the conductance of two decoupled quantum dots of different size in series. This simple model can illustrate some aspects of the experimental data. Among these are the observation of regular oscillations at relatively high temperatures, which are replaced by irregularly spaced peaks at millikelvin temperatures, and the splitting exhibited by some of the regular peaks on decreasing the temperature.

The calculations proceed as follows: Using Eq. (2.22) we calculate the conductances G_1 and G_2 of the two dots individually. The resulting conductance of the dots in series is obtained via Ohmic addition ($G^{-1} = G_1^{-1} + G_2^{-1}$), i.e., it is assumed that the dots are separated by a reservoir. The parameter values for the first dot were chosen equal to those used to model the peak in Fig. 3.8: $e^2/C_1 = 0.53$ meV and $\alpha_1 = 0.265$, but with twofold-degenerate levels, randomly spaced within a bandwidth of 25% around the average spacing $\Delta E_1 = 0.088$ meV. The tunnel rates were chosen to vary randomly within a bandwidth of 50% around the average tunnel rates $h\Gamma^l = h\Gamma^r = 0.065$ meV. The parameter values for the second dot were obtained using a scaling argument. It is assumed that the relevant capacitances C and C_{gate} are approximately proportional to the length L of the conductance-limiting segment (see section 3.4.1), while the

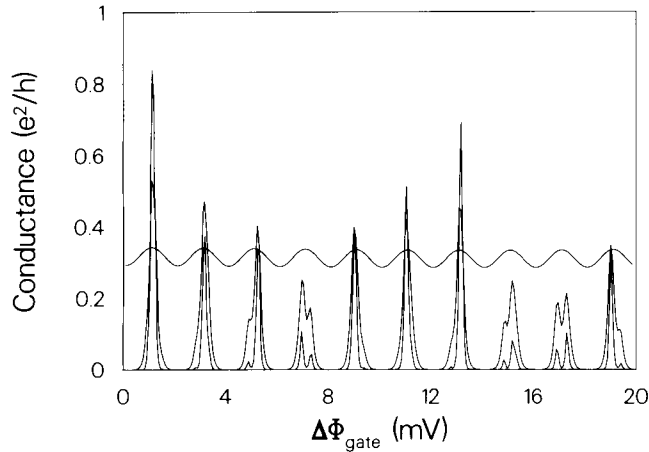


Figure 3.14: Calculations of the conductance oscillations of two quantum dots in series, separated by a reservoir. The temperatures are 1.5 K, 240 mK, and 130 mK. The parameter values are given in the text.

average level spacing $\Delta E \propto 1/L$ and the parameter α is independent of L . The second dot was chosen to be approximately 2.7 times as long as the first dot, and accordingly we have used $e^2/C_2 = 0.097$ meV, $\alpha_2 = 0.273$, $\Delta E_2 = 0.033$ meV, and $h\Gamma^l = h\Gamma^r = 0.065$ meV (the energy levels and tunnel rates were chosen randomly within the same bandwidths as for the first dot). The results of the calculations are shown in Fig. 3.14.

Figure 3.14 illustrates several points. At the relatively high temperature of 1.5 K, the conductance oscillations are very regular. The reason is that at this temperature the oscillations of the second dot are smeared completely, because $e^2/C_1 > k_B T > e^2/C_2$. Additionally, since $k_B T > \Delta E$ the period is determined by an average level spacing and tunnel rate, rather than by a particular level separation and tunnel rate for each individual peak. As the temperature is decreased, the quantum regime $k_B T < \Delta E$ is entered (in particular for the first dot), and the oscillations of the second dot become important since $k_B T < e^2/C_2$. The resulting irregularity in the conductance as a function of gate voltage is apparent from Fig. 3.14. In addition, it shows that at low temperatures a splitting of the peaks can result from differences in period and activation energy of the oscillations

in the two dots. As in the experimental data, peaks exhibiting such a splitting are smaller than peaks that do not split. In contrast to the experimental data, however, the split peaks decrease rather than increase (see Fig. 3.9) with decreasing temperature. This may be due to the intrinsic broadening of the transmission resonances through the dot, which becomes important for $k_B T < h\Gamma$ and which is not accounted for by the calculations (cf. section 3.4.2).

An alternative model of a large and small quantum dot which are directly coupled (not via a reservoir, as in our calculation), has recently been studied by Ruzin *et al.* [22]. They find a crossover from periodic Coulomb-blockade oscillations to aperiodic fluctuations at low temperatures, when $k_B T$ is smaller than the level spacing in both quantum dots. A conductance peak then requires that the levels in both the quantum dots line up, which occurs at random.

3.5 Discussion

In this section we discuss those aspects of the data that are not so well understood, as well as the connection with other work. Our disordered quantum wires exhibit *periodic* conductance oscillations as a function of gate voltage. This effect has also been observed in electron and hole gases in Si (Refs. [1], [9], and [23]) and in the electron gas in GaAs [18, 24]. In contrast, earlier work by Fowler *et al.* [25] and by Kwasnick *et al.* [26] on narrow inversion and accumulation layers in Si has revealed sharp but *aperiodic* conductance peaks. Structure reminiscent of their results is visible in some of our samples at low temperature (50 mK) in zero or very strong magnetic fields [cf. Figs. 3.2 (lower left panel) and 3.6(c) (traces for $B = 0$ and 7.59 T)]. How can these observations be reconciled? We surmise that the explanation is to be found in differences in strength and spatial scale of the potential fluctuations in the wires. Coulomb-blockade oscillations require two large potential spikes, which delimit a conductance-limiting segment in the quantum wire [Fig. 3.13] containing a large number of states. The random conductance fluctuations seen previously [25, 26] are thought instead to be due to variable range hopping between individual localized states, distributed randomly along the length of the channel [27, 28, 29]. As proposed by Ruzin *et al.* [22] the periodic Coulomb-blockade oscillations of multiple segments in series can transform into sharp aperiodic fluctuations at low

temperatures. This may explain our observation (Fig. 3.2) that periodic oscillations are found at temperatures around 1 K, whereas irregular structure occurs at millikelvin temperatures. On increasing the Fermi energy, a transition to the diffusive transport regime occurs eventually, regardless of the type of disorder. Then both the Coulomb-blockade oscillations and the random conductance fluctuations due to variable range hopping are replaced by the “universal” conductance fluctuations characteristic of the diffusive transport regime [2, 30, 31].

In very short channels (0.5 μm long and 1 μm wide) Fowler *et al.* [32] have found well-isolated, temperature-independent (below 100 mK) conductance peaks, which they attributed to resonant tunneling. At very low temperatures fine structure was observed, some of which was time dependent. A numerical simulation [33] of the temporal fluctuations in the distribution of electrons among the available sites also showed fine structure if the time scale of the fluctuations is short compared to the measurement time, but large compared to the tunnel time. It is possible that a similar mechanism is responsible for some fine structure on the Coulomb-blockade oscillations in disordered quantum wires as well.

A curious phenomenon that we have found is the effect of a perpendicular magnetic field on the amplitude of the periodic conductance oscillations. The height of the conductance peaks is enhanced for intermediate field strengths ($1 \text{ T} \lesssim B \lesssim 5 \text{ T}$), but decreases again at stronger fields. The largest isolated peaks [found in channel D1 at 5 T, see Fig. 3.6(c)] approach a height of e^2/h , measured two terminally. We have observed a similar enhancement of the amplitude of the Coulomb-blockade oscillations by a magnetic field in a quantum dot [34], see chapter 4. (However, in this case the amplitude increase is predominantly due to a suppression of the conductance in the minima of the oscillations, rather than an increase of the peak height.) In the fractional quantum Hall effect regime, Alphenaar *et al.* [35] have observed an anomalous enhancement of one of the conductance peaks of a quantum wire to approximately e^2/h , exceeding the two-terminal conductance of the wide 2DEG leads at filling factor $\frac{1}{3}$. One explanation for the observed enhancement of the peak height is that the inelastic scattering rate is reduced by a magnetic field. In the low-temperature regime $k_B T \lesssim \hbar\Gamma$ this presumably increases the peak height and decreases the width (see Ref. [7]). In disordered quantum wires the magnetic suppression of backscattering provides another mechanism for an

enhancement of the peak height because of the resulting reduced series resistance in the wire. Finally, the strong magnetic field regime in a wide high-mobility 2DEG is the realm of the fractional quantum Hall effect and the magnetic-field-induced transition to the Wigner crystal. It is possible that the suppression of the Coulomb-blockade oscillations for $B > 6$ T is related in some unknown way to these phenomena.

For noninteracting electrons, one would expect to observe Aharonov-Bohm type oscillations in the conductance of a quantum dot as a function of magnetic field in the quantum Hall effect regime. The reason is that such a dot effectively has a ring geometry if the magnetic length $l_m \equiv (\hbar/eB)^{1/2}$ is much smaller than the dot radius, due to the presence of circulating edge states. The Aharonov-Bohm (AB) effect in such a dot may be interpreted as resonant tunneling through zero-dimensional states [36, 37]. In the absence of Coulomb interaction, the period ΔB of the AB oscillations for a hard-wall dot of area A is $\Delta B = h/eA$ (it may be larger for a soft-wall confining potential [36]). Such oscillations have indeed been observed in large quantum dots [36, 38, 39], but in our experiment at high magnetic fields, no periodic oscillations with the estimated $\Delta B \approx 0.1$ T are found. Previously [18, 19], we have argued that our observations are consistent with the Coulomb blockade of the Aharonov-Bohm effect [6]. Each AB oscillation corresponds to an increase of the number of electrons in the dot by one. One can show from Eq. (2.12) that the period of the AB oscillations is enhanced due to the charging energy, according to [6]

$$\Delta B^* = \Delta B \left(1 + \frac{e^2}{C\Delta E} \right), \quad (3.1)$$

where ΔE is the energy level spacing of the circulating edge states. Meanwhile, it has become clear that this is true only for a single spin-resolved Landau level occupied in the dot. In our high-field experiments, however, it is likely that more than a single Landau level is occupied in the dot. The electron density in the dot is approximately 1.5×10^{11} cm⁻² (estimated from an extrapolation of the periodicity of the Shubnikov-de Haas oscillations, measured at several gate voltages), so that occupation of the dot by only one single spin-resolved Landau level requires $B \gtrsim 6$ T. Therefore, a different explanation must be given for the irregularity of the magnetoconductance at magnetic fields below this value [see Fig. 3.11(a)]. We point

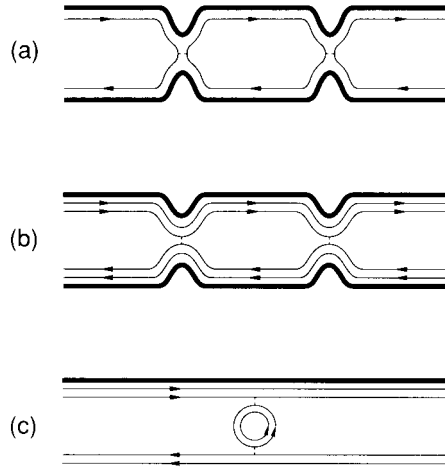


Figure 3.15: Schematic view of the edge channels (thin lines) in the quantum wire, with a conductance-limiting segment (a), and without such a segment (b), (c).

out that such an explanation should take the magnetic-field dependence of the Fermi energy into account, which is difficult to model reliably in a disordered quantum wire, however.

In one of our channels ($D1$, see Fig. 3.7 we have observed a crossover from resonant transmission at $G < e^2/h$ (conductance *peaks*), to resonant reflection at $G > e^2/h$ (conductance *dips*) at $T = 50$ mK. To explain the difference, we show schematically in Fig. 3.15 the boundaries of the quantum wire (thick lines), with the thin lines representing the edge channels which are formed in a strong magnetic field [16]. Electrons can tunnel between the edge channels when they are close together, as indicated by the dashed lines. In Fig. 3.15(a) a conductance-limiting segment is formed because of the presence of two potential barriers or constrictions, and the conductance exhibits periodic Coulomb-blockade oscillations (section 3.4). The temperature scale of these conductance peaks is set by the charging energy, which is relatively large. At less negative gate voltages, the guiding center energy of the edge channels near the Fermi level may exceed the height of the potential barriers. The edge channels are then transmitted adiabatically through the wire [Fig. 3.15(b)]. Backscattering can now occur due to tunneling between edge channels at opposite edges. This

will happen predominantly near the potential barriers (dashed lines). The backscattering can be enhanced resonantly due to constructive interference among these tunneling paths, leading to dips in the conductance. Alternatively, resonant backscattering may occur also due to the presence of a circulating edge state in the center of the quantum wire, associated with a single potential spike [40]. This mechanism is illustrated in Fig. 3.15(c). Experimentally we can not discriminate between the two mechanisms. The strong temperature dependence of the conductance dips in Fig. 3.7 implies a low activation energy, indicating that charging effects do not affect the resonant backscattering strongly. [The occurrence of charging effects in closed-loop edge channels, such as drawn schematically in Fig. 3.15(c), is considered in chapter 4 (section 4.4).]

In summary, we have reported on an experimental study of the periodic conductance oscillations as a function of gate voltage in split-gate disordered quantum wires in the 2DEG in a GaAs–Al_xGa_{1-x}As heterostructure. From the persistence up to a few kelvin of the dominant oscillations, and from the insensitivity of the period to a strong magnetic field, it is concluded that they are Coulomb-blockade oscillations. The appearance of additional periodicities and the onset of irregular conductance fluctuations at very low temperatures in some of the wires is attributed to the presence of multiple segments in these wires. We have compared the temperature dependence of the periodic conductance oscillations to a theory for Coulomb-blockade oscillations in the classical regime $k_B T > \Delta E$ and in the quantum regime $k_B T < \Delta E$. Qualitative agreement with this theory is obtained, using physically reasonable parameter values, although our lowest temperature data appear to be in the intrinsically broadened resonance regime $k_B T < h\Gamma$, for which a theory has not yet been worked out. The effect of a perpendicular magnetic field on the oscillations is to enhance their amplitude at intermediate field strengths (between about 1 and 5 T), but to suppress them at stronger fields. This remains to be understood fully. In contrast to traces of the conductance as a function of gate voltage, magnetoconductance traces at constant gate voltage show no periodic oscillations.

References

- [1] J. H. F. Scott-Thomas, S. B. Field, M. A. Kastner, H. I. Smith, and D. A. Antoniadis, Phys. Rev. Lett. **62**, 583 (1989).
- [2] J. C. Licini, D. J. Bishop, M. A. Kastner, and J. Melngailis, Phys. Rev. Lett. **55**, 2987 (1985); W. J. Skocpol, P. M. Mankiewich, R. E. Howard, L. D. Jackel, D. M. Tennant, and A. D. Stone, *ibid.* **56**, 2865, (1986).
- [3] A. I. Larkin and P. A. Lee, Phys. Rev. B **17**, 1596 (1978).
- [4] P. A. Lee and T. M. Rice, Phys. Rev. B **19**, 3970 (1979).
- [5] H. van Houten and C. W. J. Beenakker, Phys. Rev. Lett. **63**, 1893 (1989).
- [6] C. W. J. Beenakker, H. van Houten, and A. A. M. Staring, Phys. Rev. B **44**, 1657 (1991); in: *Granular Nanoelectronics*, edited by D. K. Ferry (Plenum, New York, 1991).
- [7] C. W. J. Beenakker, Phys. Rev. B **44**, 1646 (1991).
- [8] Y. Meir, N. S. Wingreen, and P. A. Lee, Phys. Rev. Lett. **66**, 3048 (1991).
- [9] S. B. Field, M. A. Kastner, U. Meirav, J. H. F. Scott-Thomas, D. A. Antoniadis, H. I. Smith, and S. J. Wind, Phys. Rev. B **42**, 3523 (1990).
- [10] M. A. Kastner, S. B. Field, U. Meirav, J. H. F. Scott-Thomas, D. A. Antoniadis, and H. I. Smith, Phys. Rev. Lett. **63**, 1894 (1989).
- [11] L. I. Glazman, I. M. Ruzin, and B. I. Shklovskii, Phys. Rev. B **45**, 8454 (1992); D. V. Averin and K. K. Likharev, in: *Nanostructures and Mesoscopic Systems*, edited by W. P. Kirk and M. A. Reed (Academic, Boston, 1992).
- [12] F. M. de Aguiar and D. A. Wharam, Phys. Rev. B **43**, 9984 (1991).
- [13] J. Mašek and B. Kramer (unpublished).
- [14] S. E. Laux, D. J. Frank, and F. Stern, Surf. Sci. **196**, 101 (1988).

- [15] J. A. Nixon and J. H. Davies, Phys. Rev. B **41**, 7929 (1990).
- [16] For a review of theoretical and experimental aspects of quantum transport in semiconductor nanostructures, see C. W. J. Beenakker and H. van Houten, Solid State Physics **44**, 1.
- [17] G. Timp, R. Behringer, J. E. Cunningham, and R. E. Howard, Phys. Rev. Lett. **63**, 2268 (1989).
- [18] A. A. M. Staring, H. van Houten, C. W. J. Beenakker, and C. T. Foxon, in: *High Magnetic Fields in Semiconductor Physics III*, edited by G. Landwehr (Springer, Berlin, 1992).
- [19] A. A .M. Staring, H. van Houten, C. W.J . Beenakker, and C. T. Foxon, Phys. Rev. B **45**, 9222 (1992).
- [20] A. M. Chang, G. Timp, T. Y. Chang, J. E. Cunningham, P. M. Mankiewich, R. E. Behringer, and R. E. Howard, Solid State Commun. **67**, 769 (1988).
- [21] L. D. Landau and E. M. Lifshitz, *Electrodynamics of Continuous Media* (Pergamon, New York, 1960).
- [22] I. M. Ruzin, V. Chandrasekhar, E. I. Levin, and L. I. Glazman, Phys. Rev. B **45**, 13469 (1992).
- [23] C. de Graaf, J. Caro, S. Radelaar, V. Lauer, and K. Heyers, Phys. Rev. B **44**, 9072 (1991).
- [24] U. Meirav, M. A. Kastner, M. Heiblum, and S. J. Wind, Phys. Rev. B **40**, 5871 (1989).
- [25] A. B. Fowler, A. Hartstein, and R. A. Webb, Phys. Rev. Lett. **48**, 196 (1982); R. A. Webb, A. Hartstein, J. J. Wainer, and A. B. Fowler, *ibid.* **54**, 1577 (1985).
- [26] R. F. Kwasnick, M. A. Kastner, J. Melngailis, and P. A. Lee, Phys. Rev. Lett. **52**, 224 (1984); M. A. Kastner, R. F. Kwasnick, J. C. Licini, and D. J. Bishop, Phys. Rev. B **36**, 8015 (1987).
- [27] P. A. Lee, Phys. Rev. Lett. **53**, 2042 (1984).

- [28] R. K. Kalia, W. Xue, and P. A. Lee, Phys. Rev. Lett. **57**, 1615 (1986).
- [29] C. J. Adkins, in: *Hopping and Related Phenomena*, edited by H. Fritzsche and M. Pollak (World Scientific, New Jersey, 1990).
- [30] B. L. Al'tshuler, Pis'ma Zh. Eksp. Teor. Fiz. **41**, 530 (1985) [JETP Lett. **41**, 648 (1985)].
- [31] P. A. Lee and A. D. Stone, Phys. Rev. Lett. **55**, 1622 (1985).
- [32] A. B. Fowler, G. L. Timp, J. J. Wainer, and R. A. Webb, Phys. Rev. Lett. **57**, 138 (1986); A. B. Fowler, J. J. Wainer, and R. A. Webb, IBM J. Res. Dev. **32**, 372 (1988).
- [33] M. Green and M. Pollak, in: *Hopping and Related Phenomena*, edited by H. Fritzsche and M. Pollak (World Scientific, New Jersey, 1990).
- [34] A. A. M. Staring, J. G. Williamson, H. van Houten, C. W. J. Beenakker, L. P. Kouwenhoven, and C. T. Foxon, Physica B **175**, 226 (1991).
- [35] B. W. Alphenaar, J. G. Williamson, H. van Houten, C. W. J. Beenakker, and C. T. Foxon, Phys. Rev. B **45**, 3890 (1992).
- [36] B. J. van Wees, L. P. Kouwenhoven, C. J. P. M. Harmans, J. G. Williamson, C. E. Timmering, M. E. I. Broekaart, C. T. Foxon, and J. J. Harris, Phys. Rev. Lett. **62**, 2523 (1989).
- [37] U. Sivan, Y. Imry, and C. Hartzstein, Phys. Rev. B **39**, 1242 (1989).
- [38] R. J. Brown, C. G. Smith, M. Pepper, M. J. Kelly, R. Newbury, H. Ahmed, D. G. Hasko, J. E. F. Frost, D. C. Peacock, D. A. Ritchie, and G. A. C. Jones, J. Phys. Condens. Matter **1**, 6291 (1989).
- [39] D. A. Wharam, M. Pepper, R. Newbury, H. Ahmed, D. G. Hasko, D. C. Peacock, J. E. F. Frost, D. A. Ritchie, and G. A. C. Jones, J. Phys. Condens. Matter **1**, 3369 (1989).
- [40] J. K. Jain, Phys. Rev. Lett. **60**, 2074 (1988).

Chapter 4

Coulomb-blockade oscillations in quantum dots

4.1 Introduction

In semiconductor nanostructures, single-electron tunneling was first discovered in the conductance of disordered quantum wires [1, 2]. As both the width and electron density are decreased, a small number of large fluctuations in the electrostatic potential may lead to the formation of tunnel barriers in the wire. If only two such potential fluctuations are dominant, a quantum dot coupled to two narrow leads is naturally formed. As discussed in chapter 3, the conductance of the wire then exhibits Coulomb-blockade oscillations. Greater experimental flexibility is offered by an artificially defined quantum dot, since separate gates can be used to independently control the tunnel barriers and the number of electrons confined in the dot. Such a system is ideally suited for the study of the interplay of charge quantization (leading to the Coulomb blockade of tunneling), size quantization (leading to a discrete energy spectrum), and magnetic quantization (leading to the formation of Landau levels) [3, 4, 5, 6, 7, 8, 9, 10, 11, 12].

In this chapter we describe our experiments on the Coulomb-blockade oscillations in a quantum dot. After a brief introduction, given in the remainder of this section, we discuss the temperature dependence of the Coulomb-blockade oscillations in section 4.2. In sections 4.3 and 4.4 we study the effect of a quantizing magnetic field on the Coulomb-blockade

oscillations. We find that the Landau levels which are then formed lead to a *periodic* envelope [11] (section 4.3), and to the occurrence of Coulomb-blockade oscillations even in the presence of extended edge channels through the dot [12] (section 4.4). Finally, in section 4.5 we report the observation of Coulomb-blockade oscillations in the *thermopower* of a quantum dot [13].

In Fig. 4.1(a) a scanning-electron micrograph is shown of the first quantum dot that we have studied. It is based on a GaAs–Al_xGa_{1-x}As heterostructure containing a 2DEG with sheet electron density $n_s = 2 \times 10^{11}$ cm⁻² and mobility $\mu = 2 \times 10^6$ cm²/Vs, at low temperatures. The quantum dot is defined by means of electrostatic depletion of the 2DEG using three pairs of gates, as shown schematically in Fig. 4.1(b). Two adjustable tunnel barriers are formed by opposite quantum point-contacts (of 0.3 μm lithographic width and 0.7 μm separation) defined by gates (B,C) and (E,F). The number of electrons confined in the quantum dot can be controlled by two additional gates (A,D) (0.9 μm apart). The gaps between the point-contact gates and the control gates are approximately 0.2 μm wide, so that the quantum dot is formed well before the point contacts are pinched off. The diagonal measurement configuration shown in Fig. 4.1(b) yields an effective two-terminal conductance, even if a magnetic field is applied [14].

In Fig. 4.2 we show results of the Coulomb-blockade oscillations as a function of the voltage applied to the control gates (A,D), at $B = 0$ and $B = 3.75$ T perpendicular to the 2DEG. The point contacts were adjusted to the tunneling regime ($G \approx \frac{1}{2}e^2/h$ at $B = 0$). In the absence of a magnetic field, no oscillations were observed if either or both of the point contacts were set to a conductance above $2e^2/h$, in agreement with Ref. [15]. Both traces show a large number of oscillations, with each conductance peak corresponding to the electrostatic depopulation of the dot by a single electron. We observe a much larger number of oscillations in a quantum dot than in a disordered quantum wire. The reason is that a quantum dot typically contains a few hundred electrons, whereas a typical wire segment contains only about 50 electrons (chapter 3, section 3.4.1). The period of the oscillations increases slowly with decreasing gate voltage (from 2.8 mV near -0.4 V to 3.4 mV near -0.7 V), presumably because the size of the quantum dot is decreased (thereby decreasing the mutual capacitance of quantum dot and control gates). Finally, the oscillations have an amplitude of about $0.2e^2/h$ (at $B = 0$), and are superimposed on a background conductance,

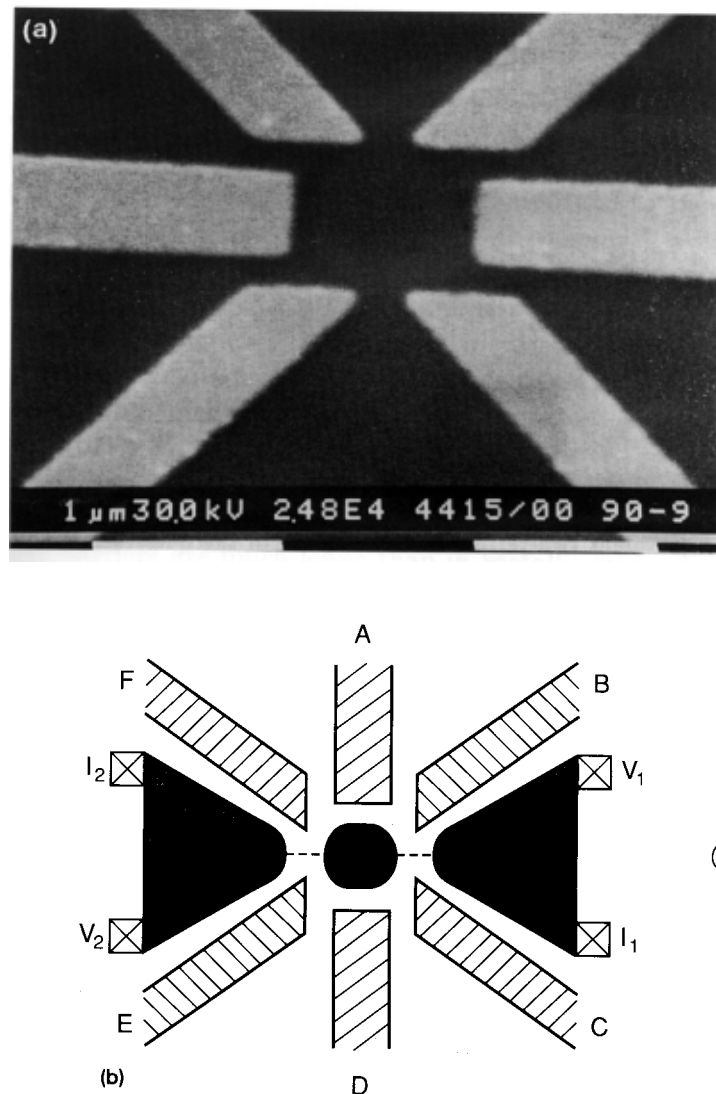


Figure 4.1: (a) Scanning-electron micrograph of the quantum dot. (b) Schematic top-view of the quantum dot. Gates (B,C) and (E,F) define tunnel barriers of adjustable transparency. Gates (A,D) control the number of electrons confined in the dot. The current contacts are labelled I_1 , I_2 , the voltage contacts V_1 , V_2 .

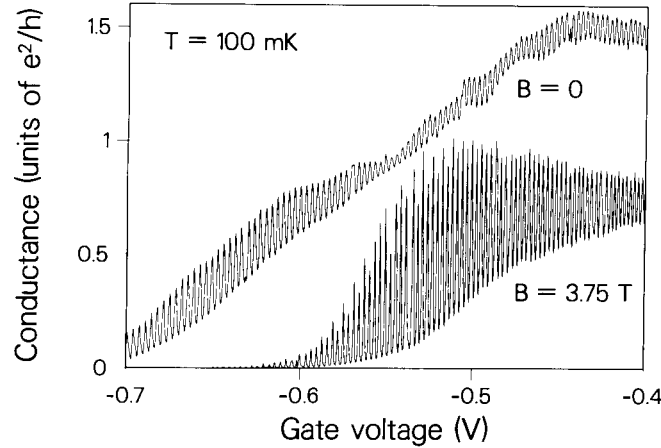


Figure 4.2: Equivalent two-terminal conductance of the quantum dot versus voltage on the control gates (A,D) (applied relative to one of the current contacts). The voltages on the point-contact gates (B,C) and (E,F) were kept fixed, at a value such that the zero-field conductance of the individual point contacts was approximately $\frac{1}{2}e^2/h$.

which increases slowly with gate voltage.

Whereas a magnetic field has almost no effect on the period, as is characteristic of Coulomb-blockade oscillations, its effect on the amplitude is quite pronounced. At $B = 3.75$ T the peak-to-valley amplitude is enhanced to approach e^2/h near a gate voltage of -0.52 V, while the background conductance is reduced in such a way that the conductance remains below e^2/h in the entire trace. We note that such effects of the magnetic field on the amplitude are not observed in metallic systems, where the Coulomb-blockade oscillations are in the classical regime. The gate voltage at which the oscillations disappear, and the conductance vanishes, increases with increasing magnetic field [10]. We attribute this to a magnetic enhancement of the effective tunnel-barrier height in the point contacts. In addition, an apparent doublet structure consisting of alternating high and low peaks is seen in a small voltage interval. Similar structure has been observed also in disordered quantum wires, see e.g. Fig. 3.5. At lower magnetic fields a nicely periodic modulation with larger period is found, which increases with decreasing magnetic field [10]. We will discuss the origin of this surprising

effect, which has been observed most of our quantum dots, in more detail in section 4.3.

The peak-to-valley amplitude does not exceed e^2/h , and in a magnetic field typically exhibits a maximum for intermediate gate voltages. We attribute the gate-voltage dependence of the amplitude to the effect of the control gates (A,D) on the transparency of the tunnel barriers. At more negative gate voltages, the tunnel barriers in the point contacts become less transparent, reducing the peak height. At less negative gate voltages, the tunnel barriers become more transparent, increasing quantum fluctuations of the charge in the quantum dot. This leads to an increased background conductance, and to conductance maxima exceeding e^2/h in the zero-field trace. It is likely that this is due to virtual tunneling processes [16, 17], known to be important in metals if the conductance of the individual barriers is of the order of e^2/h . In semiconductor nanostructures, in which the tunnel barriers are much lower than in metallic systems, a dynamical treatment is probably required since the field across the barrier changes during the tunnel process [18]. Such a treatment is not yet available.

4.2 Temperature dependence

We have studied the temperature dependence of the Coulomb-blockade oscillations using a quantum dot of the design shown in Fig. 4.3. Four gates are used to define the dot in the underlying 2DEG, which has an electron density $n_s = 3.7 \times 10^{11} \text{ cm}^{-2}$ and a mobility $\mu \approx 10^6 \text{ cm}^2/\text{Vs}$. The tunnel barriers are adjusted to a conductance of approximately $\frac{1}{2}e^2/h$, since that value yielded the best signal-to-noise ratio in our experimental set-up. In addition, this is a regime that so far has been relatively unexplored. Two-terminal conductance measurements (using contacts 1 and 2) are made as a function of the voltage applied to gate C.

In Fig. 4.4 the Coulomb-blockade oscillations are shown over a wide gate-voltage range at $B = 0$. At gate voltages close to zero, the electron gas underneath gate C is not depleted fully, and the quantum dot is not yet formed. In this regime, which extends down to approximately -0.3 V , irregular oscillatory structure is observed in the conductance. We attribute this structure to Fabry-Perot-type transmission resonances in the cavity of the partially defined dot, similar to those observed by Smith *et al.* [19] (see also Ref. [20]). The transition to Coulomb-blockade oscillations at

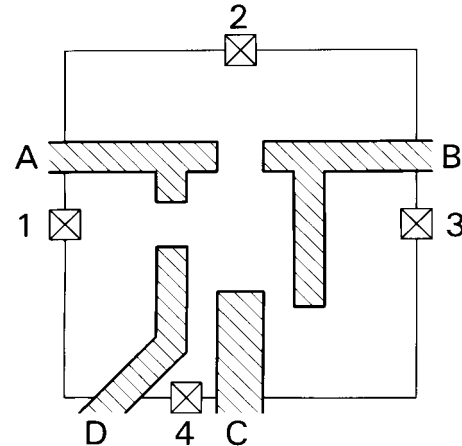


Figure 4.3: Schematic top-view of a $0.7 \times 0.8 \mu\text{m}^2$ quantum dot. Gates A, B, and D (hatched) define individually adjustable tunnel barriers, and gate C controls the electrostatic potential of the dot; the gaps between gates B and C, and between gates C and D, are pinched off in the experiment.

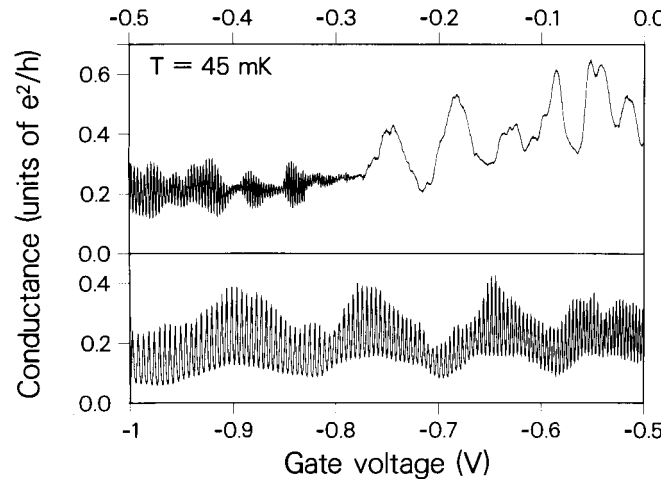


Figure 4.4: Two-terminal conductance of the quantum dot versus voltage applied to gate C. The tunnel barriers are adjusted to a conductance of approximately $\frac{1}{2}e^2/h$.

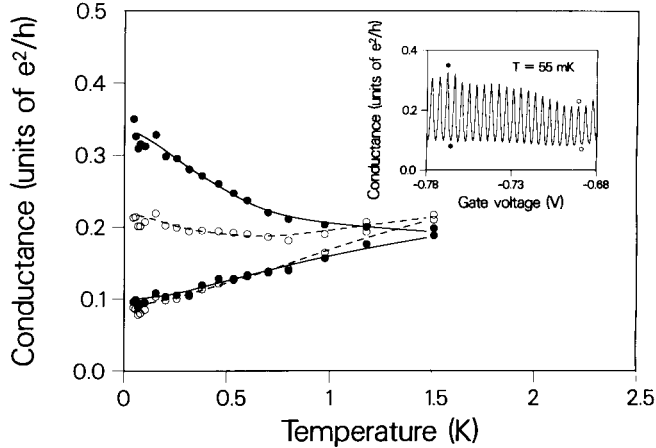


Figure 4.5: Temperature dependence of the Coulomb-blockade oscillations for two peaks and two valleys, as indicated in the inset. The solid and dashed lines guide the eye.

more negative gate voltages is quite abrupt, and presumably occurs as the electron gas underneath gate C (and underneath the gaps between gates B and C, and between gates C and D) is depleted fully. This is supported by an estimate of the depletion voltage using the capacitor formula (1.1), which yields -0.3 V [the distance between 2DEG and gate is $d = 80 \text{ nm}$, $\epsilon_r = 13$ for GaAs, and assuming an electron gas density near the dot that is about 25% lower than in the wide 2DEG regions, due to fringing electric fields of gates A, B, and D (see section 4.3)]. In the conductance trace shown, over 200 peaks are counted (and thus over 200 electrons are depopulated from the dot), which is a sizeable fraction of the number of electrons initially confined to the dot. (We estimate that the dot initially contains about 600 electrons, assuming a quantum dot of radius $d = 0.5 \mu\text{m}$ with an electron density that is approximately 25% lower than that of the 2DEG.)

In Fig. 4.5 the temperature dependence of the Coulomb-blockade oscillations is plotted for two peaks and two valleys, as indicated in the inset. The amplitude of the Coulomb-blockade oscillations exhibits irregular variations as a function of gate voltage (see also Fig. 4.4, measured using slightly different gate voltage values). The open and closed circles give the conductance of a peak and an adjacent valley where the amplitude

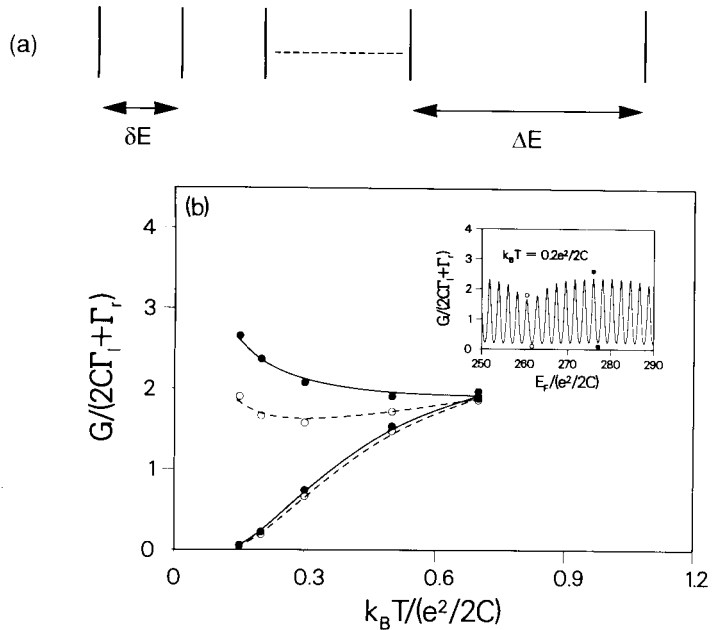


Figure 4.6: Model spectrum (a) and the associated temperature dependence of the Coulomb-blockade oscillations for two peaks and two valleys (b), as indicated in the inset. The calculations are made from Eq. (2.22), with 15 levels spaced at $\delta E = 0.075e^2/C$ per group, gaps of $\Delta E = 0.3e^2/C$, and level-independent tunnel rates.

is at a minimum and at a maximum of these variations. Whereas the large-amplitude conductance peaks increase with decreasing temperature, characteristic of resonant tunneling, the height of the small-amplitude conductance peaks is approximately temperature independent, characteristic of classical Coulomb-blockade oscillations. From the observation of oscillations up to $T \gtrsim 1.5$ K, we estimate a charging energy $e^2/C \approx 0.3$ meV.

A simple model that is able to explain at least part of the observed temperature dependence is the following. We assume an energy spectrum in the dot consisting of groups of closely spaced states separated by energy gaps, see Fig. 4.6(a). Such a spectrum is not unlikely: If the dot is modelled by a parabolic confining potential of strength ω_0 , the spectrum consists of n -fold degenerate states at energies $n\hbar\omega_0$ (ignoring spin-degeneracy). Deviations from parabolic confinement will lift the degeneracy, leading to a spectrum

as shown schematically in Fig. 4.6(a). The temperature dependence of the Coulomb-blockade oscillations calculated from Eq. (2.22) for this spectrum is shown in Fig. 4.6(b). For simplicity, level-independent tunnel rates were used. Clearly, high and low conductance peaks with different temperature-dependence result. At very low temperatures ($k_{\text{B}}T \lesssim 0.04e^2/C$), resonant tunneling through a single level becomes the dominant mechanism, leading to a $1/T$ behavior of the individual peaks, which is not observed in our experiment. This may be caused by the high impedance environment of the dot (a 100 k Ω resistor is connected in series with the dot), which results in a reduction of the peak height, as recently predicted [21]. In addition, the conductance peaks may saturate due to the finite width of the energy levels in the dot. Finally, electron-gas heating due to residual electrical noise cannot be excluded completely at these low temperatures.

In contrast to the conductance peaks, the valleys have equal temperature dependence. However, the conductance is not suppressed exponentially, but decreases approximately linearly with temperature. This indicates the importance of quantum fluctuations of the charge in the dot, due to the relatively large conductance of the individual tunnel barriers (approximately $\frac{1}{2}e^2/h$). (For tunnel-barrier conductances much smaller than e^2/h , Meirav *et al.* have found exponential suppression of the conductance in the minima [22].) Averin and Nazarov theoretically discuss “macroscopic quantum tunneling of charge” (q-mqt) [23], which is the common denominator for transport through the dot due to quantum fluctuations. They consider both inelastic- and elastic q-mqt. *Inelastic* q-mqt is due to co-tunneling [23] of two electrons through the dot: While one electron enters the dot through the first tunnel barrier, another leaves the dot through the second one. Since the two electrons involved in this process need not necessarily have equal initial and final energies, electron-hole excitations are created in the dot and leads. It is in this sense that co-tunneling is an inelastic process. *Elastic* q-mqt is due to phase-coherent tunneling of a single electron through the energy barrier imposed by the Coulomb blockade.

Co-tunneling, which in metals is the most important process by means of which the Coulomb-blockade can be overcome, leads to a conductance [23]

$$G_{\text{cot}} = \frac{e^2}{h} \frac{1}{24\pi^2} \frac{G_1 G_2}{(e^2/h)^2} \left(\frac{1}{E_-} + \frac{1}{E_+} \right)^2 \left[3(eV)^2 + (2\pi k_{\text{B}}T)^2 \right], \quad (4.1)$$

with $E_{\pm} \equiv U(N \pm 1) - U(N)$ the electrostatic charging energy associ-

ated with tunneling of a single electron into, respectively out of, the dot, $V \ll E_-, E_+$ the applied voltage across the dot, and G_1, G_2 the two tunnel conductances. At the minima of the Coulomb-blockade oscillations $E_- = E_+ = e^2/2C$. Inserting numbers relevant for our experiment, $G_1 \approx G_2 \approx \frac{1}{2}e^2/h$, $e^2/C \approx 0.3$ meV, and $V = 5$ μ V, we obtain $G_{\text{cot}} \approx 5 \times 10^{-3} e^2/h$ at $T = 0.3$ K (at this temperature, $e^2/C \approx 10k_B T$, so that transport through the dot is classically nearly suppressed). Experimentally, however, we find a conductance as large as $0.1e^2/h$. Thus, co-tunneling cannot be the only mechanism responsible for the finite conductance in the minima of the Coulomb-blockade oscillations. (We note that Glattli *et al.* [24] have studied a quantum dot of similar design to that shown in Fig. 4.1, with tunnel barrier conductances varying from 0.1 to $0.3e^2/h$. They found that co-tunneling *can* account for the temperature dependence of the conductance minima in that device.) Alternatively, elastic q-mqt may account for the relatively large conductance, but a theory relevant for the regime of our experiment is not available. Averin and Nazarov [23] discuss elastic q-mqt for the case that the dot is much larger than the electron elastic mean free path, so that the details of its geometry are not very important. In that limit, elastic q-mqt is a factor $\Delta E/(e^2/C)$ smaller than the inelastic contribution (but dominates at temperatures and voltages below the crossover values $eV_{\text{cr}}, k_B T_{\text{cr}} \approx [\Delta E(e^2/C)]^{1/2}$). Finally, as already mentioned above, electron-gas heating due to residual electrical noise cannot be excluded completely.

4.3 Periodic envelope of Coulomb-blockade oscillations in the quantum Hall regime

In this section we address the question as to what causes the variations in amplitude from peak to peak that we have observed. We will refer to these variations as the *envelope* of the Coulomb-blockade oscillations. Recently, Jalabert *et al.* have explained the occurrence of irregular envelopes in zero or weak magnetic field in terms of chaotic fluctuations of the tunnel rates [25]. In the previous section, we have discussed how a spectrum with groups of nearly degenerate levels can give rise to more regular variations in the amplitude, and to an anomalous temperature dependence. Here, we study the envelope of the Coulomb-blockade oscillations in the quantum-Hall effect regime. We find that it exhibits a *periodic* modulation, each period con-

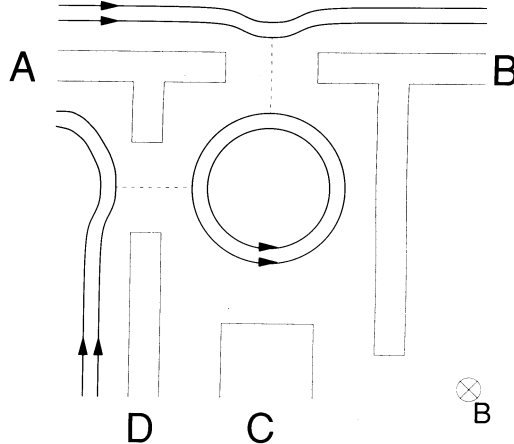


Figure 4.7: Schematic top-view of the $0.7 \times 0.8 \mu\text{m}^2$ quantum dot. Gates A, B, and D (hatched) define individually adjustable tunnel barriers, and gate C controls the electrostatic potential of the dot; the gaps between gates B and C, and between gates C and D, are pinched off in the experiment. The drawn lines represent edge channels formed by a quantizing magnetic field B perpendicular to the plane of the 2DEG, and the dashed lines indicate tunneling paths between the outermost Landau level in the dot and in the leads.

sisting of the same number of Coulomb-blockade oscillations. We argue that this surprising effect is due to electrostatic depopulation of each of the Landau levels in the dot by a *single electron* per period, with tunneling occurring predominantly through a single edge state of the outermost (lowest) Landau level. A model calculation and additional magnetoconductance data are used to support this interpretation.

Our device is shown schematically in Fig. 4.7. We used a GaAs– $\text{Al}_x\text{Ga}_{1-x}\text{As}$ heterostructure containing a two-dimensional electron gas (2DEG) with electron density $n_s = 3.7 \times 10^{11} \text{ cm}^{-2}$ and mobility $\mu \approx 10^6 \text{ cm}^2/\text{Vs}$. Part of the 2DEG is confined electrostatically to a quantum dot by patterned Ti-Au gates on top of the heterostructure. The tunnel barriers defined by gates A, B, and D were adjusted to a zero-field conductance of approximately $\frac{1}{2}e^2/h$. Two-terminal conductance measurements were made both as a function of gate voltage (applied to gate C) and magnetic field B .

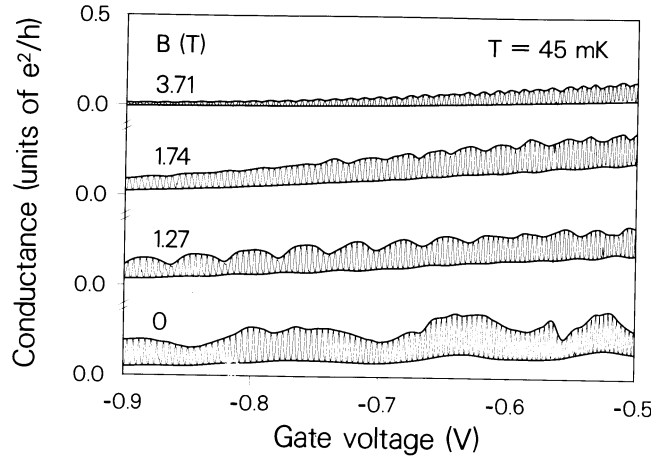


Figure 4.8: Conductance as a function of the voltage applied to gate C at $T = 45$ mK and 4 values of B . The envelope is indicated by the thick lines.

In Fig. 4.8, traces of the Coulomb-blockade oscillations as a function of gate voltage are shown at $T = 45$ mK and 4 values of the magnetic field. A large number of conductance peaks is observed in the traces, each peak corresponding to the electrostatic depopulation of the dot by a single electron. In contrast to the period of the Coulomb-blockade oscillations, which is rather insensitive to a magnetic field, the amplitude exhibits a pronounced B -dependence. Whereas in the absence of a magnetic field the envelope varies irregularly, in the quantum Hall effect regime it oscillates *periodically*, in the sense that at fixed B *each period contains the same number of conductance peaks*, and thus corresponds to the same number of electrons removed from the dot. On increasing the magnetic field, the period decreases from 9 conductance peaks per period at $B = 1.27$ T down to 3 peaks at 3.71 T. As the temperature is increased to 0.5 K, the envelope oscillations disappear (see lower right inset in Fig. 4.9), whereas the Coulomb-blockade oscillations remain clearly visible (upper left inset).

The *period* of the envelope oscillations (in terms of the number of electrons removed from the dot) corresponds to the number N_L of Landau levels occupied in the dot. This is evident from the plot in Fig. 4.9, showing the number of conductance peaks (and thus electrons) per period of

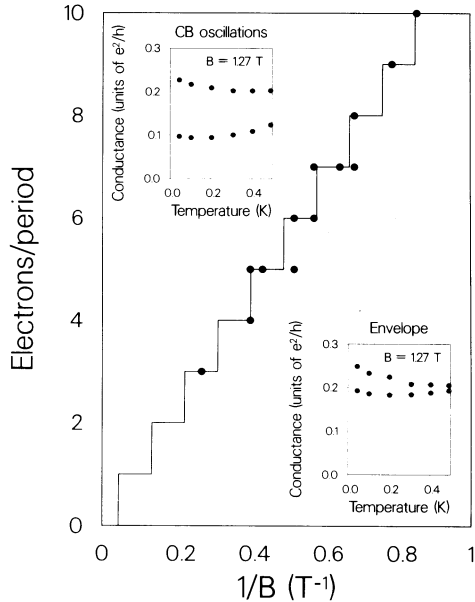


Figure 4.9: Number of conductance peaks per period of the envelope versus $1/B$ (filled circles). The drawn curve indicates the number of Landau levels in the dot. Insets: temperature dependence of the maxima and minima of the Coulomb-blockade oscillations (upper left) and envelope oscillations (lower right), averaged over a large number of periods. The drawn lines guide the eye.

the envelope oscillations versus $1/B$. The drawn staircase curve results from a fit of the data to the filling factor hn_{dot}/eB rounded to the nearest integer, which is equal to the number of spin-resolved Landau levels in the dot (treated as a 2DEG for simplicity). The value thus obtained for the electron density, $n_{\text{dot}} = 2.7 \times 10^{11} \text{ cm}^{-2}$, is about 25% smaller than the density of the ungated regions, which is quite reasonable.

We now argue that our experiment reveals a surprising new aspect of the energy spectrum of the quantum dot. Our observations can be explained if (a) the Landau levels are depopulated *cyclically*, by a single electron per Landau level per period of the envelope oscillations, and (b) only the outermost (lowest) Landau level in the dot couples to the leads. The first assumption is not a trivial one, and is in contrast to the sequential depopulation from highest to lowest Landau level in an unconfined 2DEG if the

Fermi energy is reduced. Since the number of electrons removed from the dot per period is equal to N_L , we require that in between each two states of the lowest Landau level a single state of each of the remaining occupied Landau levels is present. Such a regularity of the spectrum is unexpected, but we know of no other way to account for the periodically modulated envelope with the particular period observed.

Cyclic depopulation of the Landau levels by itself does not explain why the envelope of the Coulomb-blockade oscillations would be modulated. This requires an additional argument. The simplest explanation for a small modulation would be small differences in tunnel rates for states of different Landau levels. However, the tunnel rates through a split-gate barrier (or quantum point-contact) are known to decrease exponentially with increasing Landau level index [26]. This motivates our second assumption given above. Consecutive conductance peaks then result from tunneling through the nearest state (in energy) of the lowest Landau level, with an amplitude determined by the occupation probability of that state (which is a function of temperature and Fermi energy in the dot). The states of the remaining Landau levels serve to accomodate additional electrons induced electrostatically in the dot, but do not provide a tunneling path. Their presence affects the position of the Fermi level in the dot, and thus (indirectly) the tunneling probability. This is what explains the existence of an envelope.

In order to verify the validity of our arguments, we have made some calculations using the theory of chapter 2 [5] and the spectrum of non-interacting electrons in a dot with a parabolic confining potential of strength ω_0 , for which the energy levels within each single Landau level are equally spaced (independent of the Landau level index n) [27]:

$$E_{n,m} = \frac{1}{2}(n - m)\hbar\omega_c + \frac{1}{2}\hbar(\omega_c^2 + 4\omega_0^2)^{1/2}(n + m - 1), \quad (4.2)$$

with $\omega_c = eB/m^*$ the cyclotron frequency of electrons with effective mass m^* , and m the index of consecutive states within a Landau level. [Spin is ignored in (4.2) for simplicity]. As shown in the top panel of Fig. 4.10, at fixed B this spectrum is periodic in E , with period $\Delta E = E_{n,m} - E_{n,m-1} = -\frac{1}{2}\hbar\omega_c + \frac{1}{2}\hbar(\omega_c^2 + 4\omega_0^2)^{1/2}$ equal to the spacing of states within each single Landau level (independent of n and m). It therefore satisfies the above regularity criterium. In the bottom panel of Fig. 4.10 results of the calculations are given for a value of B indicated in the top panel by

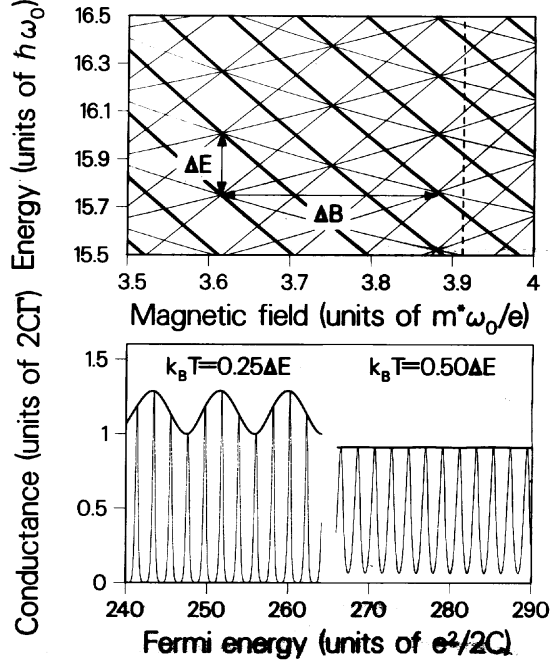


Figure 4.10: Top panel: the spectrum of non-interacting electrons in a parabolic confining potential is periodic in E with period ΔE , and quasi periodic in B with period ΔB . The states of the lowest Landau level are indicated by the thick lines. Bottom panel: model calculations using the theory of Ref. [5] for a value of the magnetic field indicated in the top panel by the dashed line (using $\hbar\omega_0 = 0.6$ meV, $e^2/2C = 0.4$ meV, and Γ respectively $10^{-2}\Gamma$ for the tunnel rates of the states of the lowest Landau level respectively remaining Landau levels).

the dashed line, corresponding to a spectrum of nearly equidistant levels with $N_L = 4$. Clearly, the amplitude of the Coulomb-blockade oscillations exhibits an envelope with a period that is determined by the number of Landau levels in the dot (left part). The modulation disappears as $k_B T$ approaches ΔE (right part). At very low temperatures, such that $k_B T \ll \delta E \approx \Delta E/N_L$, only a single peak remains per period of the envelope, associated with tunneling through a state of the lowest Landau level. In this regime, which was not accessible in our experiment, the other peaks are suppressed by orders of magnitude (not shown). We point out that the

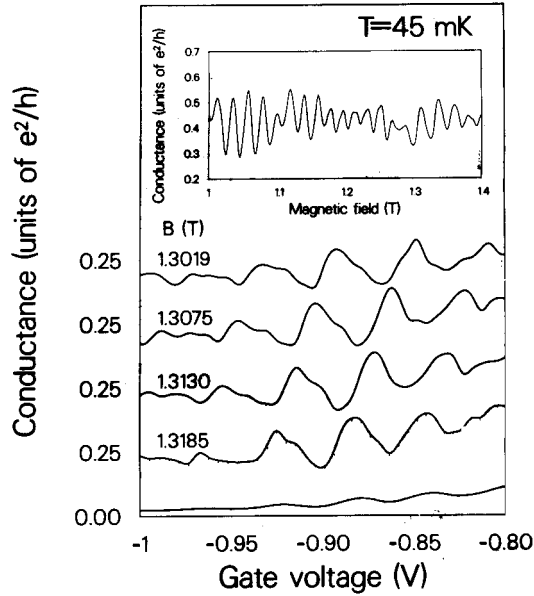


Figure 4.11: Coulomb-blockade oscillations (shown for the bottom trace only) and envelope at $T = 45$ mK and 4 values of B . Inset: magnetoconductance oscillations at a gate voltage of -0.725 V.

amplitude of the calculated envelope is not very sensitive to the distribution of the energy levels in between two consecutive states of the lowest Landau level. In our calculation we have found an increase by only about 10% if B is chosen such that the energy levels are 4-fold degenerate. The position of the envelope oscillations, however, shifts over a complete period if the magnetic field is increased by ΔB , corresponding to the nearly periodic character of the spectrum as a function of B at fixed E (see top panel of Fig. 4.10).

Experimentally, we also observe a shift of the envelope oscillations as the magnetic field is changed slightly. In Fig. 4.11 it is shown that the envelope is shifted over a full period if the magnetic field is increased by $\Delta B \approx 20$ mT. As shown in the inset, this value is equal to the period of the magnetoconductance oscillations observed at fixed gate voltage (adjusted to the maximum of a zero-field conductance peak). The amplitude and activation energy of the magnetoconductance oscillations are approximately

equal to those of the envelope oscillations, further illustrating their common origin. Note that the fact that ΔE , and not $e^2/2C$, governs the activation energy of the magnetoconductance oscillations implies that the conductance remains at a maximum of a Coulomb-blockade conductance peak as the magnetic field is changed. We have not attempted a direct comparison of experimental and calculated conductance as a function of magnetic field, because of the sensitivity to the B -dependence of the Fermi level in the leads, which is not easy to model reliably.

The results of the calculations using the single-electron energy spectrum (4.2) are in qualitative agreement with our experimental observations. We have traced the origin of the agreement to the regularity of the energy spectrum, which leads to a *cyclic depopulation of the Landau levels by one electron at a time*. McEuen *et al.* [7] have recently shown that the self-consistently calculated energy spectrum differs substantially from that of non-interacting particles. Our experiment suggests that the regularity leading to cyclic depopulation of Landau levels is a *generic* feature of a strongly interacting electron gas in a quantum dot. It would be interesting to investigate if, or to what extent, this is born out by the self-consistent model presented in Ref. [7].

4.4 Influence of adiabatically transmitted edge channels on single-electron tunneling through a quantum dot

In a two-dimensional electron gas (2DEG), selective reflection of edge channels in high magnetic fields is possible at a quantum point-contact, which consists of a constriction in the 2DEG defined by a split gate electrode [28]. The conductance of a quantum point-contact in a high magnetic field is approximately given by

$$G_{\text{pc}} \approx \frac{e^2}{h}(N_{\text{trans}} + t) , \quad (4.3)$$

with N_{trans} the number of edge channels that are fully transmitted over the barrier in the constriction, and $t \leq 1$ the tunneling transmission probability of the $(N_{\text{trans}} + 1)$ th edge channel. Edge channels corresponding to higher index Landau levels are nearly completely reflected.

With two point contacts in series and an additional gate electrode it is possible to form a quantum dot [see Fig. 4.12(a)] in which the states reflected by the point contacts form a discrete energy spectrum. For a non-

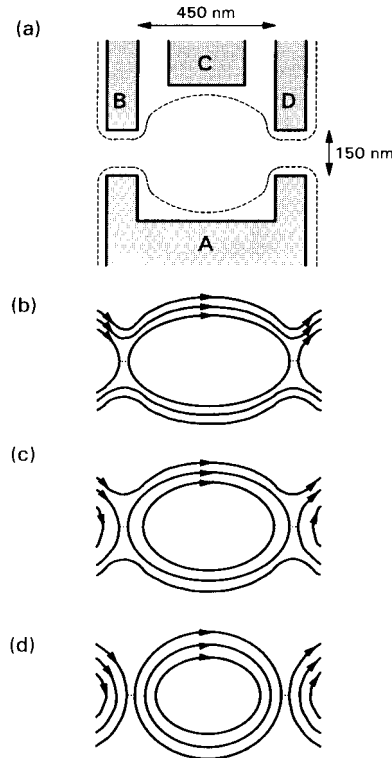


Figure 4.12: (a) Schematic drawing of the quantum dot. The dotted line indicates the edge of the depletion region. (b)–(d) Current paths through the dot in the presence of 2, 1, or 0 adiabatically transmitted edge channels as adjusted by V_B and V_D .

interacting electron gas, a peak in the conductance of the dot due to resonant tunneling should be seen when an electron state of the $(N_{\text{trans}} + 1)$ th, Landau level lines up with the Fermi energy in the leads. Periodic conductance oscillations are expected both as a function of electron density (varied by means of the voltage on gate C), and as a function of magnetic field. Such oscillations (sometimes referred to as Aharonov-Bohm oscillations [29]) have been demonstrated experimentally both as a function of magnetic field [30] and gate voltage [31] in the regime where one or more edge channels are transmitted adiabatically [i.e. $N_{\text{trans}} = 2, 1$ as shown in Figs. 4.12(b) and (c)].

Meanwhile, it has become clear that resonant tunneling through a quantum dot can be governed by single-electron charging effects. These effects are known to be important if the capacitance C of the dot is small so that the charging energy $e^2/C \gg k_B T$, and if the conductance of each point contact $G_{pc} < e^2/h$, so that no adiabatically transmitted edge channels are present [see Fig. 4.12(d)]. In the Coulomb blockade regime, periodic magnetoconductance oscillations of the type seen by van Wees *et al.* [30] are generally not observed [32].

Considering the extent to which Coulomb charging modifies electron tunneling, we have decided to re-examine its influence in the regime where it has previously been ignored: in the presence of adiabatically transmitted edge channels. In this section, we present the first direct comparison of the conductance versus gate voltage and magnetic field for different barrier transparencies, so that 2, 1, or 0 adiabatically transmitted channels are present in addition to the confined levels. We observe periodic conductance oscillations as a function of gate voltage for all three barrier transparencies. We use the oscillations observed in the full Coulomb-blockade regime (i.e., no adiabatically transmitted edge channels) as a novel electron counter to calibrate the period of the oscillations observed in the presence of adiabatically transmitted edge channels. In this way we argue that *even in the presence of the transmitted edge channels the conductance oscillations cannot be satisfactorily described in terms of resonant tunneling without invoking Coulomb charging*. In addition, magnetoconductance oscillations are observed to increase in period as the number of adiabatically transmitted edge channels decreases from 2 to 1, while irregular fluctuations with a larger activation energy comparable to $e^2/2C$ are seen in the full Coulomb-blockade regime. This observation indicates that charging effects become progressively more important as the number of transmitted edge channels decreases, while it confirms that their influence is still significant for barrier transparencies larger than e^2/h .

A schematic drawing of our device is shown in Fig. 4.12(a). Four gates (labelled A–D in the figure) define a square 450×450 nm 2 on the surface of a GaAs–Al $_x$ Ga $_{1-x}$ As heterostructure with a 2DEG of mobility 10^6 cm 2 /Vs and density 3.0×10^{11} cm $^{-2}$. When the gates are negatively biased with respect to the 2DEG, a quantum dot with a diameter of approximately $d = 400$ nm is formed in the underlying 2DEG, which is connected through two point-contacts to the two-dimensional leads. Two-terminal conductance

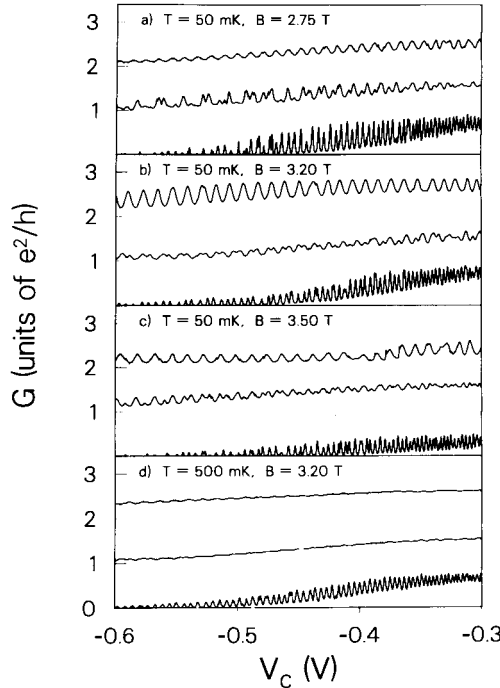


Figure 4.13: Dot conductance as a function of the voltage on gate C at a series of magnetic fields and temperatures. In the top, middle, and bottom trace of each figure (a)–(d) point contacts are adjusted to conductances of $2.5e^2/h$, $1.5e^2/h$, and $0.5e^2/h$, respectively. The three cases correspond to the three possible current paths shown in Fig. 4.12(b)–(d).

measurements are made across the dot as a function of the voltage on gate C (V_C), which determines the electron density in the dot. In the experiments, the voltage on gate A is left fixed at -0.7 V, and the voltages on gates B and D (V_B, V_D) are adjusted to control the transmission through the tunnel barriers between dot and leads. The data described below are from measurements performed on a single device; however, the salient results were accurately reproduced in several other devices.

Figures 4.13(a)–(c) show results of conductance measurements as a function of V_C for three different magnetic fields (2.75, 3.20, and 3.50 T, respectively) and a temperature of 50 mK. Each figure displays three traces,

corresponding to three different adjustments of the point-contact conductances; $G_{pc} = 2.5e^2/h$ in the top traces, $1.5e^2/h$ in the middle traces, and $0.5e^2/h$ in the bottom traces. The traces all show a series of nearly periodic oscillations in the conductance as a function of V_C , however the period of the oscillations varies from trace to trace. In Fig. 4.13(b), for example, there are 27 peaks in the top trace, 44 peaks in the middle trace, and 67 peaks in the bottom trace, indicating that the period in the top trace is about 2.5 times that in the bottom trace and the period in the middle trace is about 1.5 times that in the bottom trace. A comparison of the traces measured at the three magnetic fields shows that the number of peaks in the top trace decreases from 31 at 2.75 T to 24 at 3.50 T while the number of peaks in the middle trace decreases from 48 to 42. The number of peaks in the bottom trace however, remains fixed at 67. Figure 4.13(d) shows results of measurements taken with the same parameters as in Fig. 4.13(b) but at a temperature of 500 mK. The oscillations observed in the top two traces have now nearly vanished, while strong oscillations are still observed in the bottom trace. Further measurements (not shown) indicate that the oscillations in the bottom trace persist up to a temperature of at least 2 K.

The Coulomb charging energy $e^2/2C \approx 0.4$ meV of the dot, estimated from the self capacitance $C = 4\epsilon_0\epsilon d$ of a flat circular disk of diameter d , is greater than $k_B T$ for temperatures up to 4 K. Thus, the very regular oscillations observed for $G_{pc} = 0.5e^2/h$ (the bottom traces in Fig. 4.13) can safely be interpreted as Coulomb-blockade oscillations. The gate voltage separation between peaks is about e/C_{gate} where C_{gate} , the capacitance between gate C and the dot, is assumed to be independent of G_{pc} . This is reasonable since G_{pc} is much more sensitive to changes in voltages B and D than are the size of the dot and the dot-gate separation, which together determine C_{gate} . Since each Coulomb-blockade peak corresponds to the removal of one electron from the dot, this allows us to use the Coulomb-blockade oscillations in a new way: as a tool to determine the mechanism that governs the period of the oscillations seen at higher barrier transparencies. The number of electrons per peak for the upper traces in Fig. 4.13 can be determined by dividing the number of Coulomb-blockade peaks counted for $G_{pc} = 0.5e^2/h$ into the number of peaks counted for $G_{pc} = 1.5e^2/h$ and $2.5e^2/h$. The results of this procedure performed on a set of measurements of the type shown in Fig. 4.13 are plotted versus magnetic field in Fig. 4.14. The number of electrons per peak is considerably

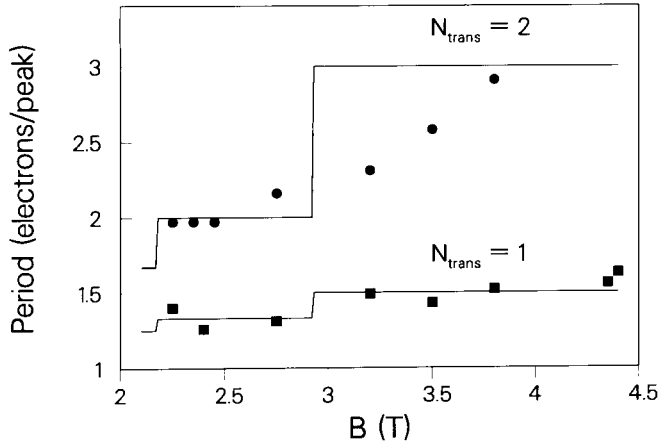


Figure 4.14: Period of the conductance oscillations (in units of electrons per peak) versus magnetic field for $G_{pc} = 2.5e^2/h$ (circles) and $G_{pc} = 1.5e^2/h$ (squares). The solid lines are fits for $N_{trans} = 2$ respectively 1 adiabatically transmitted edge channel (see text).

larger for $G_{pc} = 2.5e^2/h$ than for $G_{pc} = 1.5e^2/h$. In both cases, an increase in magnetic field results in an increase in the number of electrons per peak.

We now consider the periodic conductance oscillations for $G_{pc} > e^2/h$ [the upper two traces in Figs. 4.13(a)–(d)]. The simplest possibility is to ignore Coulomb charging. As discussed in the introduction, then a peak in the conductance is observed due to resonant tunneling when an electron state of the $(N_{trans} + 1)$ th Landau level lines up with the Fermi energy in the leads. The frequency at which this occurs corresponds to the rate at which electrons are removed from the $(N_{trans} + 1)$ th Landau level. The total number N_{dot} of spin-split Landau levels in the dot are made up of the N_{conf} Landau levels of guiding center energy E_g below the barrier height E_b , and the N_{trans} additional Landau levels that are occupied in the dot but fully transmitted over the barriers in the point contacts ($E_g > E_b$). Assuming that both the N_{conf} and N_{trans} Landau levels are depopulated at about the same rate, the number of electrons per peak should be simply N_{dot} . This argument predicts that the number of electrons per peak should decrease, rather than increase with magnetic field, in contradiction

with the observed results (Fig. 4.14). This discrepancy could in principle be eliminated if resonant tunneling through electron states of the confined Landau levels with index higher than $(N_{\text{trans}} + 1)$ also contribute to the conductance of the dot. The tunneling rate, however, decreases exponentially with decreasing E_g [26], thus there should be an order of magnitude modulation of conductance peak heights due to resonant tunneling through states of consecutive Landau levels confined in the dot [4, 5]. This is not observed in our experiment, however.[†]

We can model the results of Fig. 4.14, if we take Coulomb charging into account for $G_{\text{pc}} > e^2/h$. We extend recent arguments for the $N_{\text{trans}} = 0$ case [7] to our problem by considering a separate Coulomb charging energy of the N_{conf} Landau levels existing in the presence of the adiabatically transmitted edge channels. This is reasonable, since a magnetically induced tunnel barrier consisting of an incompressible electron-gas region exists between each of the edge channels. Resonant-tunneling electrons thus face a nonzero Coulomb-charging energy associated with a change in the electron population of the confined Landau levels. This leads to Coulomb-blockade oscillations as a function of gate voltage with a period corresponding to the removal of an electron from any one of the N_{conf} Landau levels. The removal of electrons from one of the N_{trans} Landau levels in the dot does not give rise to a conductance peak because charge in these levels is not localized and can therefore be changed continuously. This implies that

$$\frac{\text{electrons}}{\text{peak}} = \frac{N_{\text{conf}} + N_{\text{trans}}}{N_{\text{conf}}} = \frac{N_{\text{dot}}}{N_{\text{conf}}}. \quad (4.4)$$

Figure 4.14 shows solutions of Eq. (4.4) for $N_{\text{trans}} = 1$ and $N_{\text{trans}} = 2$. We determine N_{dot} assuming parabolic confinement in the dot [27] of strength $\hbar\omega_0 = 0.6$ meV and Fermi energy $E_F = 7$ meV, corresponding to an electron density of $2.2 \times 10^{11} \text{ cm}^{-2}$, and a dot diameter of 400 nm. The fit between the calculated and experimental results is fair. In both cases, the number of electrons per peak is seen to increase (from 2 to 3 in the upper curve and from 1.3 to 1.5 in the lower curve) as N_{dot} decreases from 4 to 3.

[†]The more modest amplitude modulation of the conductance peaks that we observe in the middle and bottom traces of Fig. 4.13 can be explained in terms of tunneling through the confined states associated with *only* the $(N_{\text{trans}} + 1)$ th Landau level, as discussed in section 4.3. The fact that a more dramatic amplitude modulation is not observed suggests that we are in the near classical regime where $k_B T \gtrsim \Delta E$, the average spacing of states of the $(N_{\text{trans}} + 1)$ th Landau level.

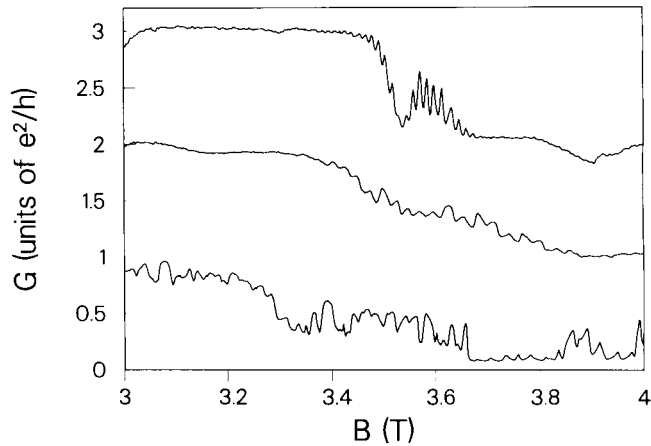


Figure 4.15: Dot conductance as a function of magnetic field for three different barrier transparencies. At $B = 3.5$ T, the top, middle, and bottom traces correspond to point-contact conductances of $2.5e^2/h$, $1.5e^2/h$ and $0.5e^2/h$, respectively.

The presence of the N_{trans} Landau levels enters only in the form of a nearby electron reservoir, coupled capacitively to both the gates and the confined Landau levels. This enhances the effective capacitance, and decreases the charging energy relative to that in the case of zero transmitted edge channels through the dot. A calculation of the charging energy of the confined Landau levels in the presence of adiabatically transmitted edge channels [33] indicates that the increase in C with the number of adiabatically transmitted edge channels can account for the reduction of the activation energy with increasing barrier transparency in the conductance traces in Fig. 4.13.

We now briefly discuss the magnetoconductance of the dot. Figure 4.15 shows the conductance as a function of magnetic field at a temperature of 50 mK. The constrictions are adjusted so that the conductance drops from $3e^2/h$ to $2e^2/h$ in the top trace, from $2e^2/h$ to e^2/h in the middle trace, and from e^2/h to 0 in the bottom trace. Magnetoconductance oscillations are observed with $\Delta B = 13$ mT in the top trace and $\Delta B = 26$ mT in the middle trace while more random fluctuations are observed in the bottom trace. The oscillations disappear for $T \approx 250$ mK, while the fluctuations observed in the bottom trace survive to $T > 1$ K.

We speculate that the magnetoconductance oscillations are due to resonant tunneling through confined states of the ($N_{\text{trans}} + 1$)th Landau level, modified by single-electron charging effects. The increase in period observed between the top two traces is thought to be due to the increasing influence of Coulomb charging with decreasing number of edge channels in contact to the 2DEG. In the bottom trace, the Coulomb-charging energy becomes dominant, and the periodic magnetoconductance oscillations are replaced by large scale fluctuations. We do not attempt to describe the magnetoconductance of the dot in more detail. What is needed is a self-consistent calculation based on precise knowledge of the full energy spectrum in the presence of both confined and adiabatically transmitted edge channels.

Our results demonstrate that the formation of Landau levels in a high magnetic field causes single-electron charging effects to be of importance for barrier conductances greater than e^2/h . This finding necessitates a reinterpretation of earlier experimental results on single [30, 31] and multiple quantum dots [34].

4.5 Coulomb-blockade oscillations in the thermopower of a quantum dot

Single-electron tunneling is the dominant mechanism governing the transport properties of a quantum dot that is weakly coupled to leads by tunnel barriers. Whereas the conductance has been studied quite extensively, the thermo-electric properties of a quantum dot remain essentially unexplored. Amman *et al.* have theoretically studied the role of Coulomb interactions on thermo-electric effects in a single mesoscopic tunnel-junction, and have used their results to interpret the thermopower of granular thin bismuth films [35]. As discussed in chapter 2, a theory was also developed for the thermopower of a quantum dot, taking the discrete energy spectrum of the dot into account [36]. The thermopower as a function of the Fermi energy in the reservoirs is predicted to exhibit sawtooth-like oscillations at low temperatures, with an amplitude that is determined by the charging energy and temperature only [36].

Here, we present an experimental study of the thermo-electric properties of a quantum dot, using the current-heating technique applied previously to study the thermovoltage across a quantum point-contact [37]. At low lattice temperatures and small heating currents, we observe the predicted [36]

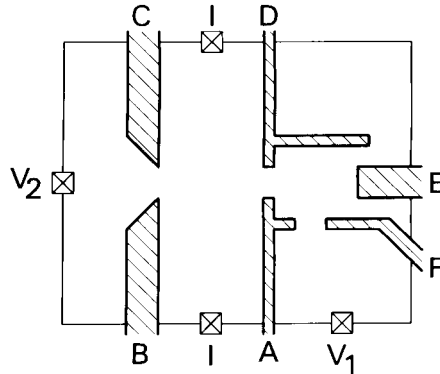


Figure 4.16: Schematic top-view of the $0.7 \times 0.8 \mu\text{m}^2$ quantum dot adjacent to a $2 \mu\text{m}$ wide, $20 \mu\text{m}$ long channel. Gates A, D, and F (hatched) define individually adjustable tunnel barriers, and gate E controls the electrostatic potential of the dot; the gaps between gates D and E, and between gates E and F, are pinched off in the experiment. An ac heating current I is passed through the channel and the thermovoltage $V_{\text{th}} \equiv V_1 - V_2$ is measured across the quantum dot and the opposite reference point-contact defined by gates B and C.

sawtooth-like oscillations as a function of gate voltage in the thermovoltage. These are compared with measured Coulomb-blockade oscillations in the conductance, and are analyzed in terms of the theory [36] outlined in chapter 2. We find that the generic lineshapes of the Coulomb-blockade oscillations in both the thermopower and the conductance are in agreement with the theory. However, the oscillations are broadened more strongly than is calculated from the known lattice temperature and the estimated charging energy of the dot. In addition, we present an unexpected sign reversal of the thermovoltage oscillations in the nonlinear regime at large heating currents.

The devices used for the experiments have a layout as shown schematically in Fig. 4.16. Patterned Ti-Au gates are used to define a quantum dot in the two-dimensional electron gas (2DEG) in a modulation doped GaAs-Al_xGa_{1-x}As heterostructure. The ungated parts of the 2DEG have an electron density $n_s = 3.7 \times 10^{11} \text{ cm}^{-2}$ and a mobility $\mu \approx 10^6 \text{ cm}^2/\text{Vs}$. Gates A, D, and F define two tunnel barriers with a conductance that is adjusted to about $0.1e^2/h$ each. Two additional gates, B and C, define a

narrow channel. A point contact in the boundary of this channel is used as a reference voltage-probe, opposite to the dot. The sample is mounted in the mixing chamber of a dilution refrigerator, and measurements of the thermopower and conductance of the dot are made as a function of the voltage V_E applied to gate E. To measure the thermopower, the electron gas in the channel is heated using an ac current I . This leads to an increase $\Delta T \propto I^2$ of the electron temperature in the channel in the low current regime [37]. Lock-in detection at twice the frequency of the current is used to measure the resulting thermovoltage $V_{\text{th}} \equiv V_1 - V_2$, which is equal to the difference in thermovoltages across the quantum dot and reference point-contact,

$$V_{\text{th}} = (S_{\text{dot}} - S_{\text{pc}})\Delta T , \quad (4.5)$$

where S_{dot} is the thermopower of the dot, and S_{pc} the thermopower of the reference point-contact. The contribution of S_{pc} to V_{th} is independent of V_E and leads to a constant offset voltage, which is minimized in our experiment by suitably adjusting the reference point-contact [37]. Thus, variations in V_{th} as a function of V_E directly reflect changes in the thermopower of the dot. In addition to the thermovoltage, the two-terminal conductance is measured using a standard lock-in technique with an excitation voltage across the dot below 9 μV . No heating current is used in this latter measurement.

In Fig. 4.17(a) we compare measurements of the Coulomb-blockade oscillations as a function of V_E in the thermovoltage (solid) and conductance (dashed) of the dot, at a lattice temperature of $T = 45$ mK. As shown in the figure, the thermovoltage V_{th} (and therefore S_{dot}) oscillates periodically as a function of V_E . The period is equal to that of the conductance oscillations, and corresponds to depopulation of the dot by a single electron. In contrast to the conductance oscillations, which consist of a series of *symmetric* peaks separated by gate-voltage regions where the conductance is suppressed, the thermopower oscillations have a distinct *sawtooth* lineshape. In addition, we find that the conductance peaks are approximately centered on the positive slope of the thermopower oscillations, with the steeper negative slope occurring in between two conductance peaks. These data comprise the first experimental demonstration of the key characteristics of the thermopower oscillations of a quantum dot, as predicted theoretically [36].

Using the linear-response formulas of chapter 2 [36], the thermopower and conductance can be calculated as a function of Fermi energy. As shown

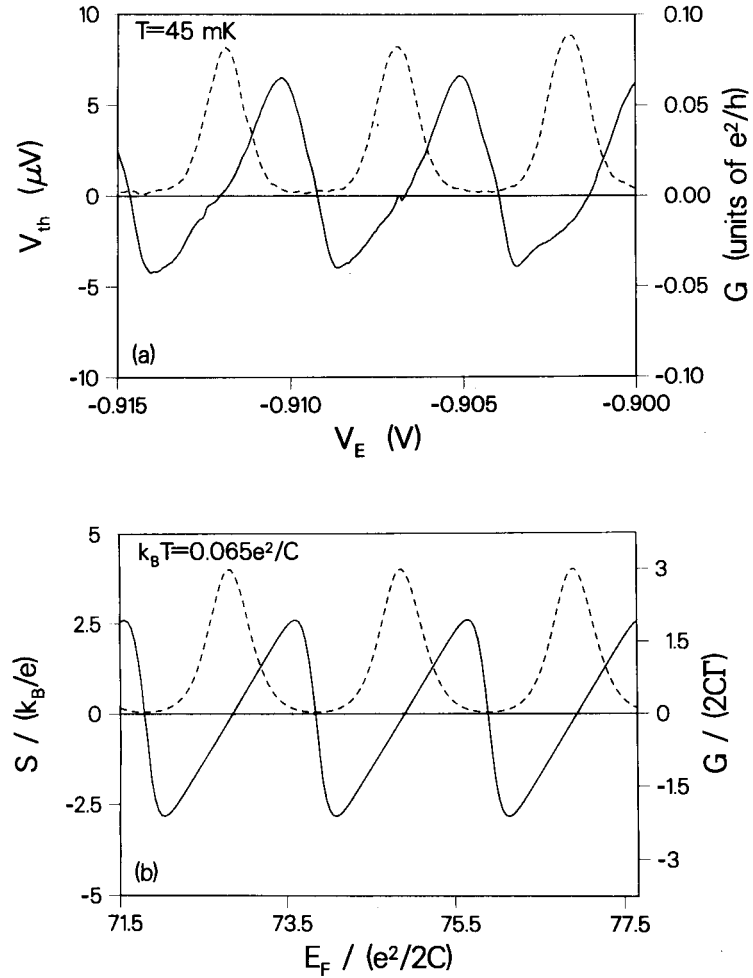


Figure 4.17: (a) Thermovoltage V_{th} at a heating current of 58 nA (solid) and conductance (dashed) of the dot as a function of V_E at a lattice temperature of $T = 45 \text{ mK}$. (b) Calculated thermopower (solid) and conductance (dashed) of a quantum dot as a function of Fermi energy using Eqs. (2.35) and (2.22). The parameters used in the calculations are discussed in the text.

in Fig. 4.17(b), the calculated lineshapes of the Coulomb-blockade oscillations in both the thermovoltage and the conductance reproduce the experimental lineshapes in Fig. 4.17(a) quite well. In the calculations, we have assumed an energy spectrum in the dot consisting of equidistantly spaced, twofold degenerate levels, with spacing $\Delta E = 0.05e^2/C$; the tunnel rates Γ to the individual states have been taken to be independent of energy, so that they do not appear in the final result for the thermopower; and the lattice-temperature parameter has been set to $k_B T = 0.065e^2/C$. In spite of the similarity between the experimental and calculated lineshapes, it becomes evident that there is some discrepancy between experiment and theory if a reasonable value for the charging energy e^2/C is inserted.

From the observation of the Coulomb-blockade oscillations up to $T \gtrsim 1.5$ K, we estimate $e^2/C \approx 0.3$ meV (cf. section 4.2). This implies that the temperature parameter used in the calculations corresponds to approximately 0.23 K, which is about four times as high as the actual temperature in the experiment (45 mK). If we would have used a lower temperature in the calculations, the conductance peaks would have been too narrow and the thermopower oscillations too skewed, as compared to the experiments. Since in the experiment the anomalous broadening is observed in *both* S_{dot} and G , excess heating of the electron gas by the heating current in the narrow channel can be excluded as a source for the broadening. It may be due to the intrinsic broadening of the levels in the dot in the regime $k_B T \lesssim h\Gamma$, which is not taken into account theoretically [36]. In addition, electron-gas heating due to residual electrical noise cannot be excluded completely at these low temperatures.

The lattice-temperature dependence of the thermovoltage oscillations is shown in Fig. 4.18, where traces of V_{th} versus V_E are given for three different temperatures (obtained using a heating current of $I = 18$ nA). The poor signal-to-noise ratio is due to the very low heating current, which we choose to ensure that the measurements are made in the linear response regime (see also Fig. 4.19, below). The sawtooth lineshape of the thermopower oscillations is most pronounced at the lowest lattice temperature of $T = 45$ mK, and is gradually replaced by a more symmetric lineshape as T is increased to 313 mK. If the temperature is further increased to 750 mK, the oscillations are no longer observable using $I = 18$ nA, due to the large noise level. If larger heating currents are used, however, the oscillations can still be observed even at 1.5 K (not shown).

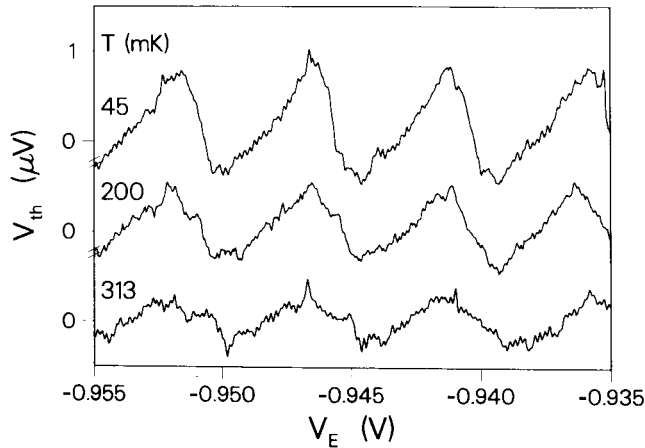


Figure 4.18: Thermovoltage as a function of V_E at lattice temperatures of $T = 45$, 200 and 313 mK, obtained using a heating current of 18 nA.

A comparison of the temperature dependence of the thermovoltage oscillations with theory (Ref. [36] and chapter 2, section 2.4) requires knowledge of the applied temperature difference ΔT across the dot. This is difficult if ΔT is applied using a current-heating technique, however, since in that case ΔT depends on several parameters that are not well known. The order of magnitude of ΔT may be estimated using a heat balance argument [37], $c_v \Delta T = (I/W)^2 \rho \tau_\varepsilon$, with $c_v = (\pi^2/3)(k_B T/E_F) n_s k_B$ the heat capacity per unit area of the 2DEG, I the heating current, W the channel width, ρ the channel resistivity, and τ_ε an energy relaxation time associated with energy transfer from the electron gas to the lattice. Using the theoretical result for the peak-to-peak amplitude of the thermopower oscillations $\Delta V_{\text{th}} \approx (e/2CT)\Delta T$, and inserting the measured ΔV_{th} from the 200 mK trace in Fig. 4.18 and our estimate for the charging energy, we obtain $\Delta T \approx 0.5$ mK. This implies for the heat balance that $\tau_\varepsilon = 10^{-10}$ s, which is not unreasonable [37].

We now turn to a discussion of an intriguing result found in experiments beyond the regime of linear response. In Fig. 4.19 the peak-to-peak amplitude ΔV_{th} of the thermovoltage oscillations is shown as a function of heating current at a lattice temperature of $T = 45$ mK (using another device, with tunnel barriers adjusted to a conductance of approximately $0.5e^2/h$). It is

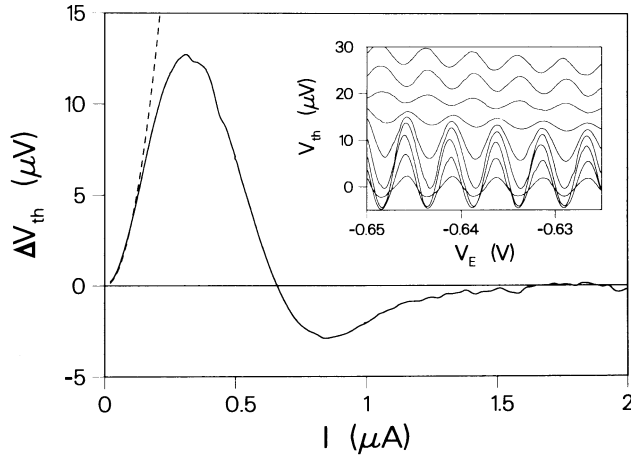


Figure 4.19: Peak-to-peak amplitude of the thermovoltage oscillations as a function of the heating current, at a lattice temperature of $T = 45 \text{ mK}$. The dashed line indicates a quadratic increase of the amplitude with heating current. Inset: Thermovoltage versus V_E at a lattice temperature of $T = 45 \text{ mK}$. From top to bottom, the heating current is $0.1, 0.2, \dots, 0.9 \mu\text{A}$.

obtained by subtracting traces of V_{th} as a function of heating current at a maximum and at an adjacent minimum of the thermovoltage oscillations. (Note that the oscillations do not shift in gate voltage as the heating current is increased, see inset in Fig. 4.19.[‡]) As shown by a comparison with the dashed curve, which corresponds to a quadratic increase of the amplitude with current, the linear-response regime extends up to $I \lesssim 0.1 \mu\text{A}$. (We assume that Joule heating is the dominant mechanism for the increase in temperature of the electron gas in the channel, so that linear response to a temperature difference corresponds to $V_{\text{th}} \propto I^2$ [37].) As the current is increased further, a remarkable damped oscillatory behavior of ΔV_{th} is found. At approximately $0.65 \mu\text{A}$ the *amplitude reverses sign* (as is also clear from the inset). Using the heat balance argument discussed above, we estimate that the temperature of the electron gas in the channel is as high as a few kelvin at this current level, so that $\Delta T \gg T, \Delta E/k_{\text{B}}$. It may

[‡] V_{th} becomes more negative with increasing current. We attribute this to the increasing negative contribution of the reference point-contact to V_{th} [cf. Eq. (4.5)].

be significant that $k_B\Delta T$ is comparable to e^2/C under these conditions. A theoretical study of the thermovoltage of a quantum dot beyond the regime of linear response is called for.

In conclusion, we have presented an experimental study of the thermopower of a quantum dot in the Coulomb-blockade regime. The thermopower is observed to oscillate in a sawtooth-like fashion as the dot is depopulated, with a period equal to that of the Coulomb-blockade oscillations in the conductance. This is in agreement with a recent theory [36]. In the nonlinear regime at large heating currents, a remarkable change of sign of the amplitude of the thermopower oscillations is observed, which remains to be understood.

References

- [1] J. H. F. Scott-Thomas, S. B. Field, M. A. Kastner, H. I. Smith, and D. A. Antoniadis, Phys. Rev. Lett. **62**, 583 (1989).
- [2] H. van Houten and C. W. J. Beenakker, Phys. Rev. Lett. **63**, 1893 (1989).
- [3] U. Meirav, M. A. Kastner, and S. J. Wind, Phys. Rev. Lett. **65**, 771 (1990).
- [4] Y. Meir, N. S. Wingreen, and P. A. Lee, Phys. Rev. Lett. **66**, 3048 (1991).
- [5] C. W. J. Beenakker, Phys. Rev. B **44**, 1646 (1991).
- [6] P. L. McEuen, E. B. Foxman, U. Meirav, M. A. Kastner, Y. Meir, N. S. Wingreen, and S. J. Wind, Phys. Rev. Lett. **66**, 1926 (1991).
- [7] P. L. McEuen, E. B. Foxman, J. Kinaret, U. Meirav, M. A. Kastner, N. S. Wingreen, and S. J. Wind, Phys. Rev. B **45**, 11419 (1992).
- [8] C. J. B. Ford, IOP Conference Series **108**, 85 (1991).
- [9] R. J. Haug, K. Y. Lee, and J. M. Hong, in: *Superconducting Devices & Their Applications*, edited by H. Koch and H. Lubbig (Springer, New York, 1992).
- [10] A. A. M. Staring, J. G. Williamson, H. van Houten, C. W. J. Beenakker, L. P. Kouwenhoven, and C. T. Foxon, Physica B **175**, 226 (1991).
- [11] A. A. M. Staring, B. W. Alphenaar, H. van Houten, L. W. Molenkamp, O. J. A. Buyk, M. A. A. Mabesoone, and C. T. Foxon, Phys. Rev. B, to be published.
- [12] B. W. Alphenaar, A. A. M. Staring, H. van Houten, O. J. A. Buyk, M. A. A. Mabesoone, and C. T. Foxon, Phys. Rev. B, to be published.
- [13] A. A. M. Staring, L. W. Molenkamp, H. van Houten, B. W. Alphenaar, O. J. A. Buyk, M. A. A. Mabesoone, C. W. J. Beenakker, and C. T. Foxon, submitted to Phys. Rev. Lett.

- [14] For a review of quantum transport in semiconductor nanostructures, see: C. W. J. Beenakker and H. van Houten, Solid State Physics **44**, 1 (1991).
- [15] L. P. Kouwenhoven, N. C. van der Vaart, A. T. Johnson, W. Kool, C. J. P. M. Harmans, J. G. Williamson, A. A. M. Staring, and C. T. Foxon, Z. Phys. B **85**, 367 (1991).
- [16] D. V. Averin and A. A. Odintsov, Phys. Lett. A **140**, 251 (1989); D. V. Averin and Yu. V. Nazarov, Phys. Rev. Lett. **65**, 2446 (1990).
- [17] L. I. Glazman and K. A. Matveev, Pis'ma Zh. Eksp. Teor. Fiz. **51**, 425 (1990) [JETP Lett. **51**, 484 (1990)].
- [18] Yu. V. Nazarov, Solid State Commun. **75**, 669 (1990); A. N. Korotkov and Yu. V. Nazarov, Physica B **173**, 217 (1991).
- [19] C. G. Smith, M. Pepper, J. E. F. Frost, D. G. Hasko, R. Newbury, D. C. Peacock, D. A. Ritchie, and G. A. C. Jones, J. Phys. Condens. Matter **1**, 9035 (1989).
- [20] S. Datta, Superlattices and Microstructures **6**, 83 (1989).
- [21] A. A. Odintsov, G. Falci, and G. Schön, Phys. Rev. B **44**, 13089 (1991).
- [22] U. Meirav, P. L. McEuen, M. A. Kastner, E. B. Foxman, A. Kumar, and S. J. Wind, Z. Phys. B **85**, 457 (1991).
- [23] D. V. Averin and Yu. V. Averin, in: *Single Charge Tunneling*, edited by H. Grabert and M. H. Devoret, NATO ASI Series B (Plenum, New York, 1992).
- [24] D. C. Glattli, C. Pasquier, U. Meirav, F. I. B. Williams, Y. Jin, and B. Etienne, Z. Phys. B **85**, 375 (1991).
- [25] R. A. Jalabert, A. D. Stone, and Y. Alhassid, Phys. Rev. Lett. **68**, 3468 (1992).
- [26] H. A. Fertig and B. I. Halperin, Phys. Rev. B **36**, 7969 (1987).
- [27] V. Fock, Z. Phys. **47**, 446 (1928); C. G. Darwin, Proc. Cambridge Pilos. Soc. **27**, 86 (1930).

- [28] B. J. van Wees, L. P. Kouwenhoven, H. van Houten, C. W. J. Beenakker, J. E. Mooij, C. T. Foxon, and J. J. Harris, Phys. Rev. B **38**, 3625 (1988).
- [29] J. K. Jain, Phys. Rev. Lett. **60**, 2074 (1988); U. Sivan and Y. Imry, *ibid.* **61**, 1001 (1988).
- [30] B. J. van Wees, L. P. Kouwenhoven, C. J. P. M. Harmans, J. G. Williamson, C. E. Timmering, M. E. I. Broekaart, C. T. Foxon, and J. J. Harris, Phys. Rev. Lett. **62**, 2523 (1989).
- [31] R. J. Brown, H. Ahmed, J. E. F. Frost, D. G. Hasko, G. A. C. Jones, M. J. Kelly, D. A. Ritchie, D. C. Peacock, M. Pepper, C. G. Smith, and R. Newbury, J. Phys. Condens. Matter **1**, 6291 (1989).
- [32] For a review see H. van Houten, C. W. J. Beenakker, and A. A. M. Staring, in: *Single Charge Tunneling*, edited by H. Grabert and M. H. Devoret, NATO ASI Series B (Plenum, New York, 1992).
- [33] I. K. Marmorkos and C. W. J. Beenakker, submitted to Phys. Rev. B.
- [34] L. P. Kouwenhoven, F. W. J. Hekking, B. J. van Wees, C. J. P. M. Harmans, C. E. Timmering, and C. T. Foxon, Phys. Rev. Lett. **65**, 361 (1990).
- [35] M. Amman, E. Ben-Jacob, and J. Cohn, Z. Phys. B **85**, 405 (1991).
- [36] C. W. J. Beenakker and A. A. M. Staring, Phys. Rev. B, to be published. This is an extension of existing theory for the conductance, see C. W. J. Beenakker, Phys. Rev. B **44**, 1646 (1991).
- [37] L. W. Molenkamp, H. van Houten, C. W. J. Beenakker, R. Eppenga, and C. T. Foxon, Phys. Rev. Lett. **65**, 1052 (1990).

Summary

Fundamental solid-state physics has benefitted greatly from the industrial effort to increase the performance of semiconductor devices. The advances in microfabrication technology this effort has led to, underlie major breakthroughs that have been established in the past decade in the field of mesoscopic physics. This is a new branch of solid-state physics that is concerned with the study of “small” systems, where small means dimensions comparable to some relevant physical length scale. As a result mesoscopic systems have interesting properties and exhibit many novel physical phenomena.

This thesis deals with the phenomenon of “Coulomb-blockade oscillations in quantum dots and wires.” In a quantum dot, the electron gas is confined to a small volume, such that its energy spectrum consists of discrete levels; in a quantum wire, it is confined in two directions only. Both quantum dots and wires can be defined in the two-dimensional electron gas (2DEG) in a modulation-doped GaAs–Al_xGa_{1-x}As heterostructure by means of an appropriate pattern of split gate-electrodes, fabricated on top of the heterostructure using electron-beam lithography. Application of a negative voltage (with respect to the 2DEG) replicates this pattern into the 2DEG. Coulomb blockade refers to the suppression of tunneling through a system with ultra-small capacitance, e.g., a quantum dot or small metal particle, at low temperatures and small applied voltages. The reason for this suppression is that the electrostatic charging energy required to add a single electron to such a system is not available (because it is large compared to the thermal energy). The charging energy can be reduced by means of a voltage applied to a gate electrode that is capacitively coupled to the system. This lifts the Coulomb blockade which results in periodic conductance oscillations as a function of the gate voltage. These are the

Coulomb-blockade oscillations.

After an introduction in chapter 1 to the basic concepts used in this thesis, a theory for Coulomb-blockade oscillations in quantum dots is summarized in chapter 2. The periodicity of the oscillations at zero temperature is derived from equilibrium properties of the system, and a discussion is given of limiting cases of the general result of a kinetic theory for transport through the dot at finite temperatures. These consist of the classical limit, in which the energy spectrum of the dot can be treated as a continuum (as in metals), and the quantum limit, in which transport proceeds by resonant tunneling through a single discrete energy level in the dot. In addition, Coulomb-blockade oscillations in the *thermopower* of a quantum dot are discussed. In contrast to the conductance oscillations, which consist of a series of sharp peaks, the thermopower oscillations have a sawtooth line shape.

Chapter 3 deals with disordered quantum wires. In spite of the *disordered* nature of these wires, the conductance is found to exhibit *periodic* oscillations as a function of gate voltage. This is the case in both intentionally (Be doped) and unintentionally disordered wires. The oscillations, which persist up to a few kelvin, have a period that does not correlate with wire length, and that is quite insensitive to a strong magnetic field. These observations can be interpreted consistently in the frame work of Coulomb-blockade oscillations, if one assumes that the disorder results in the natural formation of a quantum dot in the wire.

Chapter 4 deals with Coulomb-blockade oscillations in quantum dots. The irregular envelope, i.e., the variation of the amplitude of the oscillations from peak to peak, is found to change into a periodic modulation in quantizing magnetic fields. This is interpreted in terms of *cyclic* depopulation of the Landau levels in the dot by a single electron per Landau level per period, with tunneling occurring predominantly through a single edge state of the outermost Landau level. In addition, it is shown that Coulomb charging effects have to be taken into account even in the presence of adiabatically transmitted edge channels through the dot. This is because edge channels confined to the dot are separated from transmitted edge channels by incompressible regions, i.e. dielectric-like regions, acting as tunnel barriers. Finally, an account is given of the first observation of sawtooth like Coulomb-blockade oscillations in the *thermopower* of a quantum dot, in agreement with theory.

Samenvatting

De fundamentele vaste-stoffysica heeft veel profijt gehad van de industriële inspanning om de prestatie van halfgeleiderdevices op te voeren. De vooruitgang in microfabricagetechnieken waartoe deze inspanning heeft geleid, ligt ten grondslag aan belangrijke doorbraken die in het afgelopen decennium tot stand zijn gebracht op het gebied van de mesoscopische fysica. Dit is een nieuwe tak van de vaste-stoffysica die zich bezig houdt met de studie van “kleine” systemen. Klein betekent hier afmetingen vergelijkbaar met een relevante fysische lengteschaal, waardoor mesoscopische systemen interessante eigenschappen bezitten en veel nieuwe fysische verschijnselen vertonen.

Dit proefschrift behandelt het verschijnsel van “Coulomb-blokkade oscillaties in quantum dozen en draden”. In een quantum doos is het elektronengas in een klein volume opgesloten, zodanig dat het energiespectrum uit discrete niveaus bestaat; in een quantum draad is het in slechts twee richtingen opgesloten. Zowel quantum dozen als draden kunnen in het tweedimensionale elektronengas (2DEG) in een modulatie-gedoteerde GaAs-Al_xGa_{1-x}As heterostructuur worden gedefinieerd door middel van een geschikt patroon van split-gate elektroden, dat met behulp van elektronbundel lithografie boven op de heterostructuur wordt aangebracht. Door een negatieve gatespanning (ten opzichte van het 2DEG) aan te leggen wordt dit patroon in het 2DEG gekopieerd. Coulomb blokkade verwijst naar de onderdrukking van tunneling door een systeem met ultra-kleine capaciteit, bijvoorbeeld een quantum doos of klein metaaldeeltje, bij lage temperaturen en kleine aangelegde spanningen. De reden voor deze onderdrukking is dat de elektrostatische ladingsenergie, die nodig is om één enkel elektron aan het systeem toe te voegen, niet beschikbaar is (omdat die groot

is ten opzichte van de thermische energie). De ladingsenergie kan worden gereduceerd door middel van een spanning die wordt aangelegd op een gate elektrode die capacitief aan het systeem is gekoppeld. Hierdoor wordt de Coulomb blokkade opgeheven, hetgeen periodieke geleidingsoscillaties als functie van de gatespanning tot gevolg heeft. Dit zijn de Coulomb-blokkade oscillaties.

Na een inleiding in hoofdstuk 1 in de basisconcepten die in dit proefschrift worden gebruikt, wordt in hoofdstuk 2 een samenvatting gegeven van een theorie voor Coulomb-blokkade oscillaties in een quantum doos. De periodiciteit van de oscillaties bij temperatuur nul wordt afgeleid van de evenwichtseigenschappen van het systeem, en limiet gevallen van het algemene resultaat van een kinetische theorie voor transport door de doos bij eindige temperaturen worden besproken. Deze bestaan uit de klassieke limiet, waarin het energiespectrum van de doos als een continuüm mag worden behandeld (zoals in metalen), en de quantum limiet, waarin het transport plaatsvindt door resonant tunnelen door één enkel energie niveau in de doos. Voorts worden de Coulomb-blokkade oscillaties in de *thermokracht* van een quantum doos besproken. In tegenstelling tot de oscillaties in de geleiding, die uit een serie scherpe pieken bestaan, hebben de oscillaties in de thermokracht de vorm van een zaagtand.

Hoofdstuk 3 behandelt wanordelijke quantum draden. Ondanks het *wanordelijke* karakter van deze draden vertoont de geleiding hiervan *periodieke* oscillaties als functie van de gatespanning. Dit is het geval in draden waarin zowel opzettelijk (Be dotering) als onopzettelijk wanorde is aangebracht. De periode van de oscillaties, die tot een paar kelvin waarneembaar zijn, vertoont geen correlatie met de draadlengte en is vrij ongevoelig voor een sterk magnetisch veld. Deze waarnemingen kunnen consistent worden verklaard in het kader van Coulomb-blokkade oscillaties, indien men aanneemt dat de wanorde leidt tot de natuurlijke vorming van een quantum doos in de draad.

Hoofdstuk 4 behandelt Coulomb-blokkade oscillaties in quantum dozen. De onregelmatige omhullende, d.w.z. de variatie van de amplitude van de oscillaties van piek tot piek, blijkt in een quantiserend magnetisch veld te veranderen in een periodieke modulatie. Dit wordt verklaard in termen van *cyclische* depopulatie van de Landau niveaus in de doos, met één enkel elektron per Landau niveau per periode, waarbij tunneling voor namelijk optreedt door één enkele randtoestand van het buitenste Landau

niveau. Voorts wordt er aangetoond dat ladingseffecten zelfs in rekening moeten worden gebracht in de aanwezigheid van adiabatisch doorgelaten randkanalen door de doos. De reden hiervoor is dat de randkanalen die in de doos zijn opgesloten door incompressibele gebieden, d.w.z. diëlectricum-achtige gebieden, van de doorgelaten kanalen worden gescheiden. Tenslotte wordt er een verslag gegeven na de eerste waarneming van zaagtandvormige Coulomb-blokkade oscillaties in de *thermokracht* van een quantum doos, in overeenstemming met de theorie.

List of publications

1. P. Hendriks, A. A. M. Staring, R. G. van Welzenis, J. H. Wolter, W. Prost, K. Heime, W. Schlapp, and G. Weimann, "Current oscillations at high electrical fields in the two-dimensional electron gas in GaAs/AlGaAs heterostructures", *Appl. Phys. Lett.* **54**, 2668 (1989).
2. L. P. Kouwenhoven, B. J. van Wees, W. Kool, C. J. P. M. Harmans, A. A. M. Staring, and C. T. Foxon, "Transition from Ohmic to adiabatic transport in quantum point contacts in series", *Phys. Rev. B* **40**, 8083 (1989).
3. L. W. Molenkamp, A. A. M. Staring, C. W. J. Beenakker, R. Eppenga, C. E. Timmering, J. G. Williamson, C. J. P. M. Harmans, and C. T. Foxon, "Electron-beam collimation with a quantum point contact", *Phys. Rev. B* **41**, 1274 (1990).
4. A. A. M. Staring, L. W. Molenkamp, C. W. J. Beenakker, L. P. Kouwenhoven, and C. T. Foxon, "Magnetoconductance of two point contacts in series", *Phys. Rev. B* **41**, 8461 (1990).
5. A. A. M. Staring, H. van Houten, C. W. J. Beenakker, and C. T. Foxon, "Coulomb-regulated conductance oscillations in a disordered quantum wire", in *High magnetic fields in semiconductor physics III*, edited by G. Landwehr (Springer-Verlag, Berlin Heidelberg, 1992).
6. C. W. J. Beenakker, H. van Houten, and A. A. M. Staring, "Coulomb blockade of the Aharonov-Bohm effect", in *Granular Nanoelectronics*, edited by D. K. Ferry (Plenum Press, New York, 1991).

7. C. W. J. Beenakker, H. van Houten, and A. A. M. Staring, "Influence of Coulomb repulsion on the Aharonov-Bohm effect in a quantum dot", *Phys. Rev. B* **44**, 1657 (1991).
8. L. P. Kouwenhoven, N. C. van der Vaart, A. T. Johnson, C. J. P. M. Harmans, J. G. Williamson, A. A. M. Staring, and C. T. Foxon, "Charging effects in quantum dots", in *Festkörperprobleme/Advances in Solid State Physics*, edited by U. Rössler (Vieweg, Braunschweig, 1991), Vol. 31, p. 329.
9. L. P. Kouwenhoven, N. C. van der Vaart, A. T. Johnson, W. Kool, C. J. P. M. Harmans, J. G. Williamson, A. A. M. Staring, and C. T. Foxon, "Single electron charging effects in semiconductor quantum dots", *Z. Phys. B* **85**, 367 (1991).
10. A. A. M. Staring, J. G. Williamson, H. van Houten, C. W. J. Beenakker, L. P. Kouwenhoven, and C. T. Foxon, "Coulomb-blockade oscillations in a quantum dot", *Physica B* **175**, 226 (1991).
11. J. G. Williamson, A. A. M. Staring, L. P. Kouwenhoven, H. van Houten, C. W. J. Beenakker, C. E. Timmering, M. Mabesoone, and C. T. Foxon, "Lateral electron transport through a quantum dot: Coulomb blockade and quantum transport", in *Nanostructures and Mesoscopic Systems*, edited by W. P. Kirk (Academic Press, Boston, 1992).
12. H. van Houten, C. W. J. Beenakker, and A. A. M. Staring, "Coulomb-blockade oscillations in semiconductor nanostructures", in *Single Charge Tunneling*, edited by H. Grabert and M. H. Devoret (Plenum Press, New York, 1992).
13. A. A. M. Staring, H. van Houten, and C. W. J. Beenakker, "Coulomb-blockade oscillations in disordered quantum wires", *Phys. Rev. B* **45**, 9222 (1992).
14. H. van Houten, C. W. J. Beenakker, and A. A. M. Staring, "Coulomb-blockade oscillations in quantum wires and dots", in *Single-Electron Tunneling and Mesoscopic Devices*, edited by H. Koch and H. Lübbig (Springer-Verlag, Berlin Heidelberg, 1992).

15. C. W. J. Beenakker and A. A. M. Staring, "Theory of the thermopower of a quantum dot", Phys. Rev. B, to be published.
16. A. A. M. Staring, B. W. ALphenaar, H. van Houten, L. W. Molenkamp, O. J. A. Buyk, M. A. A. Mabesoone, and C. T. Foxon, "Periodic envelope of Coulomb-blockade oscillations in the quantum Hall regime", Phys. Rev. B, to be published.
17. B. W. Alphenaar, A. A. M. Staring, H. van Houten, O. J. A. Buyk, M. A. A. Mabesoone, and C. T. Foxon, "The influence of adiabatically transmitted edge channels on single-electron tunneling through a quantum dot", Phys. Rev. B, to be published.
18. A. A. M. Staring, L. W. Molenkamp, B. W. Alphenaar, H. van Houten, O. J. A. Buyk, M. A. A. Mabesoone, C. W. J. Beenakker, and C. T. Foxon, "Coulomb-blockade oscillations in the thermopower of a quantum dot", submitted to Phys. Rev. Lett.

Dankwoord

Dit proefschrift zou niet tot stand zijn gekomen zonder de bijdragen van Bruce Alphenaar, Marcel Broekaart Hans Buyk, Carlo Beenakker, Rob Eppenga, Tom Foxon, Cees Harmans, Henk van Houten, Leo Kouwenhoven, Menno Mabesoone, Laurens Molenkamp, Ad Nagelkerke, Martin Schuurmans, Eugene Timmering, Bart van Wees, John Williamson, Fred de Wit, en Joachim Wolter. Ik dank hen hiervoor hartelijk.

Curriculum Vitae

9 oktober 1964 geboren te Tilburg

1977 – 1983 Gymnasium B, Sint Pauluslyceum te Tilburg

1983 – 1988 Technische Natuurkunde (cum laude) aan de
Technische Universiteit Eindhoven

1988 – 1990 twee-jarige onderzoekersopleiding aan het
Instituut voor Vervolgopleidingen van de
Technische Universiteit Eindhoven,
met praktisch werk op het
Philips Natuurkundig Laboratorium

1990 in dienst bij het Philips Natuurkundig Laboratorium;
groep Experimental and Theoretical Physics,
onder leiding van Prof. Dr. Ir. M. F. H. Schuurmans;
thans groep Experimental Physics,
onder leiding van Dr. H. van Houten

Stellingen

behorende bij het proefschrift

Coulomb-Blockade Oscillations in Quantum Dots and Wires

1. Bij resonant tunnelen van elektronen door gelocaliseerde quantum-toestanden zijn ladingseffecten veelal dominant.

– *Dit proefschrift*

2. De gangbare opvatting dat de Coulomb blokkade uitsluitend kan optreden in systemen met een weerstand groter dan h/e^2 is onjuist.

– *K. K. Likharev, IBM J. Res. Dev. **32**, 144 (1988)*

3. De door Nejoh met behulp van een “scanning-tunneling” microscoop (STM) waargenomen structuur in de I-V karakteristiek van een vloeibaar-kristalmolecuul is geen Coulomb ladder.

– *H. Nejoh, Nature **353**, 640 (1991)*

4. De contactweerstand die optreedt bij metingen aan verticaal transport door een metallische multilaag kan niet worden geëlimineerd door een standaard vierpuntsgeometrie te kiezen.

5. Een quantum puntcontact kan als locale thermometer in een tweedimensionaal elektronengas worden gebruikt.

– *L. W. Molenkamp, Th. Gravier, H. van Houten, O. J. A. Buyk en M. A. A. Mabesoone, Phys. Rev. Lett. **68**, 3765 (1992)*

6. De polaire molecuul-oriëntatie in het centrum van een vloeibaar-kristalcel wordt bepaald door de azimuthale verdeling in de eerste moleculaire monolaag op het gewreven polymer-glas substraat.
 - *M. Barmentlo, R. W. J. Hollering en N. A. J. M. van Aerle, Phys. Rev. A* **46**, 15 oktober 1992
7. Het grote externe rendement waargenomen bij fotoluminescentiemetingen aan poreus Si kan worden verklaard op grond van de onderdrukking van niet-stralende processen.
 - *G. W. 't Hooft, Y. A. R. R. Kessener, G. L. J. A. Rikken en A. H. Venhuizen, Appl. Phys. Lett.* **61**, 9 november 1992
8. Metingen aan hagelruit leveren informatie die niet kan worden verkregen uit geleidingsmetingen.
 - *C. W. J. Beenakker en M. Büttiker, Phys. Rev. B* **46**, 1889 (1992)
9. Mesoscopische fysica is een bijzonder geschikt werkterrein voor een onderzoeker in opleiding.
10. Het is inzichtlijker om in demografische beschouwingen over de bevolkingsgroei een verdubbelingstijd te hanteren in plaats van een groeipercentage per jaar.

Eindhoven, 5 november 1992

Toine Staring